UNCLASSIFIED

DEFENCE RESEARCH ESTABLISHMENT
CENTRE DE RECHERCHES POUR LA DEFENSE
VALCARTIER, QUEBEC

DREV TM-1999-134

Unlimited Distribution/Distribution illimitée

WIND TUNNEL TESTS ON DREV - ISL REFERENCE AFTERBODIES AT MACH 2.0 (SERIES ISLPWT-2)

by

Bertrand Girard

March/mars 2000

Approved by / approuvé par

Head, Delivery Systems Section
Chef, Section systèmes de lancement

6 March 00
Date

SANS CLASSIFICATION

ABSTRACT

In support to a co-operative research programme between the Defence Research Establishment Valcartier (DREV), Canada and the Institut franco-allemand de recherches de St-Louis (ISL) France, under the auspices of Theme 25 - Aeroballistics of the Franco-Canadian Accord, wind tunnel tests were performed in the DREV 0.6 m x 0.6 m facility at a Mach number of 2.0 with two configurations of afterbody models of reference: Cylinder with/without fins based on the Southampton University Calibration Body. Boundary layer characterization tests were performed with a smooth afterbody model without fins and surface pressure distribution surveys were made with afterbody models with and without fins. The rationale for this test series was to compare test results with those from similar tests performed at ISL in test conditions that differ to some extent. This memorandum describes the experiment and is complementary to other DREV and ISL publications on wind tunnel and aeroballistic range tests and on CFD simulations.

RÉSUMÉ

Dans le cadre du programme de coopération de recherches entre le Centre de recherches pour la défense, Valcartier (CRDV), au Canada et l'Institut franco-allemand de recherches de St-Louis (ISL), en France, relativement au thème 25 de l'Accord franco-canadien, des essais dans la soufflerie 0,6 m x 0,6 m du CRDV ont été faits à Mach 2.0 sur deux modèles de référence de corps arrière: cylindrique avec ou sans empennage et basés sur le "Southampton University Calibration Body". Des mesures de caractérisation de la couche limite ont été effectuées avec un modèle lisse non empenné ainsi que des mesures de distribution de pression de surface sur des modèles de corps arrière lisses ou avec empennage. L'un des intérêts primordiaux de ces essais était de comparer les résultats obtenus à ceux d'expériences similaires effectuées à l'ISL dans des conditions expérimentales présentant certaines différences. Ce mémorandum décrit l'expérience et est complémentaire à d'autres publications du CRDV et de l'ISL sur des essais en soufflerie et dans le corridor aérobalistique ainsi que sur des simulations numériques d'écoulements.

WARNING NOTICE

The information contained herein is proprietary to Her Majesty and is provided to the recipient on the understanding that it will be used for information and evaluation purposes only. Any commercial use, including use for manufacture, is prohibited. Release to third parties of this publication or of information contained herein is prohibited without the prior written consent of DND Canada.

© Her Majesty the Queen in Right of Canada as represented by the Minister of National Defence, 2000

TABLE OF CONTENTS

ABSTRACT/RÉSUMÉ i

EXECUTIVE SUMMARY v

NOMENCLATURE vii

1.0 INTRODUCTION 1

2.0 MODEL AND SUPPORT CONFIGURATIONS 10

2.1 Boundary Layer Characterization 11

2.2 Base Pressure Distribution 15

3.0 DREV TRISONIC FACILITY - DESCRIPTION 55

4.0 BOUNDARY LAYER CHARACTERIZATION - EXPERIMENTAL METHODOLOGY AND DESCRIPTION OF APPARATUS 60

5.0 BASE PRESSURE DISTRIBUTION - EXPERIMENTAL METHODOLOGY AND DESCRIPTION OF APPARATUS 73

6.0 DATA ACQUISITION SYSTEM 84

6.1 Boundary Layer Characterization Tests 85

6.2 Base Pressure Distribution Tests 85

7.0 TREATMENT OF DATA - BOUNDARY LAYER CHARACTERIZATION IN A COMPRESSIBLE FLOW 86

7.1 Velocity Ratio Profiles as a Function of Mach Number Inside Boundary Layer 86

7.2 Relationship Between Mach Number and Pitot Probe Total Pressure Measurement at Supersonic Regime Inside Boundary Layer 88

7.3 Relationship Between Mach Number and Pitot Probe Total Pressure Measurement at Subsonic Regime Inside Boundary Layer 90

7.4 Algorithm Used to Calculate the Boundary Layer Velocity Ratio Profile 91

7.5 Equations to Characterize the Boundary Layer 94

7.6 Algorithms Used to Determined Boundary Layer Thickness and the Velocity Profile Power Law Exponent 96

7.7 Algorithm Used to Calculate the Boundary Layer Displacement Thickness and Momentum Thickness 99

8.0 TREATMENT OF DATA - BASE PRESSURE DISTRIBUTION 102

9.0 RESULTS 104

9.1 Boundary Layer Characterization 104

9.2 Base Pressure Distribution Tests 104

10.0 BOUNDARY LAYER CHARACTERIZATION AND PRESSURE DISTRIBUTION MEASUREMENT ERRORS 118

11.0 DISCUSSIONS 123

12.0 CONCLUSIONS 130

13.0 ACKNOWLEDGEMENT 133

14.0 REFERENCES 134

FIGURES 1 to 77

TABLES I to VI

APPENDIX A - Summary of Runs

APPENDIX B - Upstream-Sting Alignment

APPENDIX C - Boundary Layer Aspiration

APPENDIX D - Boundary Layer - Summary of Results

APPENDIX E - Base Pressure - Summary of Results

APPENDIX F - Measurement Errors

EXECUTIVE SUMMARY

The development of new projectiles or missiles for weapons systems and improvements to current ones depend on our ability to model and experiment accurately the aerodynamic behaviour of the projectile/missile. Because of the number of design approaches to improve flight vehicles, a configuration of reference was therefore defined. New design concepts could be implemented and tested with respect to that configuration of reference in order to evaluate accurately the net benefits related to each improvement concept.

The wind tunnel testing of a complete model of reference with flat base involves important aerodynamic interactions on the base flow from the sting support. Since the base drag represents a significant percentage of the total drag of artillery projectiles configured with a flat base it was also important to specifically investigate the base flow recirculation. To improve our knowledge in that area DREV and the Institut franco-allemand de recherches de St-Louis (ISL), France, set up an initial cooperative agreement in aeroballistics/aerodynamics. The project is divided into two phases. In Phase I, the model of reference was experimentally investigated through aeroballistic range tests and wind tunnel tests at DREV and ISL. In Phase II, complementary tests on the base flow recirculation were performed by using a model of an afterbody section installed on an upstream-sting system in the DREV wind tunnel facility.

This memorandum describes Phase II of the wind tunnel tests performed in the DREV 0.6 m x 0.6 m indraft wind tunnel at a Mach number of 2.0. These tests were to characterize the boundary layer approaching a flat base and to perform surface pressure distribution measurements on the base/afterbody of DREV-ISL reference models. These reproduced the afterbody of the "Southampton University Calibration Model, 6D Configuration" with/without trapezoidal fins. This wind tunnel test runs series (made at subcritical Reynolds numbers) provided us with data complementary to the ISL facility's (obtained at supercritical Reynolds numbers). The results describe the boundary layer velocity profile and related characterization. These results are complementary to data from aeroballistics tests (DREV) and to computational fluid dynamics (CFD) simulations performed at DREV and ISL. All the necessary details are included to enable a pursuit of subsequent experiments. This data of reference will potentially make us capable of characterizing with accuracy future artillery projectiles configured with a flat base.

VI

NOMENCLATURE

C_p	Specific heat at constant pressure
C_r	Crocco number, used to determine boundary layer characterization
C_v	Specific heat at constant volume
d	Body diameter (or calibre), for all configurations = 40.0 mm or 1.575 in
$d^1 = d = D$	Base diameter for the configurations investigated in this test series
g_c	Newton constant
L	Model total length, (SOUTHAMPTON UNIVERSITY CALIBRATION MODEL)
n	Number of experimental readings
n	Inverse exponent of boundary layer velocity profile exponential law
$Ma \approx M_\infty \approx \overline{M}$	Nominal Mach number obtained by flow calibration during the wind tunnel commissioning (use to identify set of nozzle blocks in use)
Mbl	Measured Mach number at a specific level inside boundary layer
M_i	Measured Mach number in test section (free stream) at the time of the ith reading
$\overline{M} = \frac{1}{n}\sum_{i=1}^{n} M_i = M$	Average Mach number between 3.5 to 6.0 s run time

$M = M_\infty$	Average Mach number during data acquisition run time (stability or aerodynamic coefficient tests)
$M_\infty \approx M_a$	Mach number outside the boundary layer (on model surface)
M_1	Mach number inside the boundary layer (model surface)
M_2	Mach number after pitot tube bow shock wave
P_{base}	Model base flow static pressure as measured by the pressure transducer (PSI pressure module)
$P_{ij} = P_{ij\ \text{as read}}$	Static pressure read at the j^{th} pressure tap at the i^{th} reading
$P_{ij\ \text{as read}} = P_{ij}$	Static pressure read at the j^{th} pressure tap at the i^{th} reading, used in the text and several equation to make it more readily clear
$P_{ij\ \text{TRUE}}$	True static pressure read at the j^{th} pressure tap at the i^{th} reading
PITOT	Data results vector related to boundary layer characterization tests
P_{mstat_i}	Model surface static pressure at the i^{th} reading (boundary layer tests)
$P_{pitot_i} \approx P_{t_2}$	Total pressure as measured from pitot tube at the i^{th} reading
$p_p \approx P_{t_2}$	Total pressure from pitot tube (after bow shock wave)

P_{ref}	Pressure of reference used in conjunction with the pressure module and obtained from an absolute pressure sensor and appropriate manifold and tubing system
P_S	Average value of the measured test section static pressure at wall (average from wall taps nos: 7 and 8) $= \frac{1}{n}\sum_{i=1}^{n} P_{s_i}$
$p_s \approx P_\infty \approx P_S$	Static pressure at pitot tube location but just ahead of bow shock wave
P_{s_i}	Test section static pressure measured at the time of the i^{th} reading (average from wall taps nos: 7 and 8) corresponding to flow conditions at wall just aside model base/afterbody
$P\ STAT = P_S$	Average of the measured test section static pressure at wall (average from wall taps nos: 7 and 8)
$P_T = \sum_{i=1}^{n} P_{t_i}$	Average air pressure in bag during data acquisition run time, between 3.5 to 6.0 s run time
P_t	Total pressure in a flow, when used in thermodynamics or gas dynamics equations in the text
P_{t_i}	Measured air pressure in bag at the i^{th} reading
P_{t_∞}	Total pressure outside model boundary layer

P_{t_1}	Total pressure inside model boundary layer
P_{t_2}	Total pressure after pitot tube bow shock wave
P_{t_2}/P_∞	Pitot tube total pressure over test section static pressure ratio used to derive velocity inside boundary layer
$P_{tap}/P_{stat} = \frac{P_{ij\ TRUE}}{P_\infty}$	= Pressure ratio for the jth pressure tap at the time of the ith reading, displayed in tabulated data for each 0.1 s between 3.5 to 6.0 s run time
$P_\infty \approx P_S \approx P_V \approx P_{s_i}$	Free stream static pressure (≈ average from wall taps nos: 7 and 8 corresponding to flow conditions at wall just abeam of model base/afterbody)
P_1	Static pressure inside model boundary layer
P_2	Static pressure after pitot tube bow shock wave
Q	Dynamic pressure in test section $= \frac{1}{2}\rho V^2 = \frac{\gamma}{2} P_\infty M_\infty^{\ 2}$
Q_i	Dynamic pressure in test section at the ith reading
$\overline{Q} = \frac{1}{n}\sum_{i=1}^{n} Q_i$	Average dynamic pressure in test section between 3.5 and 6.0 s run time

$q_i = P_{t_1}$	Indicated dynamic pressure at pitot tube location but just ahead of bow shock wave
$R_{Pmstat_i} = \frac{P_{mstat_i}}{P_\infty}$	Model surface static pressure ratio at the i^{th} reading (boundary layer tests)
$\overline{R_{Pmstat}}$	Average model surface static pressure ratio for all readings between 3.5 to 6.0 s run time (boundary layer tests)
$R_{Ppitot_i} \approx \frac{P_{t_2}}{P_\infty} = \frac{P_{pitot_i}}{P_\infty}$	Reduced total pressure from pitot tube measurements at the i^{th} reading
$\overline{R_{Ppitot}} \equiv \frac{P_{t_2}}{P_\infty}$	Average total pressure from pitot tube measurements for all readings between 3.5 and 6.0 s run time
$R_{PRij} = \frac{P_{ij\,TRUE}}{P_\infty}$	Pressure ratio for the j^{th} pressure tap at the i^{th} reading
$\overline{R_{PRij}}$	Average pressure ratio for the j^{th} pressure tap for all readings between 3.5 and 6.0 s run time
R	Perfect gas constant
R	Model radius = D/2
REY/M	Reynolds number per meter of model characteristic length

R_{∞_D} = RE(D)	$\frac{V \bullet \rho \bullet d}{\mu}$ = Reynolds number based on diameter
R_{∞_L} = RE(L)	$\frac{V \bullet \rho \bullet L}{\mu}$ = Reynolds number based on total length
R_{CF} = RE(CF)	$\frac{V_{CF} \bullet \rho \bullet d}{\mu}$ = Cross-flow Reynolds number, 15 deg. angle of attack
STATIC MODEL ≈ $p_s \approx P_\infty \approx P_S$	Static pressure at pitot tube location but just ahead of bow shock wave
S_1	Entropy inside model boundary layer
S_2	Entropy after pitot tube bow shock wave
T_a	Air temperature in dry air bag, °K (Indraft wind tunnel)
T_c	Air temperature in dry air bag, °C (Indraft wind tunnel)
t_i	Time reference (sec.) at the time of the i^{th} pressure reading
T_v	Calculated air temperature in test section, °K
$T_\infty \approx T_v$	True air temperature in test section, °KT_1 Air flow temperature in model boundary layer
T_1	Air flow temperature in model boundary layer
T_2	Air flow temperature after pitot tube bow shock wave

T_t	Total temperature in test section = T_a °K
$U_\infty = V$	Air flow velocity in test section
U_1	Air flow velocity inside model boundary layer
V	Air velocity in test section
Y	Pitot tube distance from model surface to pitot tube inlet centreline
y	Vertical distance inside boundary layer from model surface
δ	Boundary layer total thickness = Y value where U/U_∞ is equal to 0.99
δ_1	Boundary layer displacement thickness, (cylindrical body)
δ_2	Boundary layer momentum thickness, (cylindrical body)
$\gamma = C_p/C_v$	Ratio of specific heat, = 1.4 for air
$\rho = \rho_\infty$	Air density in test section
ρ_1	Air density inside model boundary layer
ρ_2	Air density after pitot tube bow shock wave
$\rho_\infty = \rho$	Air density in test section
μ	Coefficient of viscosity of air in test section, units are $N \cdot s / m^2$, is used to calculate the REY/M

ρ	Air density in test section

NOTE : A consistent system of units was used throughout the analysis

1.0 INTRODUCTION

Through a cooperative project with ISL (Institut franco-allemand de recherches de St-Louis) experimental and numerical investigations were made on cone/cylinder projectile configurations identified as " DREV-ISL Reference Models ", (Refs. 1 to 6). As specified in " Projet de coopération scientifique entre le CRDV et ISL " (Ref. 7) wind tunnel models were designed and manufactured at DREV for tests in the DREV trisonic wind tunnel facility in order to obtain complementary data and experimental assessment on aerodynamic coefficients and surface pressure distribution. This memorandum presents the results of the second series of wind tunnel experiments relative to this cooperative work.

The wind tunnel test program was divided into two Phases. Trials designation " ISLFPWT-1 " (Phase I) stands for tests performed with the standard downstream sting and was reported in a separate document (Ref. 8). Figures 1 and 6 show typical models tested under this Phase. The current test series designation "ISLPWT-2" (Phase II) is related to experiments made with a new upstream sting/pivot/afterbody combination system. The main objective of the wind tunnel test series presented here was to obtain experimental data on the afterbody boundary layer velocity profile and the base flow surface pressure induced by recirculation phenomena. The static pressure on model fin trailing edges, along the afterbody and between fins was also investigated.

In order to not disturb the base flow by any kind of downstream sting-support, the test models had to be held from their fore end by the upstream sting/pivot/afterbody combination system (designed and built at DREV for testing in the 0.6 m x 0.6 m Indraft Wind Tunnel). These models were physically a cylindrical prolongation of the upstream/sting which was also cylindrical and of the same diameter. Tests were performed at Mach 2.0 and at 0.0 deg. incidence although the pivot system allows incidence (angle of attack) sweep from - 5.0 to +5.0 deg. Figure 2 shows the afterbody model in test section, while its upstream sting in nozzle throat section can be seen in Fig. 3. The pivot system which is located just downstream to the convergent section is shown in Fig. 4.

The base flow pattern of a projectile (or flight body) can be affected, to some extent, by the boundary layer characteristics along its afterbody. Although it was known in advance that the approaching boundary layer has a rather limited influence on base pressure coefficient, preliminary test runs were to study the effect of the boundary layer as controlled by the upstream-sting aspiration intensity and the flow transition strip made of various sand paper collars around the sting (Fig. 5).

Adjustments were performed to obtain a base pressure coefficient similar to that obtained in the ISL wind tunnel facility with the same configuration. Subsequent measurements demonstrated a small observable dependence of the base pressure coefficient on the boundary layer around model afterbody.

In order to make possible base/afterbody flow surveys as a function of boundary layer characteristics, the upstream sting was fitted with aspiration holes (Fig. 5) connected to a proper aspiration system in order to alter the boundary layer velocity profile around the base/afterbody test model.

Thereafter, dedicated test runs were performed to characterize the boundary layer near the model base. This was achieved by measuring air flow velocity profile from free stream down to model surface with a special pitot tube (total pressure only, configured with a duck beak) whose tip travelled in a plane located 1.75 body calibre from model base. All subsequent base pressure, fin trailing edges, afterbody and between fins surface pressure measurements were made with the same aspiration and transition strip settings giving a specific boundary layer velocity profile.

In order to reduce the geometric variations, DREV-ISL Reference Models were based on a unique generic main body configuration. These models reproduced the "Southampton University Calibration Model, 6D Configuration" (Refs. 9 and 10) and featured mainly a cylinder with and without trapezoidal fins.

Designed and built at DREV, Phase II models were produced in several units and had the appropriate mechanical configuration intended for tests on the upstream sting/pivot/afterbody combination system.

Conditions encountered in the DREV wind tunnel facility gave Reynolds numbers about 3.6 times smaller than free-flight conditions. This experiment was to validate CFD simulations and to compare DREV wind tunnel results with those from the DREV A/B range and from the ISL wind tunnel. Although flow conditions in the ISL wind tunnel feature Reynolds numbers about 20 times larger than that of the DREV wind tunnel, a comparison between the two facilities should show aerodynamic tendencies proper to specific configurations or at least be useful to show the influence of Reynolds numbers.

This memorandum presents the complete model descriptions, experimental procedures, test instrumentation and conditions, data reduction algorithms and a summary of measurement results.

For the Phase I of this project, a total of 57 runs were performed between January and April 1992.

This work was carried out between June 1990 and December 1998 under TNS 2ea14 " Flight Mechanics of Munitions ".

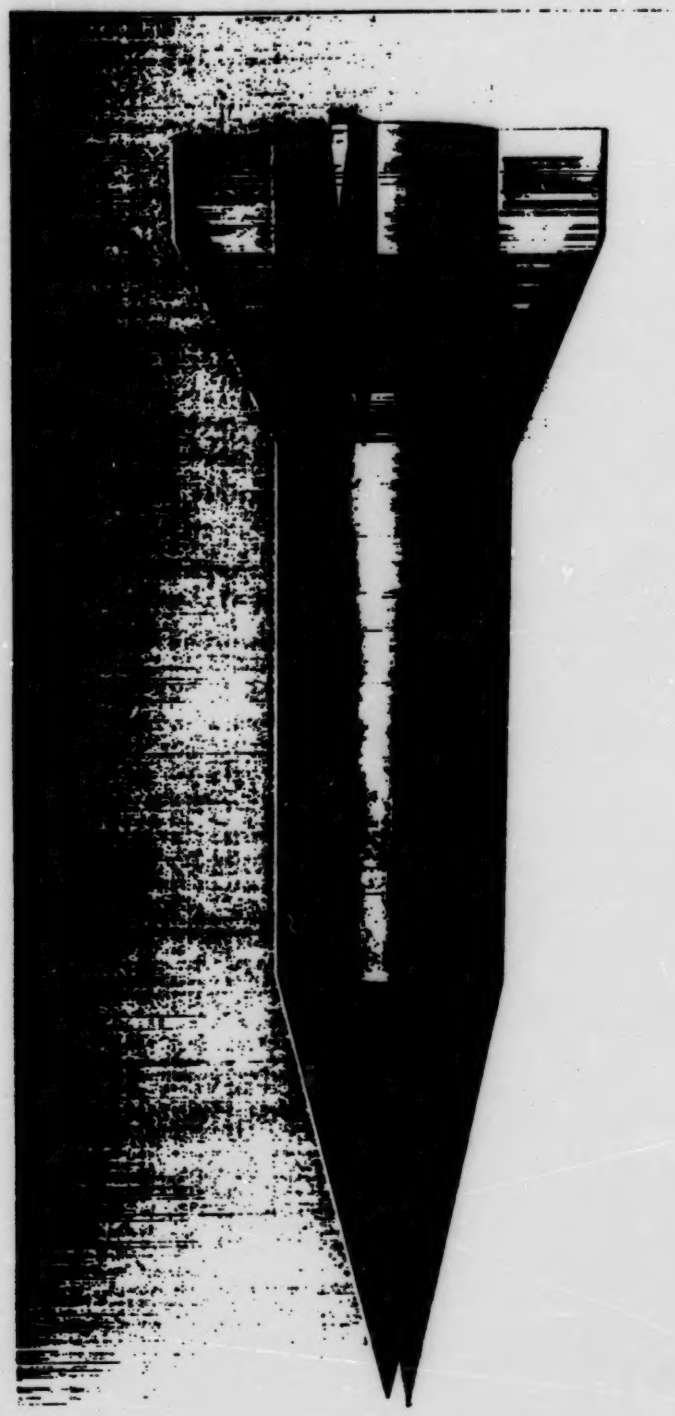

FIGURE 1 - ISL Cone/Cylinder reference model based on " SOUTHAMPTON UNIVERSITY CALIBRATION MODEL "

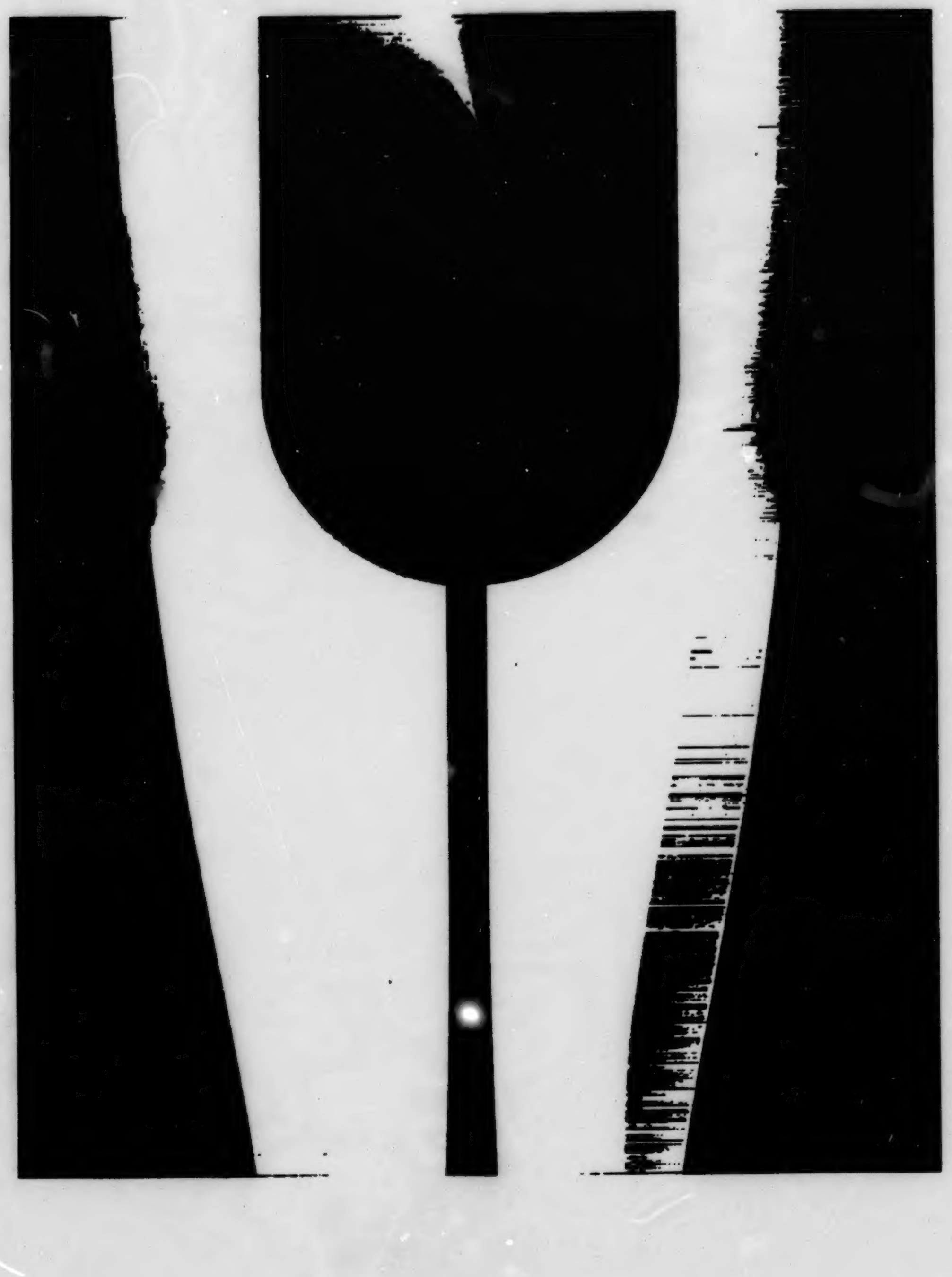

FIGURE 2 - Upstream sting fitted with afterbody model without fins, shown in Mach 2.0 test section

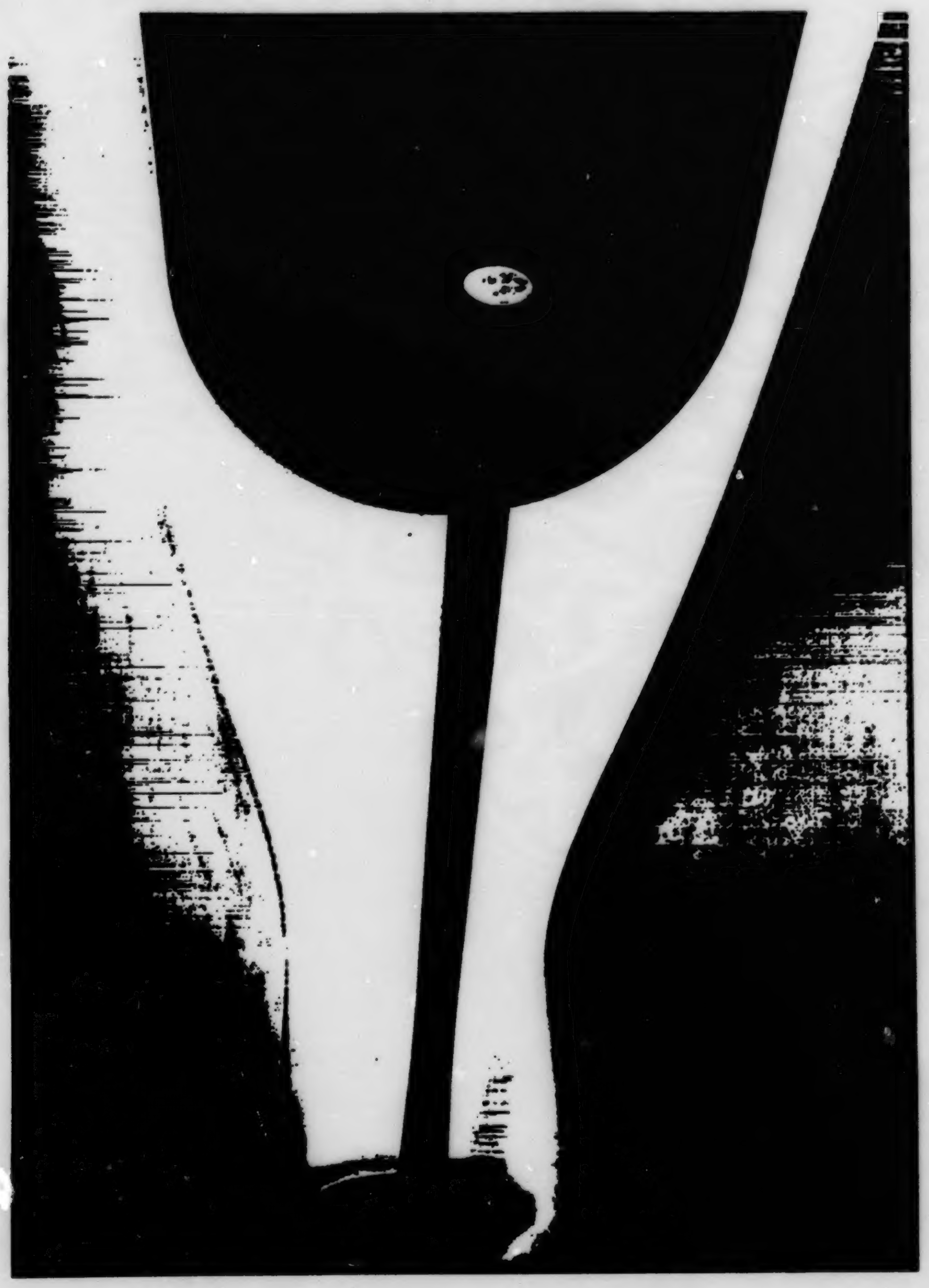

FIGURE 3 - Upstream sting across Mach 2.0 nozzle section throat, aspiration holes to be remarked

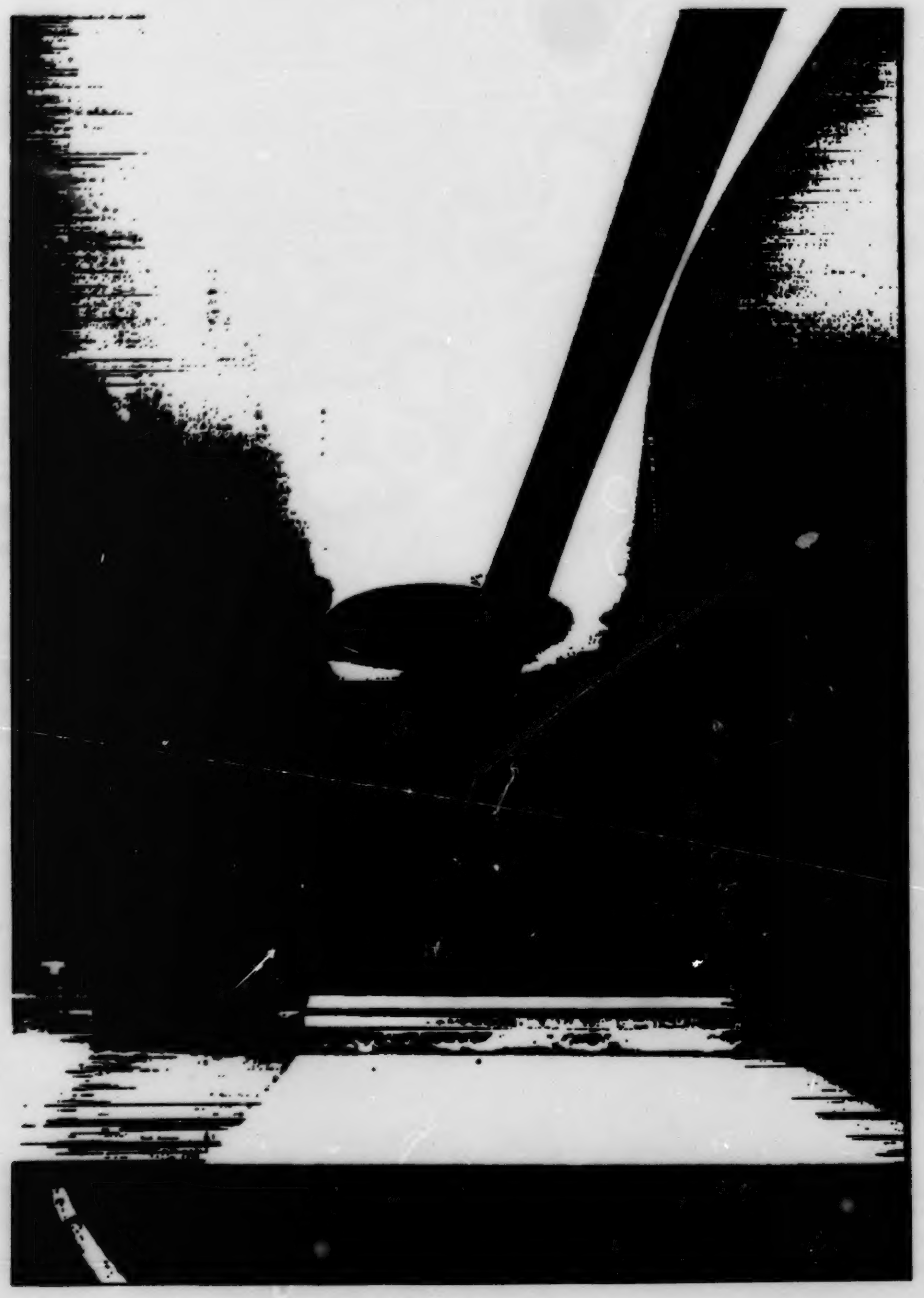

FIGURE 4 - Upstream sting pivot system, located upstream of the nozzle section

FIGURE 5 - Afterbody model with fins, sand paper collar to trip the flow and boundary layer aspiration holes

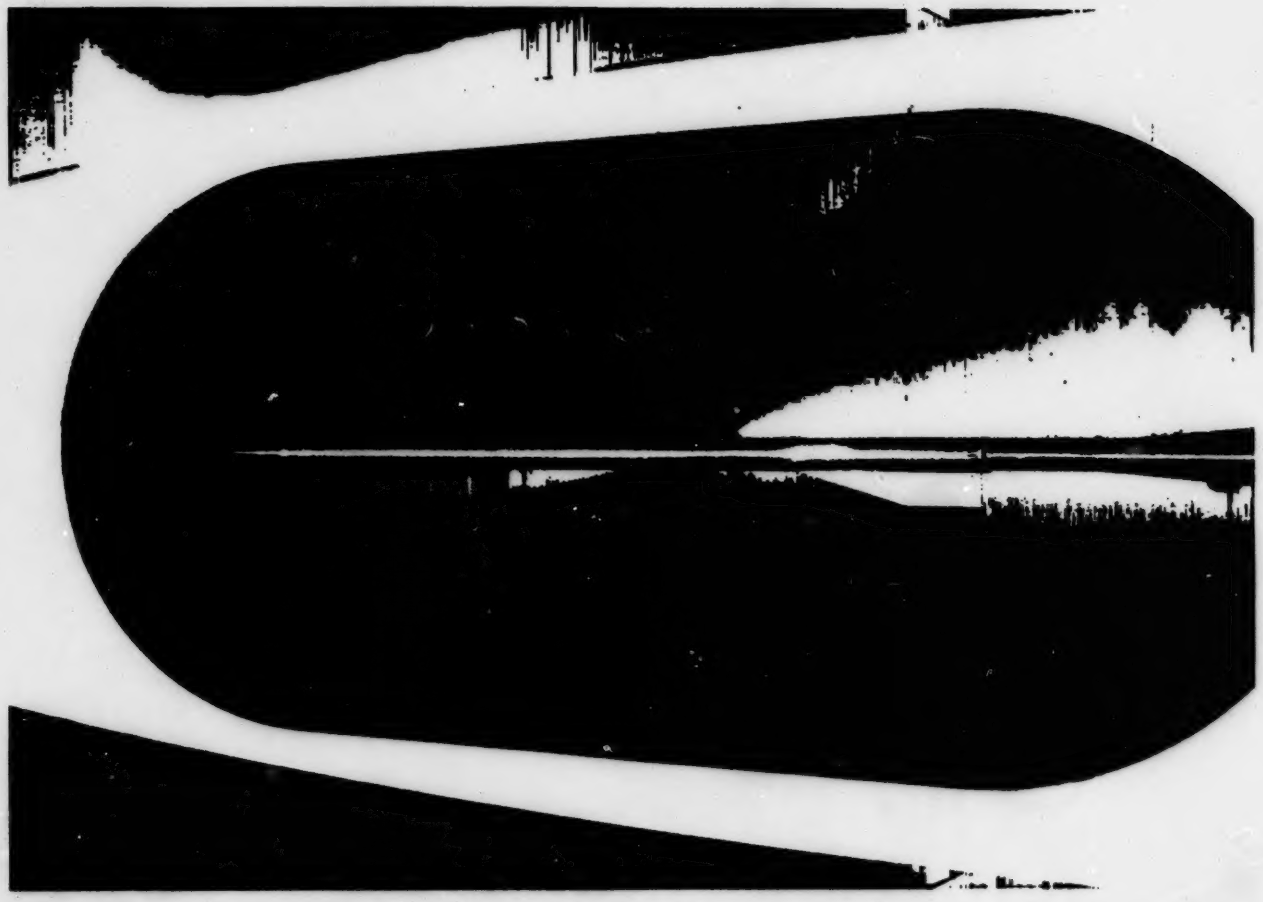

FIGURE 6 - ISL flechette model mounted on a standard downstream sting in tunnel test section fitted with the Mach 2.0 nozzle blocks

2.0 MODEL AND SUPPORT CONFIGURATIONS

The models used for the boundary layer characterization and the base pressure distribution study were all installed on the same upstream sting and boundary layer aspiration system developed at DREV for that purpose. Results on the boundary layer characterization and the base/afterbody pressure distribution were performed in different test series.

There was a need to establish a system to make distinctions between the numerous components of the models. These parts featured adapted designs to perform the boundary layer characterization and the base pressure measurements. Two families of components series were defined under the following nominatives:

a- Boundary layer characterization

A first series of components comprised the upstream sting system with its boundary layer aspiration and transition strips modular systems. It comprised all dedicated modules and components to characterize the boundary layer conditions related to the base/afterbody pressure distribution test runs series. There was only one model tested with this system. It is numbered and entitled as follows in Appendix A - SUMMARY OF RUNS :

Model no. 1 - BOUNDARY LAYER EXPLORATION
AFTERBODY MODEL

b- Base/afterbody pressure distribution

The second series consisted of a flat base/afterbody model dedicated to the base pressure distribution survey. The components were mounted on the upstream sting in replacement of the modules that were used for the boundary layer characterization. There were four models tested. They are numbered and entitled as follows in Appendix A - SUMMARY OF RUNS :

Model no. 2 - BASE PRESSURE EXPLORATION MODEL

Model no. 3 - AFTERBODY SURFACE PRESSURE MODEL

Model no. 4 - FINNED AFTERBODY MODEL, BETWEEN FINS PRESSURE SURVEY

Model no. 5 - FINNED AFTERBODY MODEL, FINS AND BASE PRESSURE SURVEY

> Note: Model no. 5 mentioned in Appendix A was physically the same unit as model no. 4 except that 32 pressure tubes from the module sensor were connected to the pressure taps on the base and the fin trailing edges instead of being connected to the pressure taps between fins. Unused pressure taps holes were filled smooth to model surface with mastic compound.

All drawings in this project were made as per ANSI (American Normalization Standard Institute) specifications for mechanical engineering. The dimensions were then expressed in inches and UNF or UNC (Unified National) screws and threads were utilized. This drawing representation is very similar to ACNOR/CSA (Association canadienne de normalisation/Canadian Standard Association).

2.1 Boundary Layer Characterization

The upstream sting/pivot/model afterbody combination system that was specially designed at DREV to study the afterbody and base flow around straight cylindrical projectiles consisted in series of interchangeable sections/modules. These units can be assembled in various combinations to fill the needs of the present test series.

Series of afterbody configurations, sting total length adjusters, sting surface rugosity and various types of boundary layer aspiration modules at different positions made possible to obtain 168 configurations and/or sting characteristics. The available boundary layer aspiration modules were of two types: canted holes or porous surface. It represented a large experimental potential. Only the aspiration modules with canted holes were used in present test series.

Figure 7 shows the upstream sting general arrangement (with/without boundary layer aspiration modules) together with the four afterbody models options that were tested in present test run series. In order to limit the risks of flow choking in the test section, a double-cone windshield was mounted on the strut hub which is normally used to hold standard downstream stings (Fig. 8).

Although tests were performed only at a constant 0 deg. sting incidence (nominal), the whole upstream sting system was mounted on a transverse wing support (Fig. 9) that can be pivoted from ± 5 deg. in order to study the influence of the angle of attack on the base flow. Figures 10 and 11 present the pivot system general arrangement and related cross-section view. In Fig. 11 it can be seen how pivots were friction held at the desired angle of incidence through conically contoured perimeters that worked like a standard conical fixation. This conical fixation was held in place by a set of 8 bolts (3/8 x 24 NF) on each side of the tunnel test section.

Figure 12 shows the air tight wall-through test section exit plug installed for the electrical wirings, calibration tubing and the high pressure servo-actuator that operate the valve of the pressure module sensor (Pressure System Inc.). This plug was located on the South side of the test section. The pressure sensor was located inside the upstream sting (Fig. 7).

Figure 13 shows the other extremity of the pivot system (located on the North side of test section) with the 1.0 in (25.4 mm) stainless steel flexible tubing that provided suction for the boundary layer aspiration. Also, two bolts (1/2 x 20 NF) located horizontally on each side of test section can be seen in Figs. 10 and 12. They were used to hold the wing support and to adjust the upstream sting in yaw for ≈ ± 1.5 deg.

Figure 14 is included herewith to show the relative positioning of the upstream sting with respect to the Mach 2.0 nozzle blocks (profile contours are represented in dash lines). The model base is drawn as per its relative position encountered during the tests. Figure 14 also displays a general arrangement of the new enlarged windows specially devised to make possible visualization effects experiments. Although no such tests were made in the present series it might be considered in near future with the Schlieren system that still have to be trial tested.

Another specific application would be the cabability to experiment on tandem projectiles aerodynamics while the upstream sting would be used in conjunction with a downstream sting to hold a follower projectile model in the test section.

For present wind tunnel test series, the upstream sting/afterbody combination modules adopted resulted into a total length of 2326 mm and a distance of 2024 mm between the pivot trunnions and afterbody model base.

From stem to stern, upstream sting components can be enumerated as follows:

a- comes in first the nose hub (Fig. 15), that also could contain the pressure module sensor if necessary, but was not used for that purpose in present test series,

b- the wing-support/body attachment (Fig. 16),

c- the horizontal wing support itself (Fig. 17),

d- the upstream sting main body with/without aspiration holes (Fig. 18), (the version with aspiration holes is represented here),

e- the tail stream-lining (Fig. 19) that also can contain the pressure sensor module for multiple pressure taps measurements (32 at a time),

f- the length adjusting anchorage (Fig. 20) that was available in 6 different lengths. Only the 8 inch long version with canted aspiration holes was used in present test series for the purpose of boundary layer aspiration, g- at the stern came the series of modular base/afterbody models (40.0 mm in diameter), in 5 different configurations. (Model no. 4 - FINNED AFTERBODY MODEL, BETWEEN FINS PRESSURE SURVEY shown in Fig. 7).

A flexible stainless-steel mesh tubing (Figs. 13, 21 and 22) was connected to the wing support tip canalization in order to achieve the boundary layer aspiration. This system used the same dump tank and valve facility which is usually utilized for the aspiration through the perforated walls of the transonic section. The other end of this tubing was connected to a pipe fitting tapped on the transonic section aspiration pipe in between the computer controlled on/off butterfly valve and the aspiration throttle valve (Fig. 22).

During tests with the upstream sting boundary layer aspiration, only the on/off valve was operated and the throttle valve was kept close, in order to get aspiration only inside the flexible mesh tubing and the upstream sting.

Figure 23 presents a general arrangement of the afterbody test rig dedicated to boundary layer velocity profile exploration. Figures 24 and 25 give the principal dimensions of its main body and its access cover. Figure 26 describes the round/conical inlet pitot tubes (made in 3 different lengths) that were used to explore the boundary layer at distances over 13 mm from model surface. Figure 27 refer to the flattened " duck beak " pitot tubes utilized for the velocity profile exploration from model surface to 13 mm .

The height adjustment gauge blocks and the alignment jig blocks utilized to adjust the height and alignment of pitot tubes are pictured and dimensioned in Figs. 28 and 29. These pitot tubes were held in place by set screws (4-40 UNC) that can be seen in the cutaway view of Fig. 23. Only the second pitot tube position, from upstream to downstream was used in the present experiment and it corresponds to a transverse plane located 69.95 mm from model base (i.e. 1.75 diameter from model base). A pressure tap located in the reference plane of the pitot tube fore tip, was used for the measurement of the surface pressure of reference needed for data reduction (Fig. 53).

2.2 Base Pressure Distribution

The general arrangement layout of the afterbody model dedicated to the base pressure measurement (Model no. 2 - BASE PRESSURE EXPLORATION MODEL) can be found in Fig. 30. The pressure taps positionning related used in the data reduction and the presentation of results in graphical form is given in Fig. 31. To be noted (Figs. 31 and 33) the 5 pressure taps located very close to model base and axially on the aft end. Figure 32 displays principal dimensions of its base shell (bearing base pressure taps) (Fig 33). The anchorage section unit is dimensioned in Fig. 34.

A general arrangement of afterbody surface pressure model (no. 3) is given in Fig. 35 and it can be seen with its access cover removed in Fig. 36. Figure 37 indicates pressure taps positionning in inches, and these dimensions were used for data reduction. Figures 38 and 39 refer to main body and anchorage dimensionning.

The most interesting model was the finned afterbody model which was based on the " SOUTHAMPTON UNIVERSITY CALIBRATION MODEL " and dedicated to base pressure exploration and also surface pressure measurement between fins (models no. 4 and 5) as referred to in Appendix A. Figure 40 presents the general arrangement. It should be noted that design and fabrication effort was invested in order to get pressure taps on base and fins trailing edge perpendicular to their surfaces. The model is shown with the access cover removed in Fig. 41 while the Fig. 42 shows access cover itself bearing two fins with base and trailing edge pressure taps. Pressure taps positionning can be found in Fig. 43. The finned afterbody module with pressure taps and anchorage component dimensionning is given in Figs. 44 and 45.

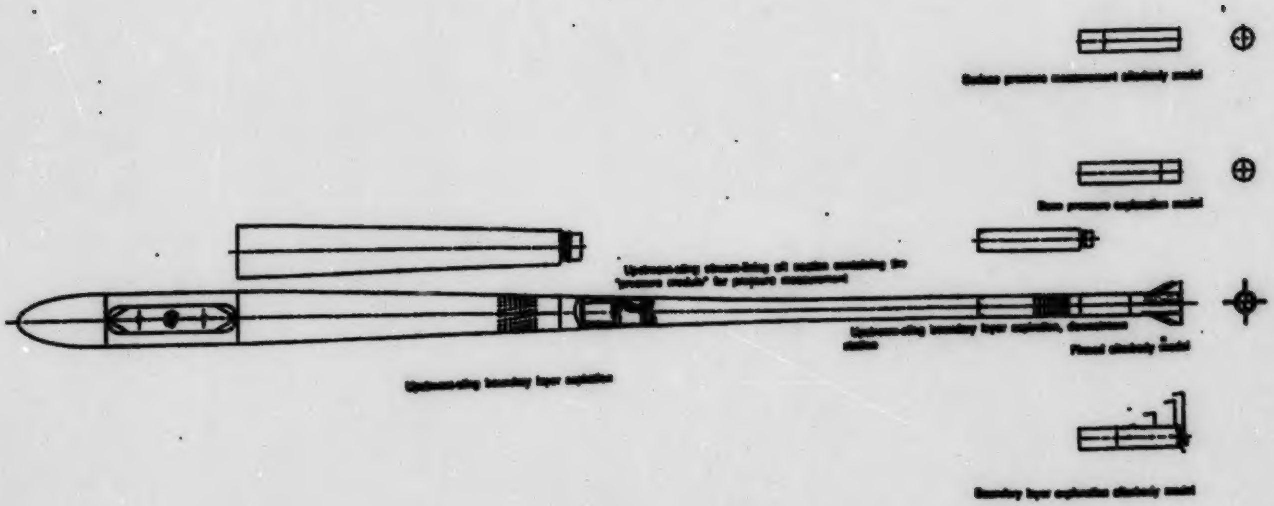

FIGURE 7 - Upstream sting/afterbody model combination system, general arrangement

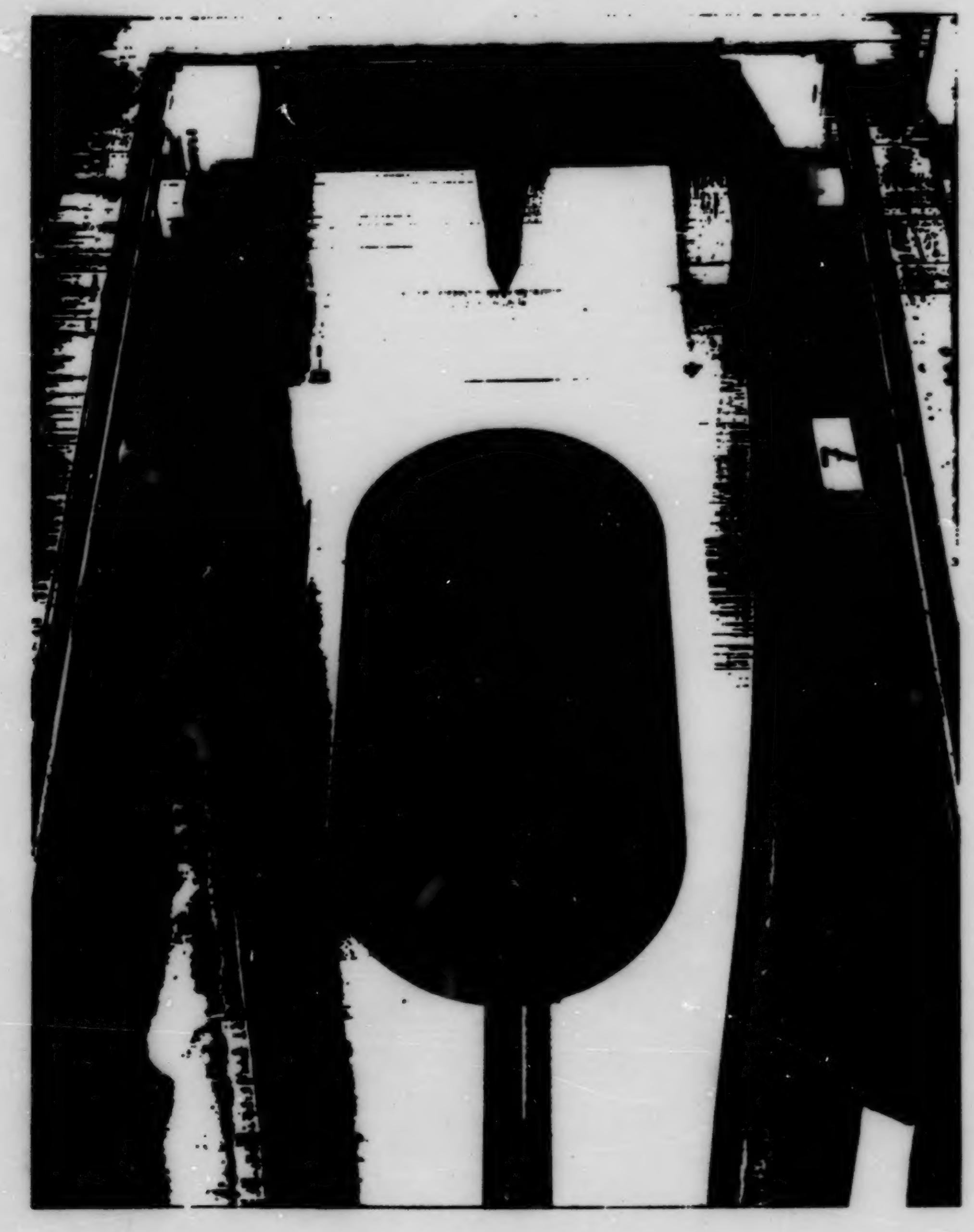

FIGURE 8 - Double-cone plug installed on strut downstream sting holding hub

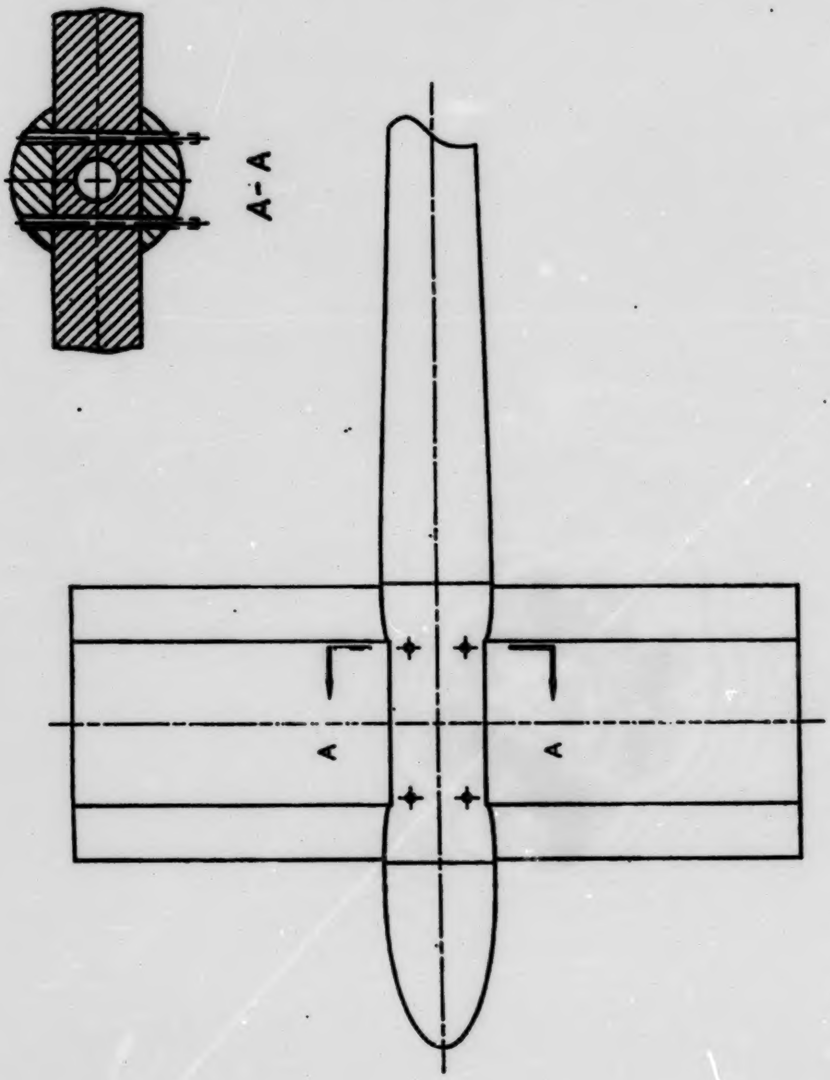

FIGURE 9 - Upstream sting wing support, general arrangement

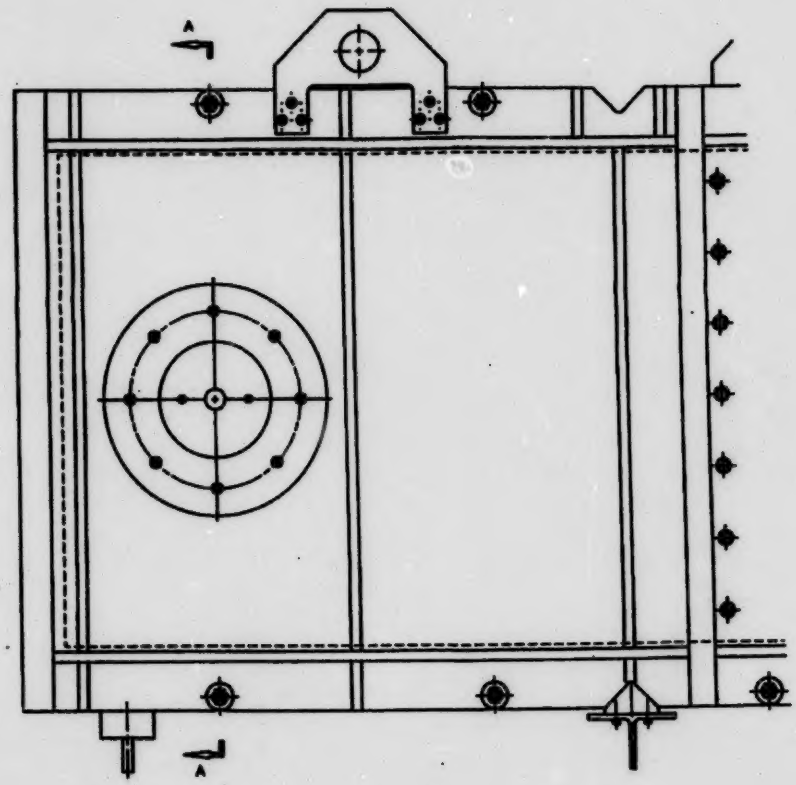

FIGURE 10 - Upstream sting pivot system, side view

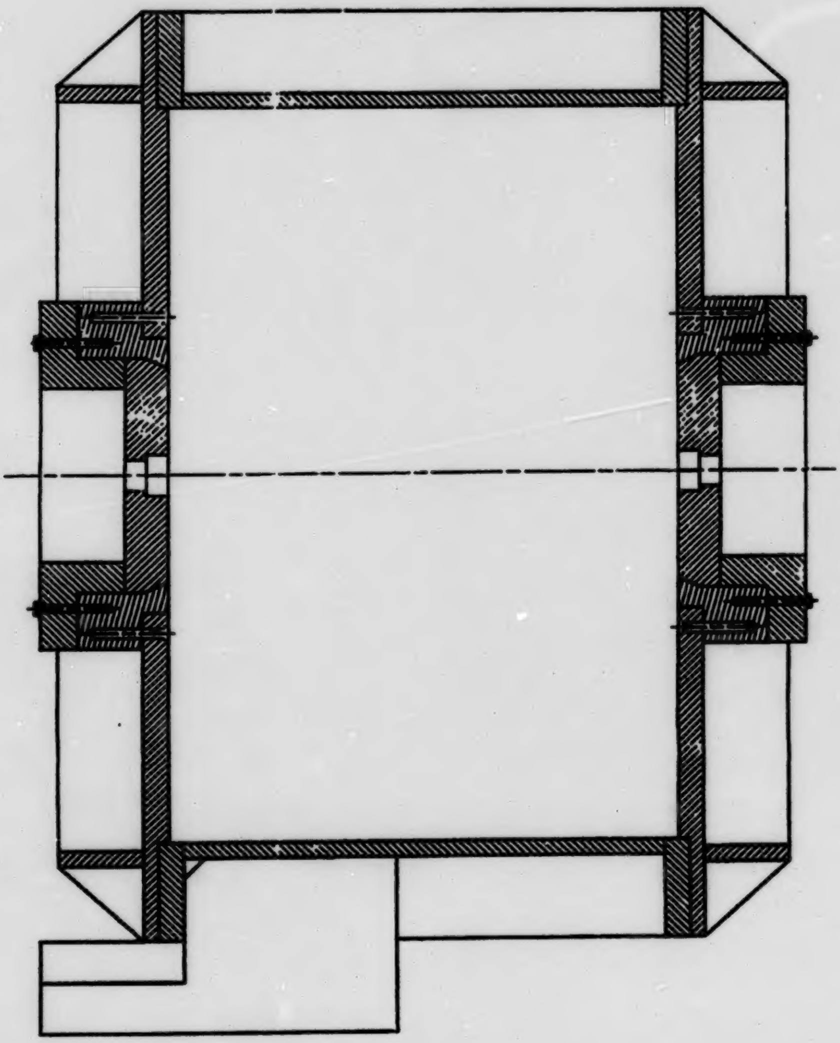

FIGURE 11 - Upstream sting pivot system, vertical cross-section view

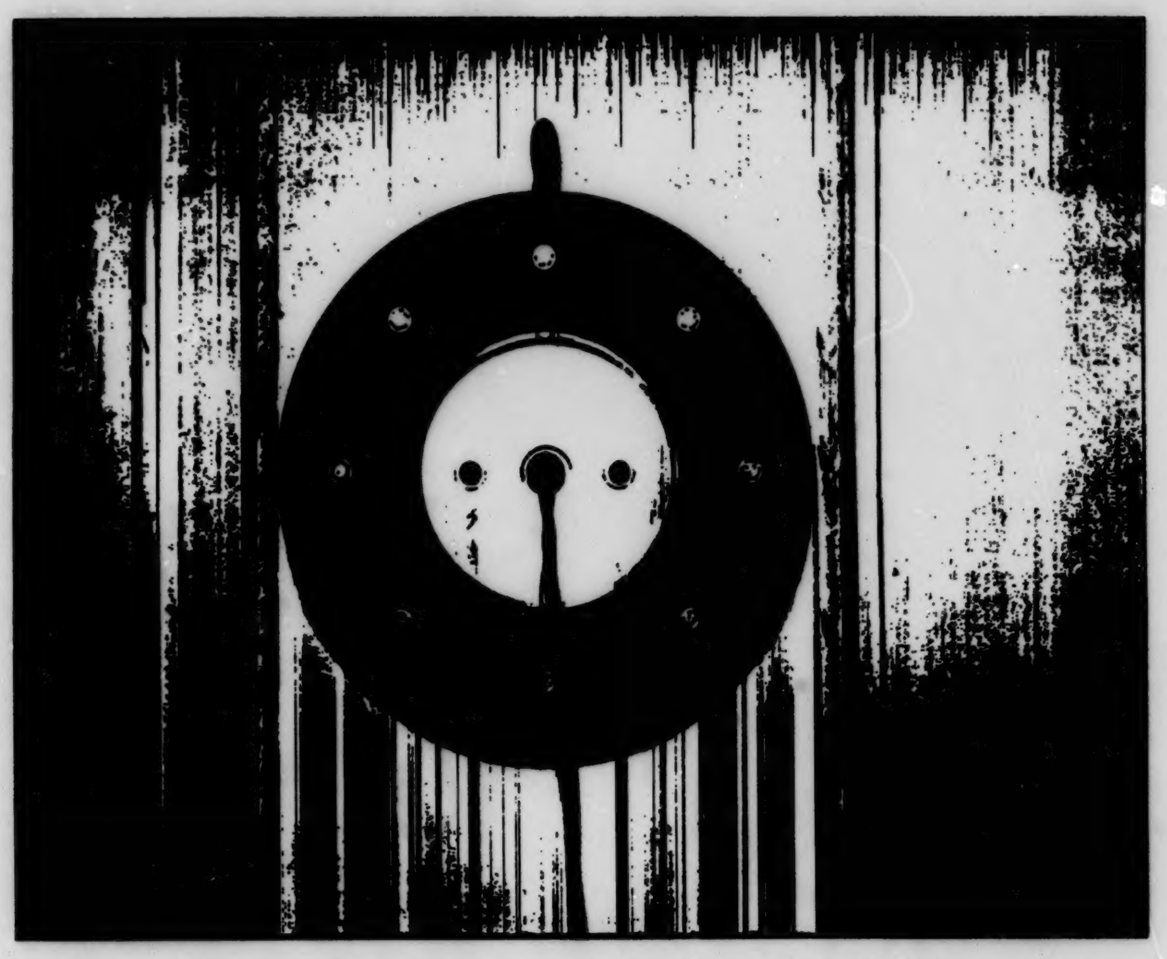

FIGURE 12 - Upstream sting pivot system, friction rings and air tight Pressure System wires with the calibration tubing exit plug

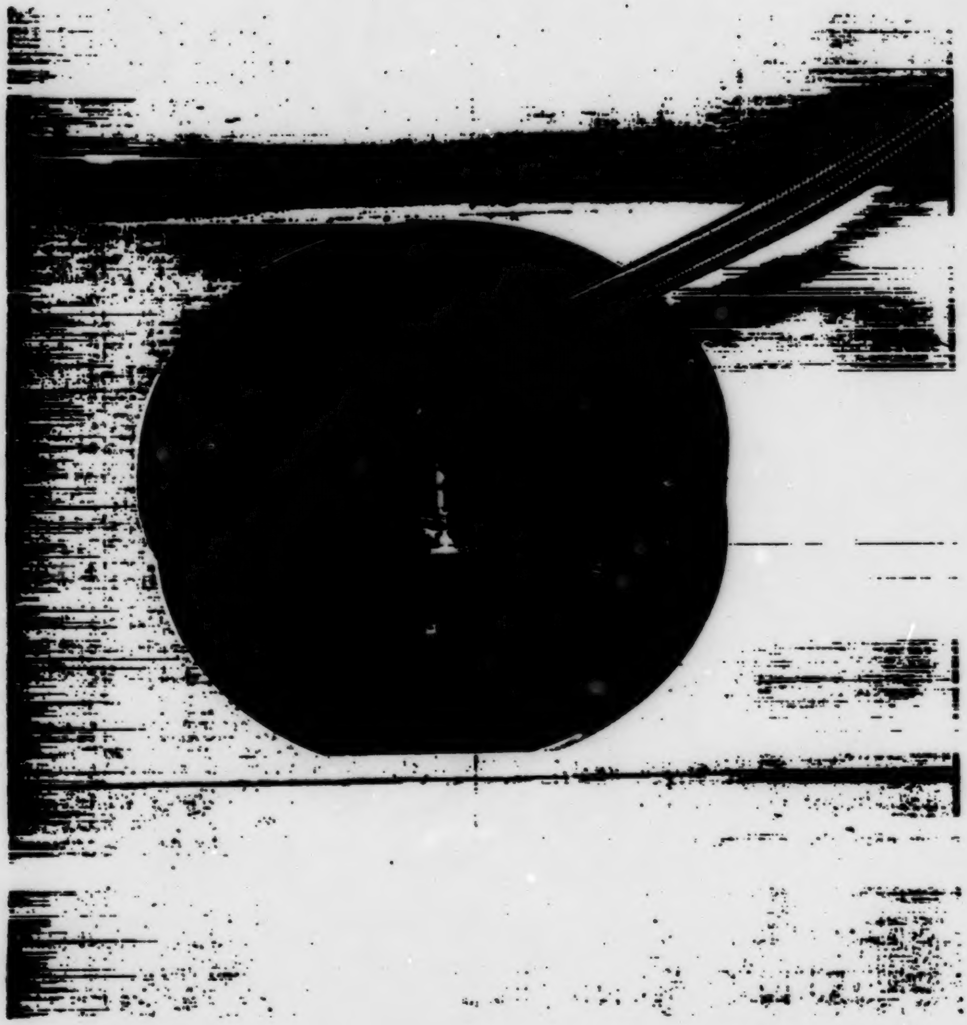

FIGURE 13 - Upstream sting pivot system and boundary layer aspiration tubing connection

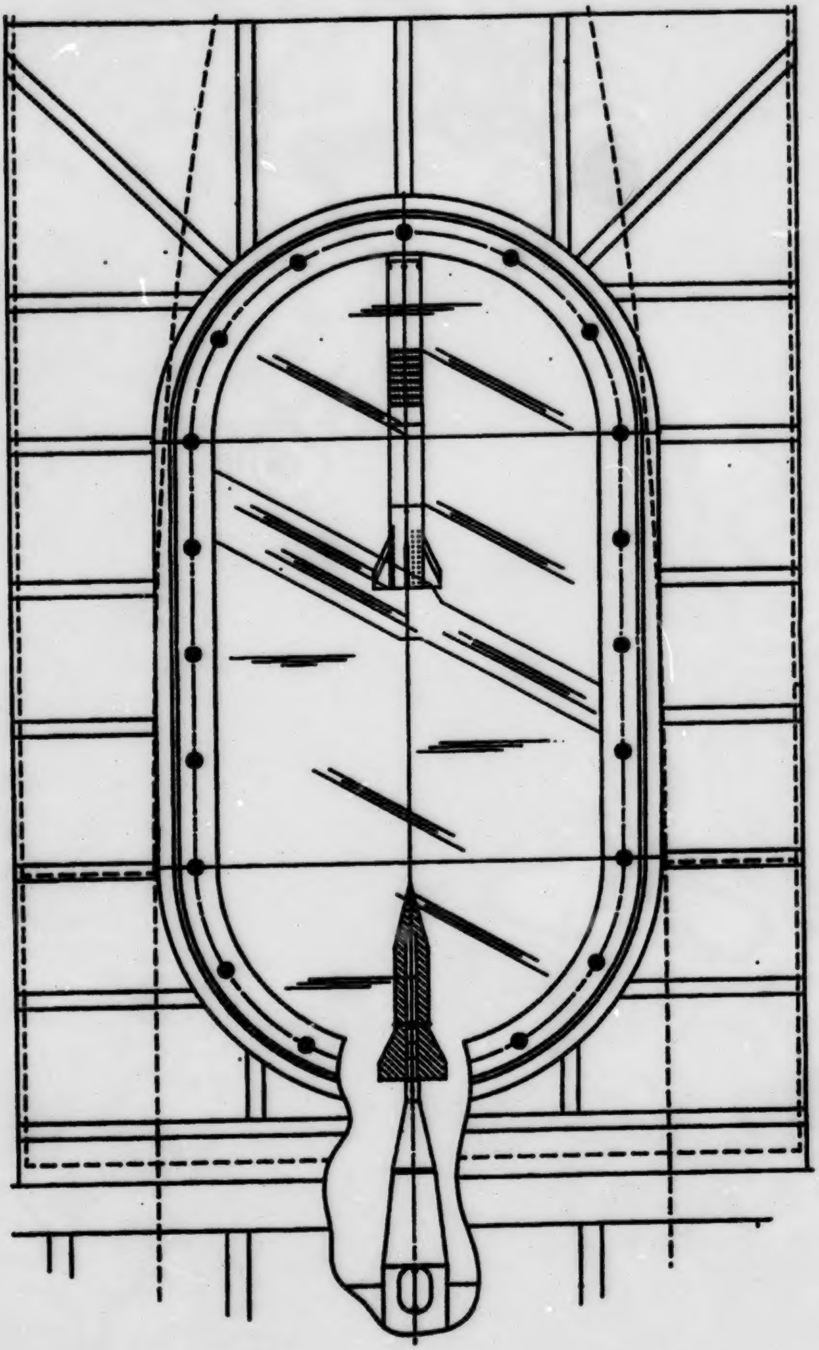

FIGURE 14 - Relative position of upstream sting with respect to the test section window and the Mach 2.0 nozzle blocks (profile indicated by dash line)

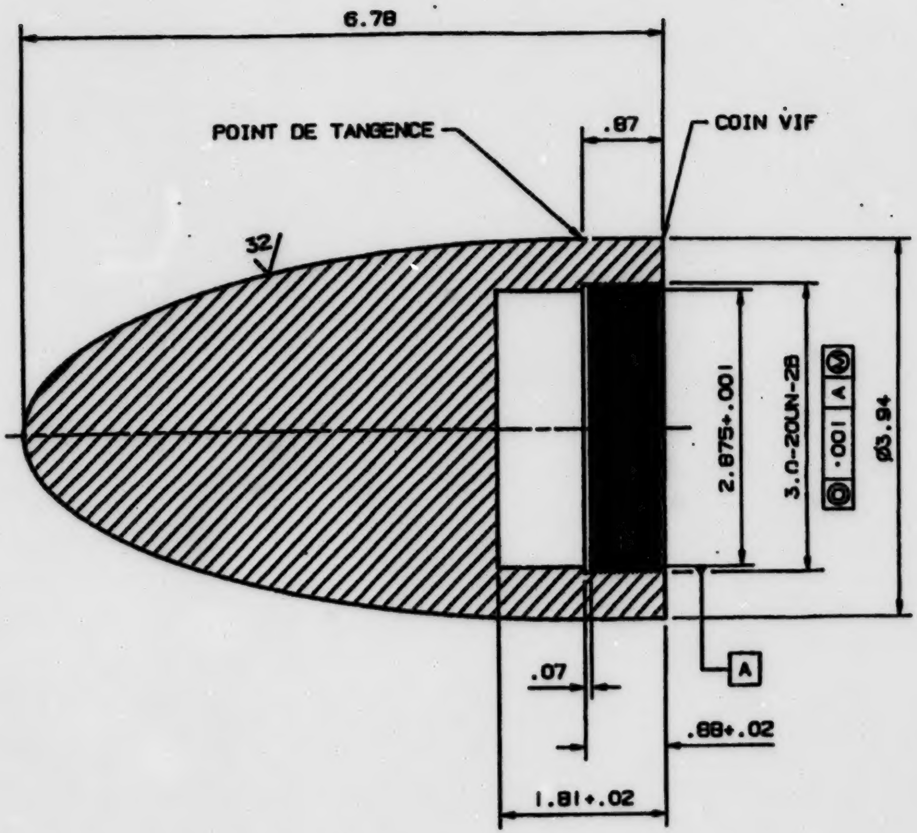
6.78
POINT DE TANGENCE
.87
COIN VIF
32
2.875+.001
3.0-20UN-2B
.001 A M
Ø3.94
A
.07
.88+.02
1.81+.02

DIS. X	DIA. Y
0	0
.250	1.134
.500	1.587
.750	1.922
1.000	2.194
1.250	2.424
1.500	2.624
1.750	2.800
2.000	2.955
2.250	3.095
2.500	3.219
2.750	3.330
3.000	3.430
3.250	3.519
3.500	3.598
3.750	3.668
4.000	3.729
4.250	3.782
4.500	3.827
4.750	3.864
5.000	3.893
5.250	3.916
5.500	3.931
5.750	3.939
5.905	3.940

FIGURE 15 - Upstream sting front nose configuration, dimensions in inches

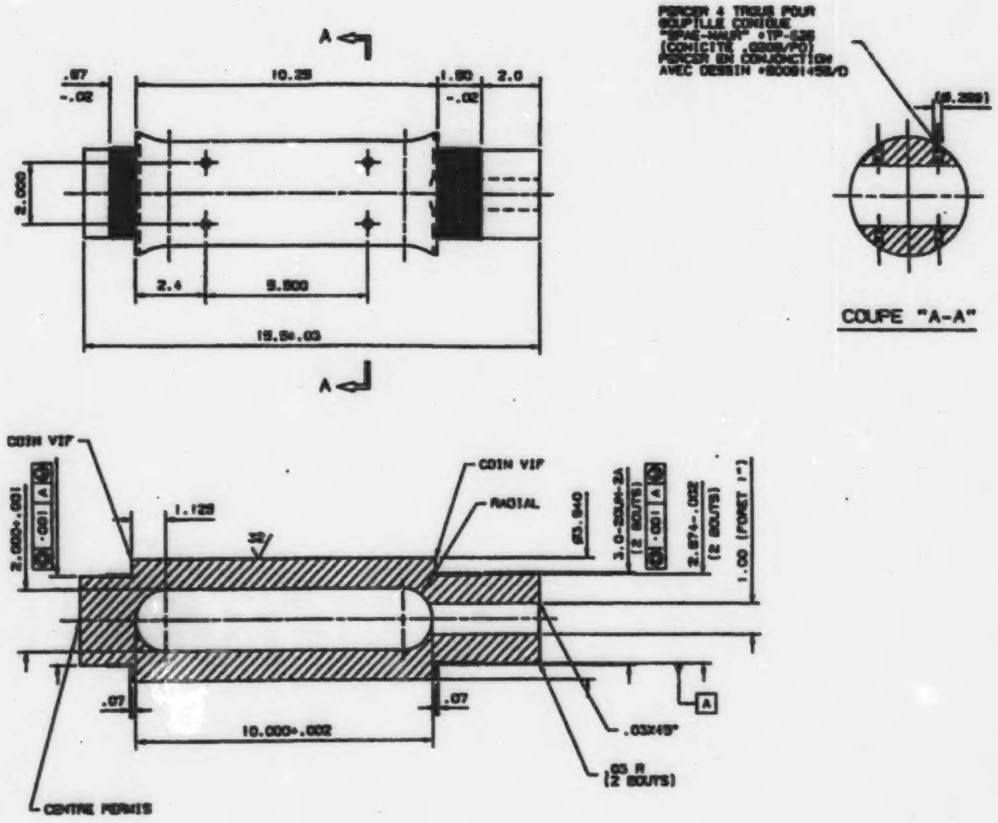
PERCER 4 TROUS POUR
GOUPILLE CONIQUE
"SPAE-NAUR" #TP-626
(CONICITE .0208/PO)
PERCER EN CONJONCTION
AVEC DESSIN #80081458/D
(0.289)
COUPE "A-A"
A
A
.87
-.02
10.25
1.90
-.02
2.0
2.000
2.4
9.500
15.9±.03
COIN VIF
1.125
32
COIN VIF
RADIAL
Ø3.940
3.0-20UN-2A
(2 BOUTS)
.001 A
2.000+.001
.001 A
2.874-.002
(2 BOUTS)
1.00 (FORET 1")
.07
.07
10.000+.002
A
.03X45°
.03 R
(2 BOUTS)
CENTRE PERMIS

FIGURE 16 - Upstream sting main body/wing support intersection and its attachment system, dimensions in inches

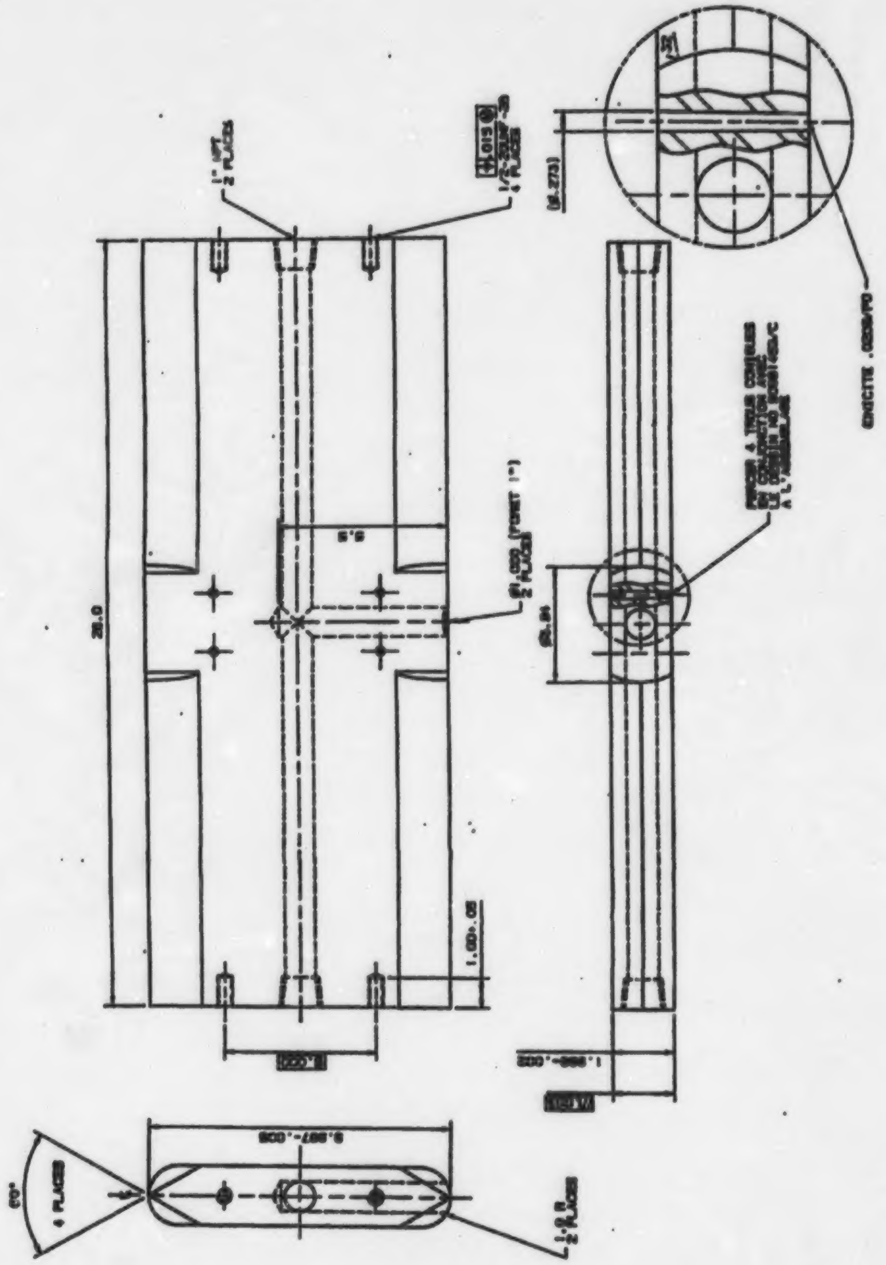
26.0
5.5
1.00±.05
3.987-.005
1.986-.002
60°
4 PLACES
1/2 R
2 PLACES
1" NPT
2 PLACES
2 PLACES
4 PLACES

FIGURE 17 - Upstream sting wing support, dimensions in inches

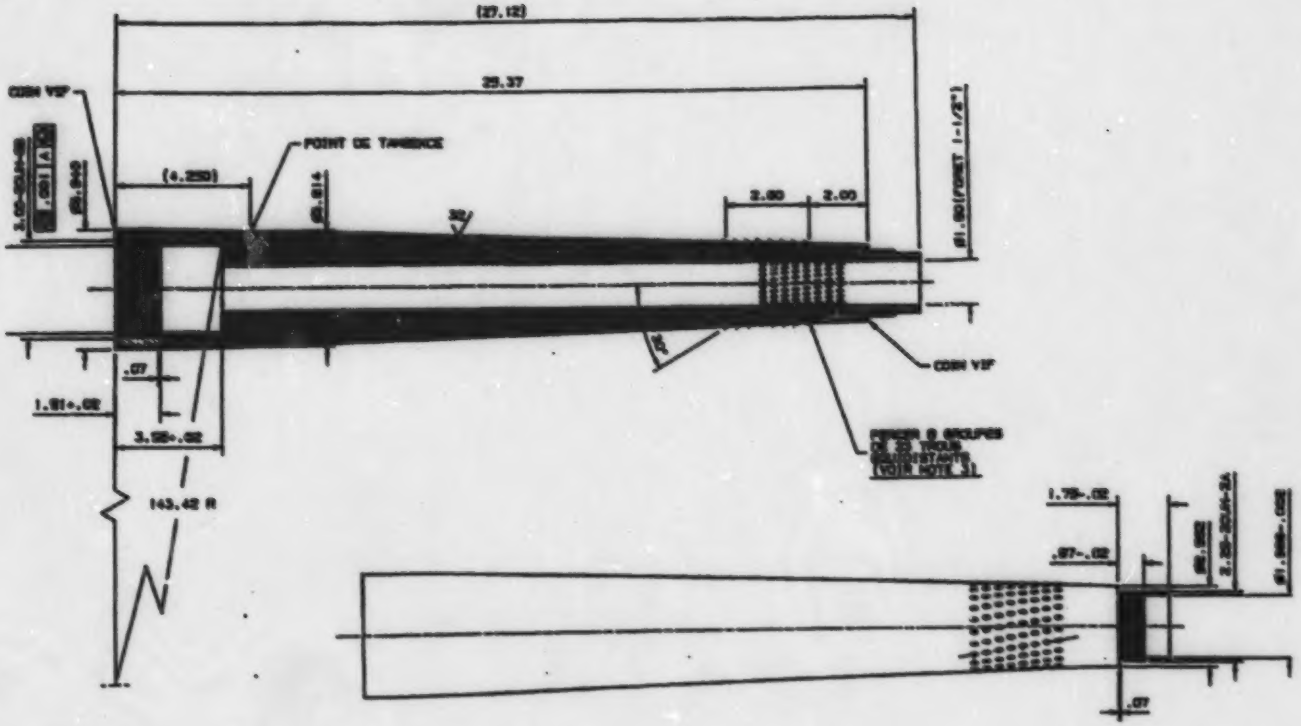
(27.12)
25.37
COIN VIF
POINT DE TANGENCE
(4.250)
Ø1.814
Ø0.940
.001 A
32/
2.00
2.00
Ø1.50(FORET 1-1/2")
30°
COIN VIF
PERCER 8 GROUPES DE 23 TROUS EQUIDISTANTS (VOIR NOTE 3)
.07
1.81+.02
3.12+.02
143.42 R
1.75-.02
.87-.02
2.25-20UN-2A
.07

FIGURE 18 - Upstream sting main body with boundary layer aspiration holes, dimensions in inches

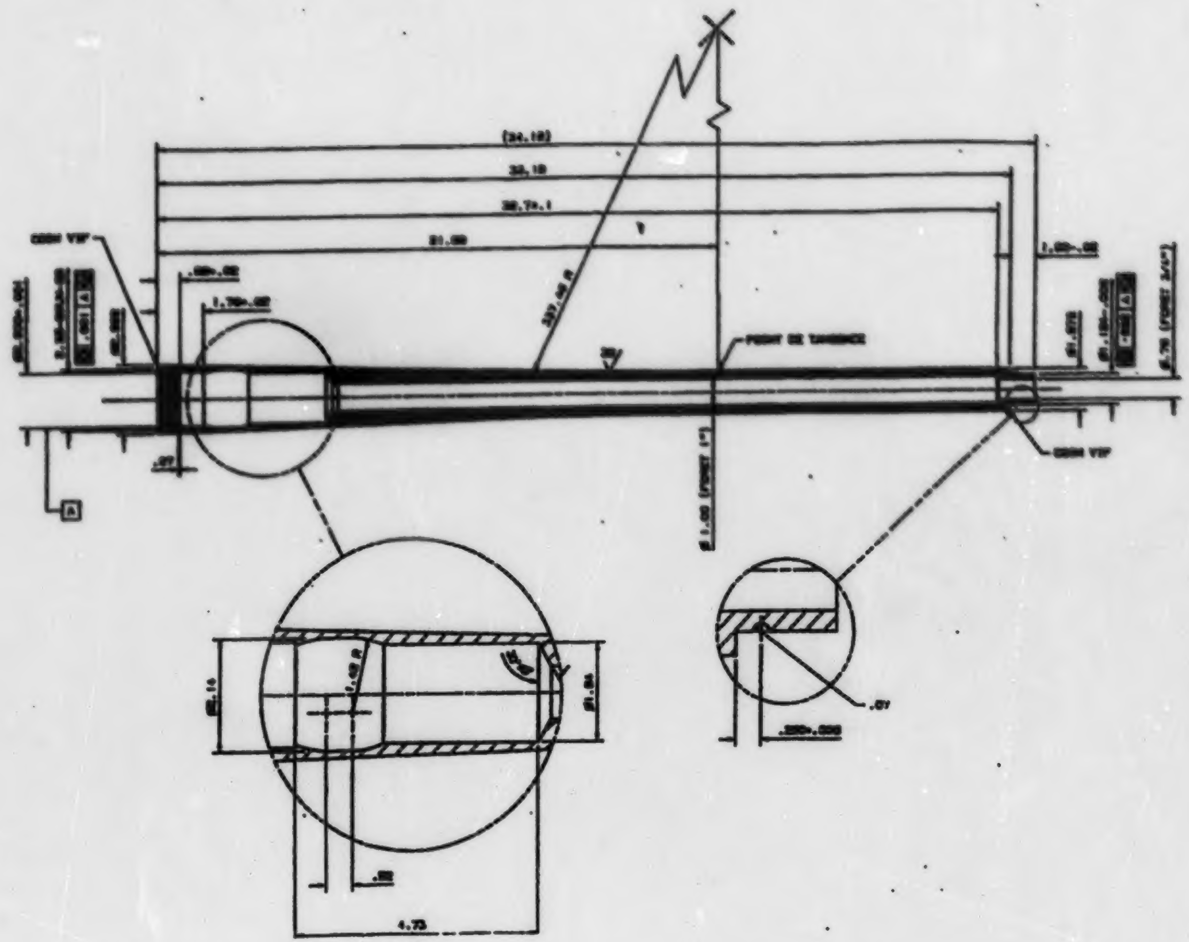
(34.18)
33.18
32.7±.1
31.00
1.70±.02
.07
POINT OF TANGENCY
CSINK V/F
4.73
.01

FIGURE - 19 Upstream sting stream-lining aft section containing the " Pressure Module " for pressure measurement, dimensions in inches

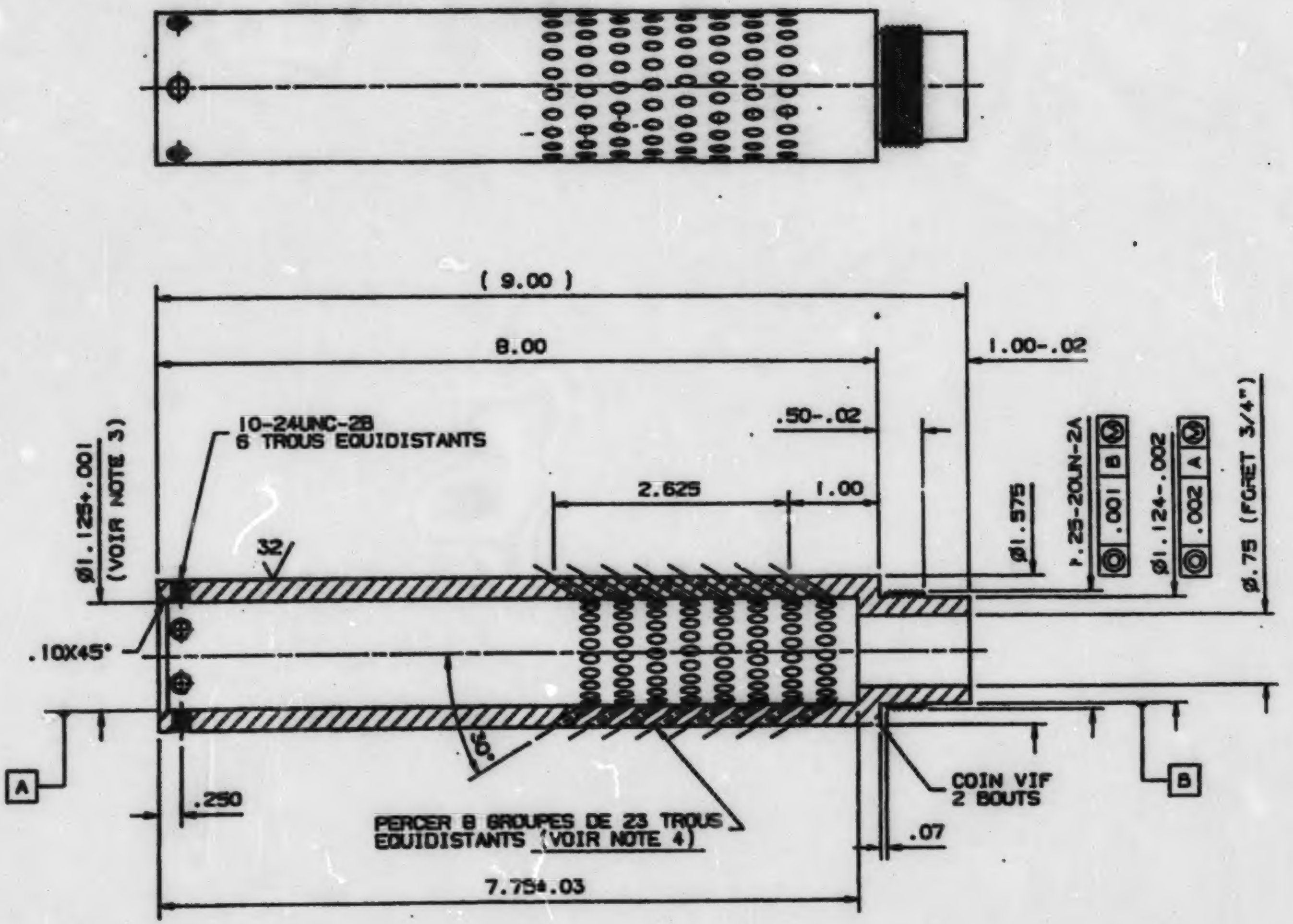
(9.00)
8.00
1.00-.02
.50-.02
2.625
1.00
Ø1.575
ƒ.25-20UN-2A
.001 B
Ø1.124-.002
.002 A
Ø.75 (FORET 3/4")
Ø1.125+.001
(VOIR NOTE 3)
10-24UNC-2B
6 TROUS EQUIDISTANTS
32
.10X45°
30°
A
B
.250
PERCER 8 GROUPES DE 23 TROUS
EQUIDISTANTS (VOIR NOTE 4)
COIN VIF
2 BOUTS
.07
7.75±.03

FIGURE 20 - Boundary layer aspiration, downstream section, dimensions in inches

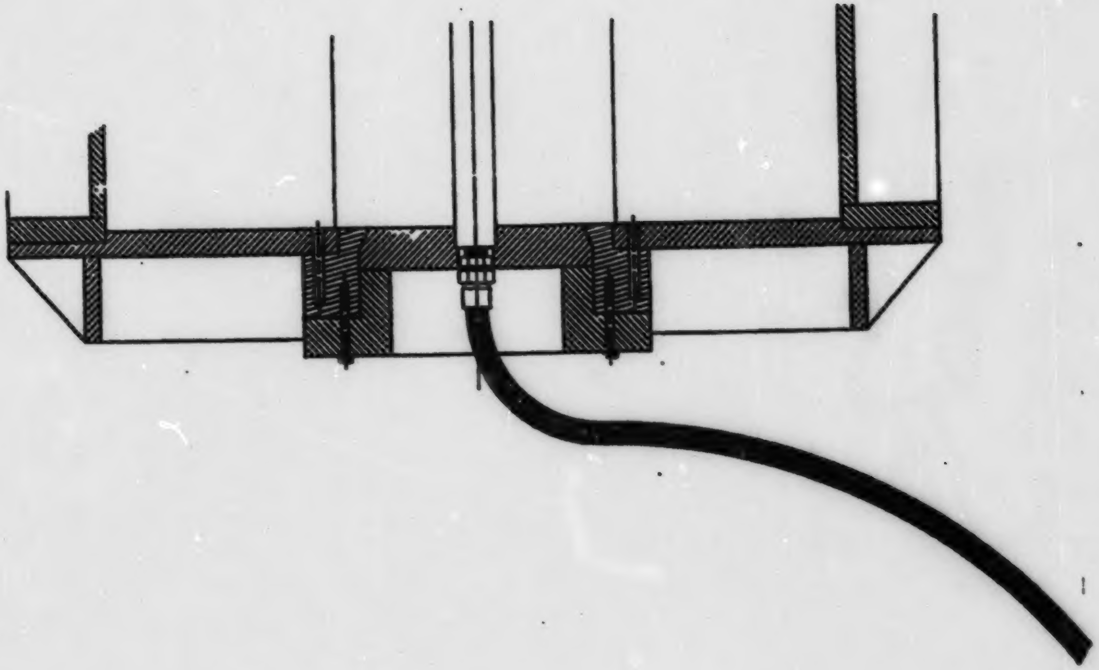

FIGURE 21 - Boundary layer aspiration system tubing

FIGURE 22 - Upstream sting boundary layer aspiration tubing with the ball valve to vary intensity, it is tapped between the computer controlled on/off valve and the throttle valve

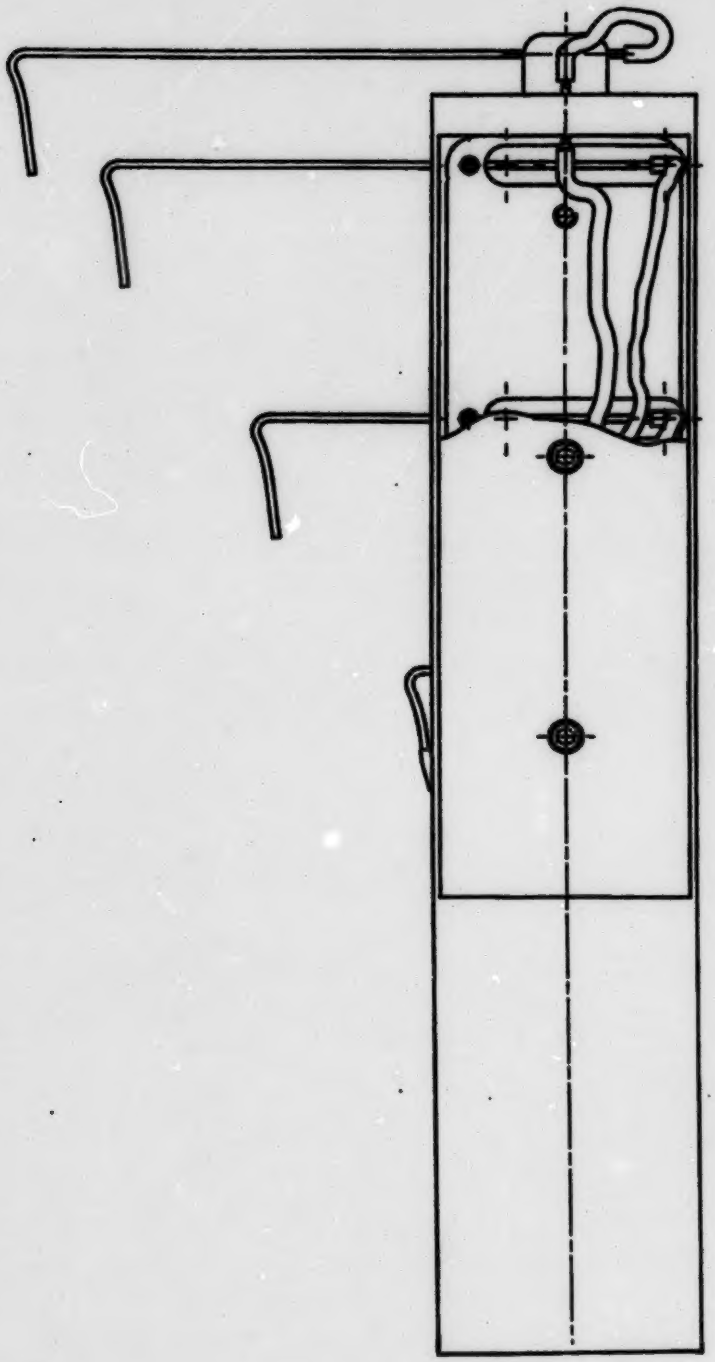

FIGURE 23 - Boundary layer exploration afterbody model, general arrangement

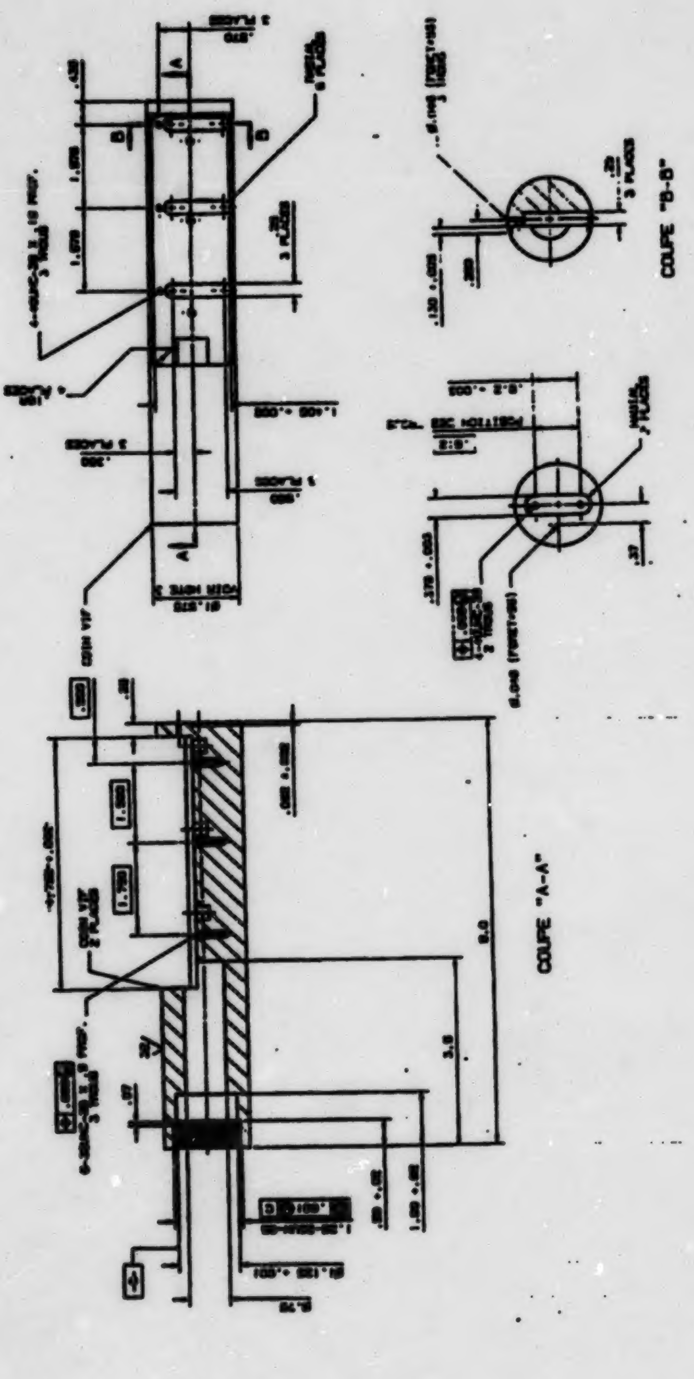
COUPE "A-A"
COUPE "B-B"
A
B
3.0
9.0
1.250
1.750
3 PLACES

FIGURE 24 - Boundary layer exploration afterbody model, main body principal dimensions in inches

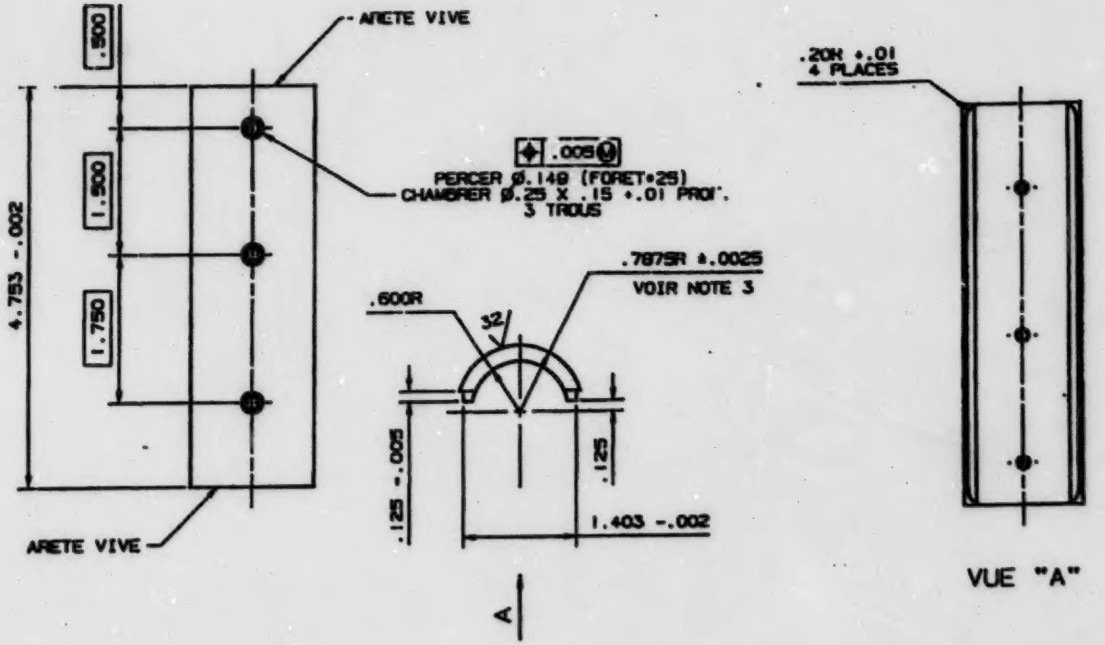
ARETE VIVE
.500
1.500
1.750
4.753 -.002
ARETE VIVE
.005 Ⓜ
PERCER Ø.148 (FORET•25)
CHAMBRER Ø.25 X .15 ±.01 PROF.
3 TROUS
.7875R ±.0025
VOIR NOTE 3
.600R
32
.125 -.005
.125
1.403 -.002
A
.20R ±.01
4 PLACES
VUE "A"

FIGURE 25 - Boundary layer exploration afterbody model, access cover, dimensions in inches

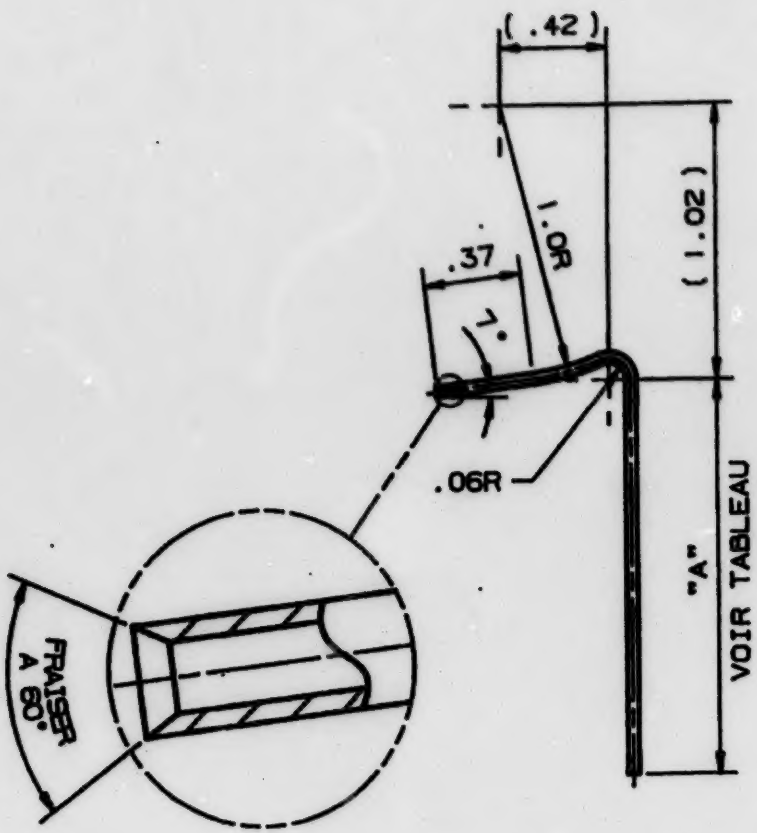
(.42)
1.0R
(1.02)
.37
7°
.06R
"A"
VOIR TABLEAU
FRAISER
A 60°

DIMENSION "A"	QTE
2.36	1
3.26	1
3.66	1

FIGURE 26 - Boundary layer exploration, round/conical inlet pitot tube, dimensions in inches

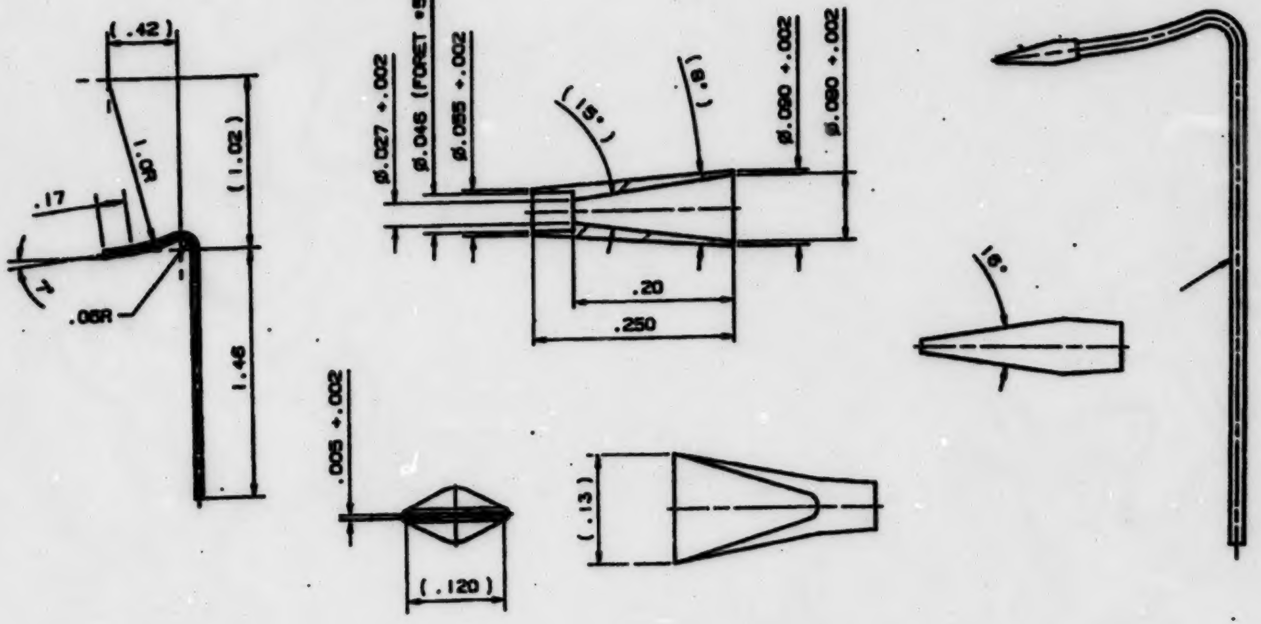
(.42)
(1.02)
1.0R
.17
7°
.08R
1.46
ø.027 +.002
ø.046 (FORET #55)
ø.055 +.002
(15°)
(8°)
ø.090 +.002
ø.090 +.002
.20
.250
.005 +.002
(.120)
(.13)
16°

FIGURE 27 - Boundary layer exploration, duck beak pitot tube, dimensions in inches

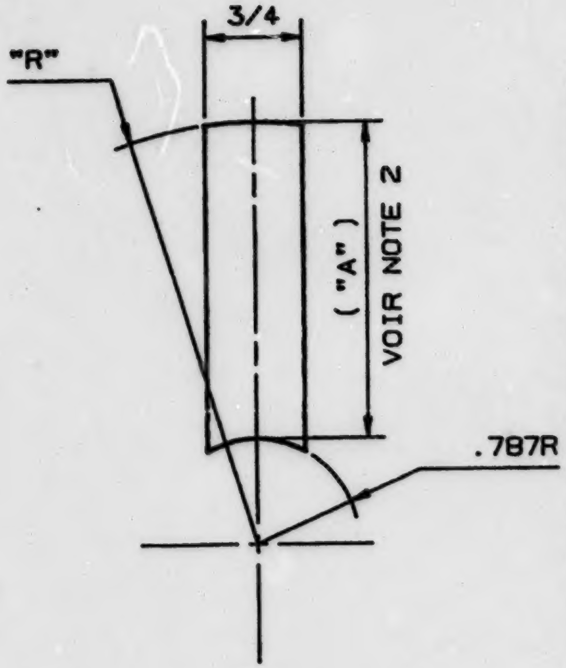

1- MATERIAU: ALUMINIUM 6061-T6, PLAQUE 1/2 EPAIS.
2- INSCRIRE LA DIMENSION "A" A L'AIDE DE POINCONS SUR CHAQUE CALE.

RAYON "R"	DIMENSION "A"	QTE	RAYON "R"	DIMENSION "A"	QTE.
.827	.04	1	1.167	.38	1
.847	.06	1	1.207	.42	1
.867	.08	1	1.247	.46	1
.887	.10	1	1.287	.50	1
.907	.12	1	1.337	.55	1
.927	.14	1	1.387	.60	1
.947	.16	1	1.437	.65	1
.967	.18	1	1.487	.70	1
.987	.20	1	1.587	.80	1
1.007	.22	1	1.787	1.00	1
1.027	.24	1	2.037	1.25	1
1.047	.26	1	2.287	1.50	1
1.067	.28	1	2.537	1.75	1
1.087	.30	1	2.787	2.00	1
1.127	.34	1	3.149	2.362	1

FIGURE 28 - Boundary layer exploration, pitot tube height adjustment gauge blocks, dimensions in inches

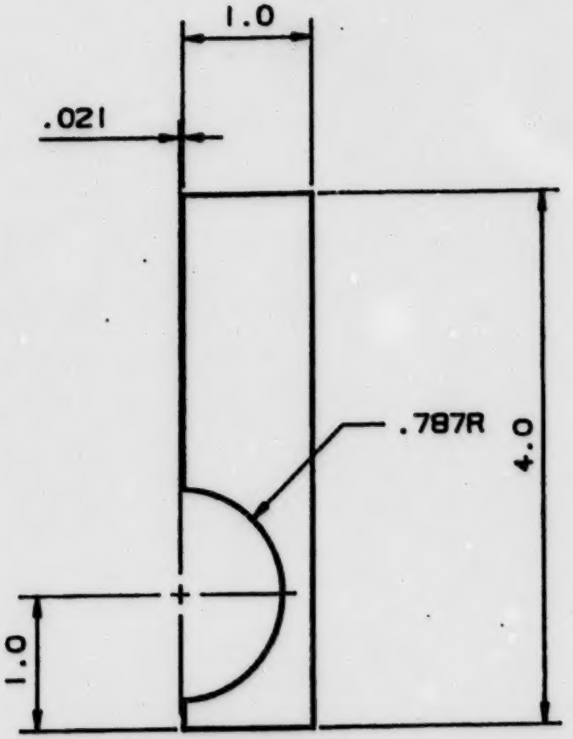
1.0
.021
.787R
4.0
1.0

FIGURE 29 - Boundary layer exploration, pitot tube alignment jig block, dimensions in inches

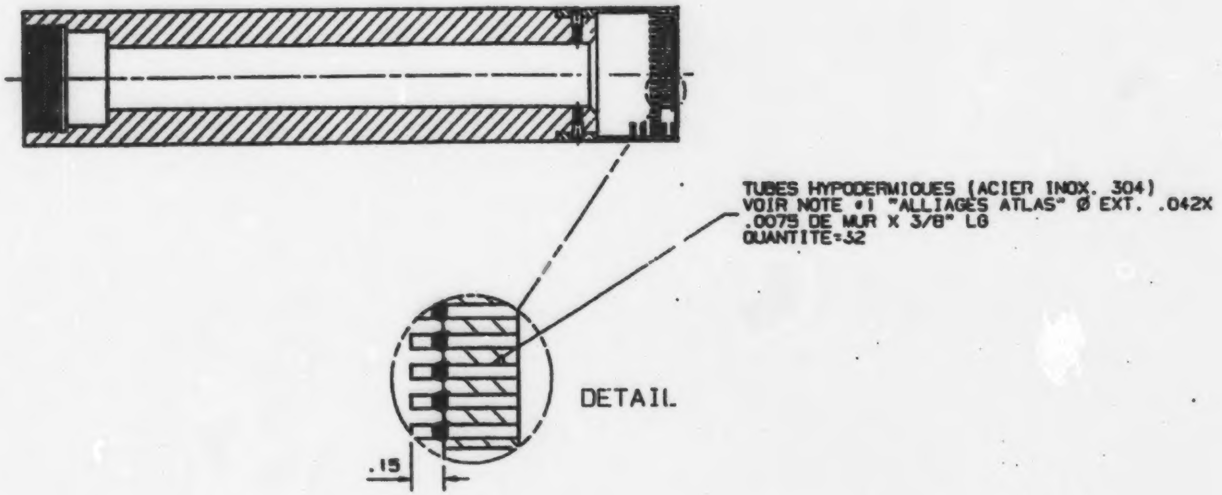
TUBES HYPODERMIQUES (ACIER INOX. 304)
VOIR NOTE #1 "ALLIAGES ATLAS" Ø EXT. .042X
.0075 DE MUR X 3/8" LG
QUANTITE=32
DETAIL
.15

FIGURE 30 - Base pressure exploration model, general arrangement

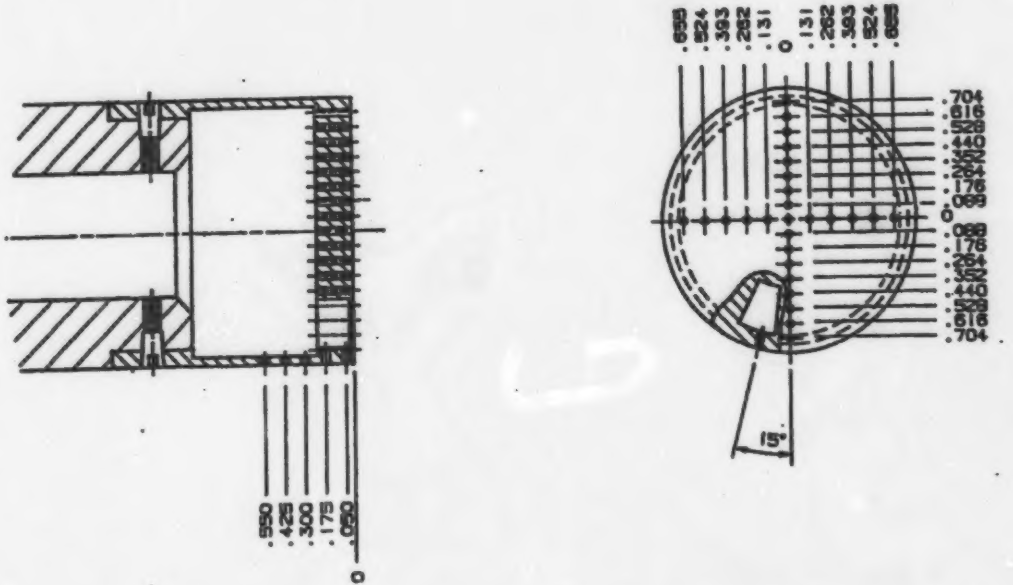
.550
.425
.300
.175
.050
0
.655
.524
.393
.262
.131
0
.131
.262
.393
.524
.655
.704
.616
.528
.440
.352
.264
.176
.088
0
.088
.176
.264
.352
.440
.528
.616
.704
15°

FIGURE 31 - Pressure taps positionning, base pressure exploration model, dimensions in inches

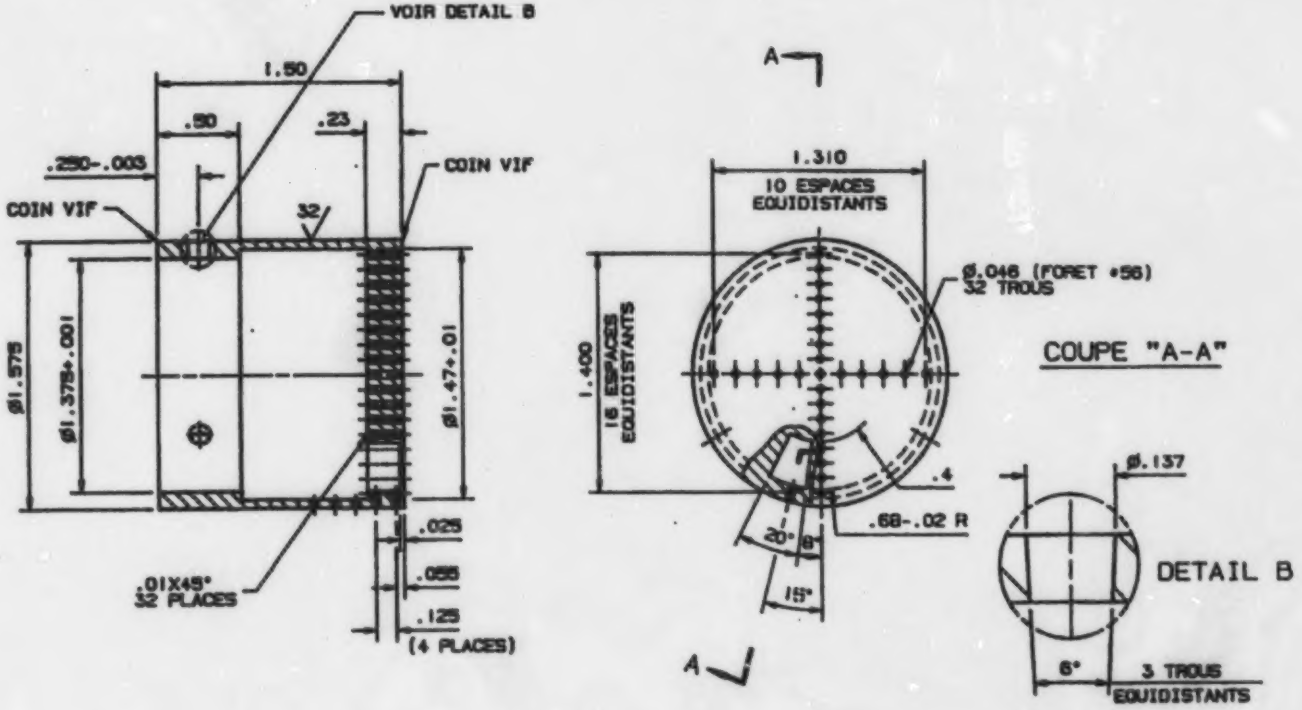
VOIR DETAIL B
1.50
.50
.23
.250-.003
COIN VIF
COIN VIF
32
Ø1.575
Ø1.375+.001
Ø1.47+.01
.01X45°
32 PLACES
.025
.055
.125
(4 PLACES)
A
1.310
10 ESPACES EQUIDISTANTS
1.400
16 ESPACES EQUIDISTANTS
Ø.046 (FORET #56)
32 TROUS
.4
.68-.02 R
20°
8°
15°
A
COUPE "A-A"
Ø.137
DETAIL B
6°
3 TROUS
EQUIDISTANTS

FIGURE 32 - Base pressure exploration model, base dimensions in inches

FIGURE 33 - Base pressure exploration model, base shell module with tubing

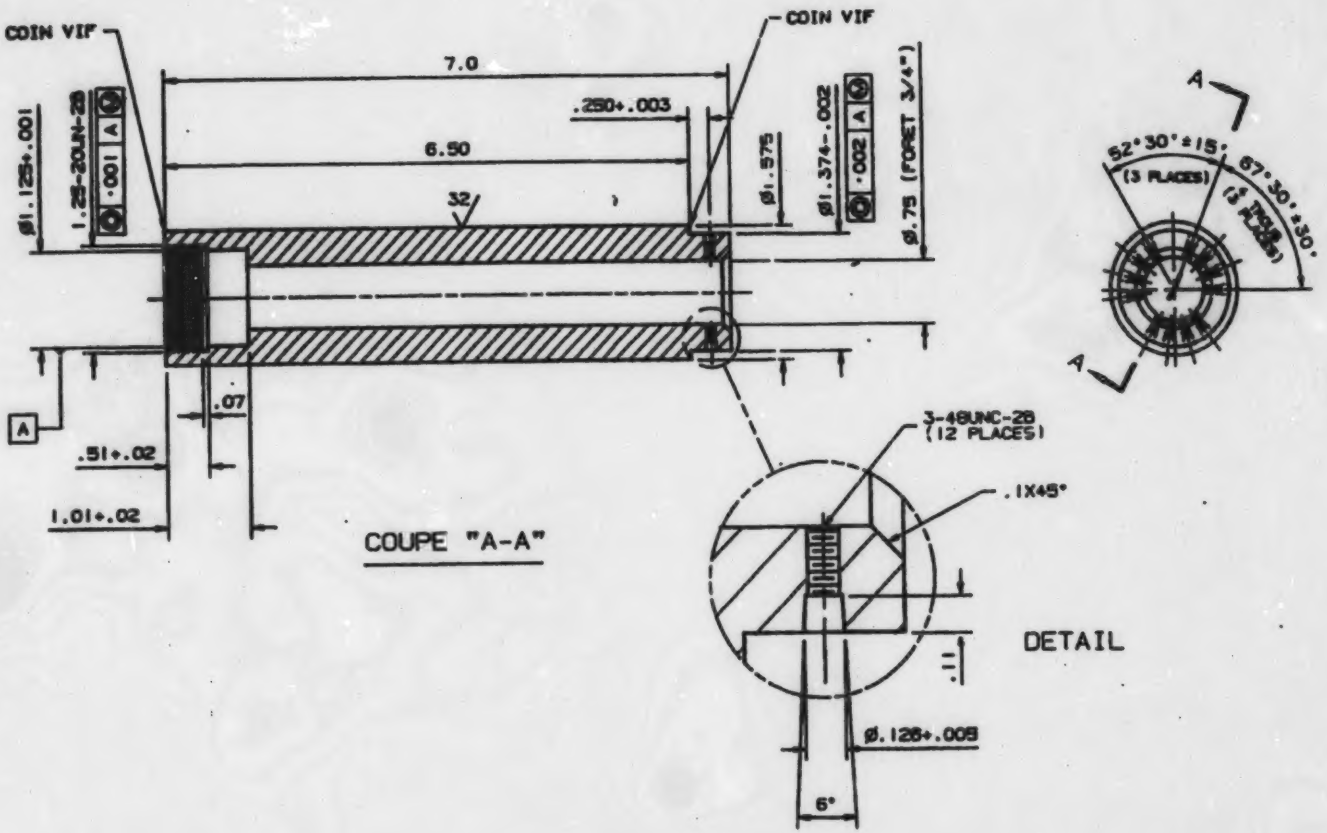
COIN VIF
COIN VIF
7.0
6.50
.250+.003
32
Ø1.125+.001
1.25-20UN-2B
.001 A
Ø1.575
Ø1.374-.002
.002 A
Ø.75 (FORET 3/4")
A
.07
.51+.02
1.01+.02
COUPE "A-A"
3-48UNC-2B
(12 PLACES)
.1X45°
DETAIL
Ø.128+.005
6°
A
A
52°30'±15'
(3 PLACES)
67°30'±30'
(3 PLACES)

FIGURE 34 - Base pressure exploration model, anchorage dimensions in inches

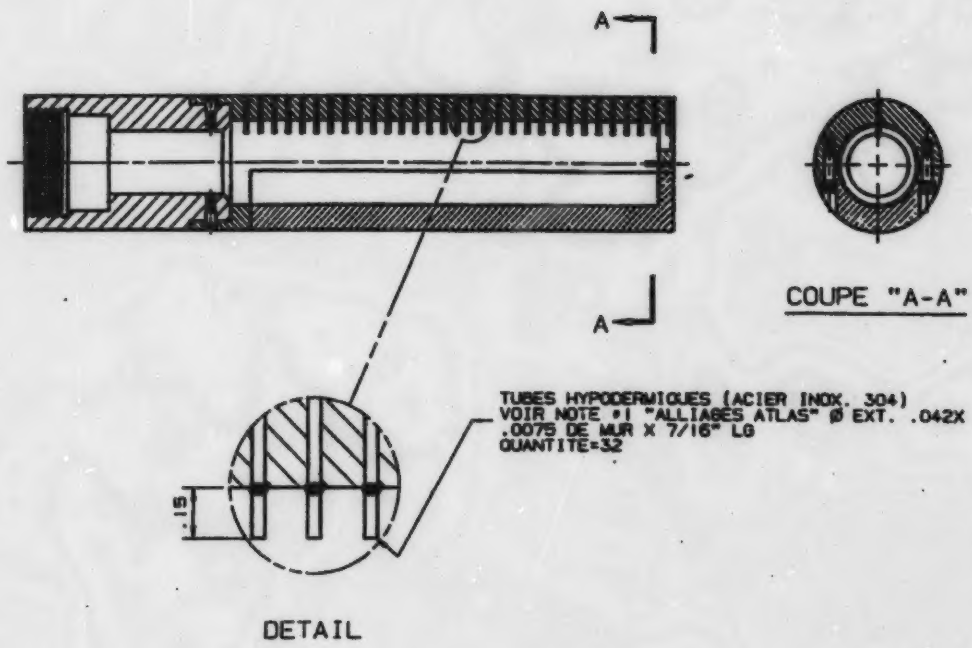
A
A
COUPE "A-A"
TUBES HYPODERMIQUES (ACIER INOX. 304)
VOIR NOTE #1 "ALLIAGES ATLAS" Ø EXT. .042X
.0075 DE MUR X 7/16" LG
QUANTITE=32
.15
DETAIL

FIGURE 35 - Afterbody surface pressure model, general arrangement

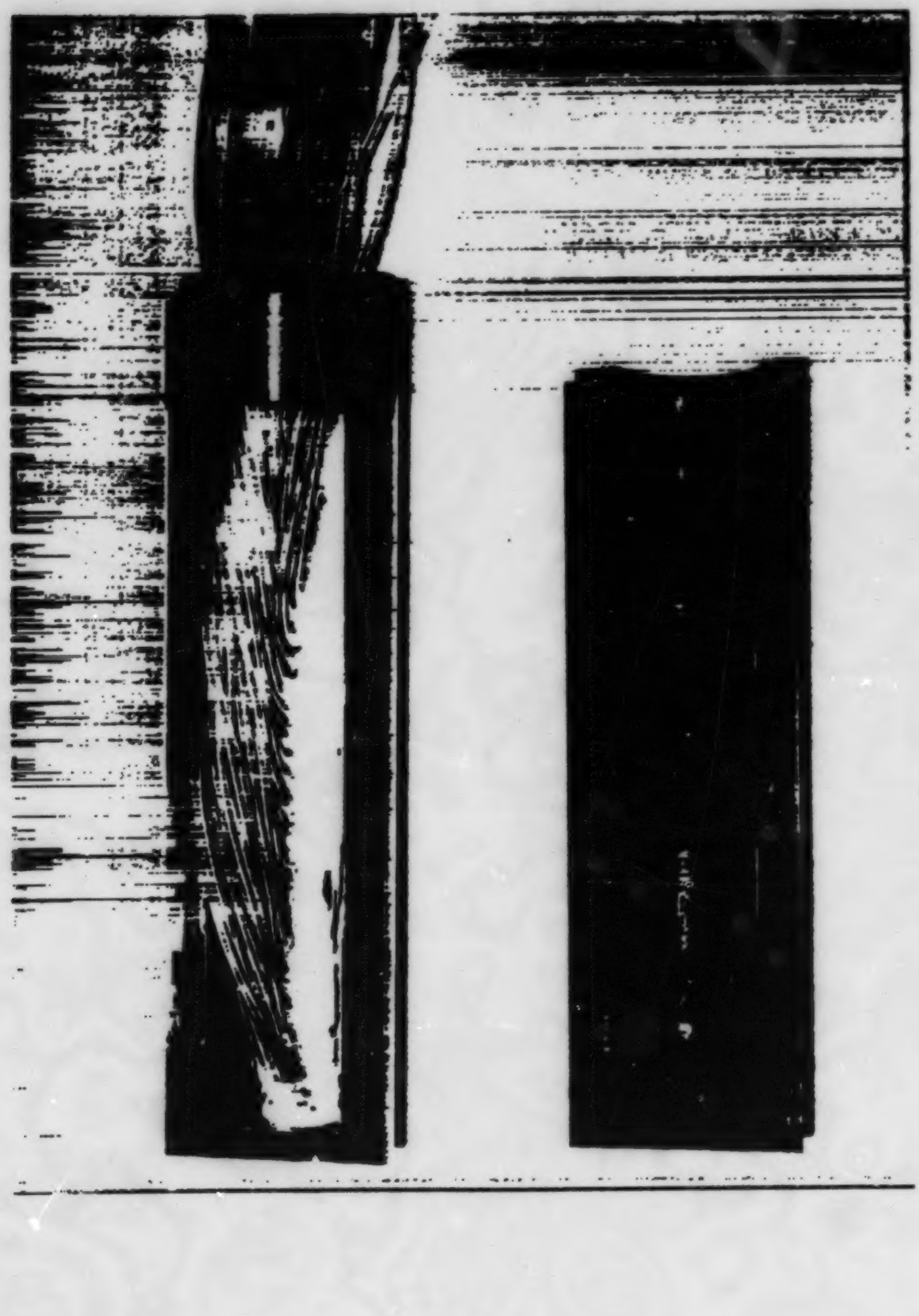

FIGURE 36 - Afterbody surface pressure model, access cover removed showing tubing running between pressure taps and pressure sensor

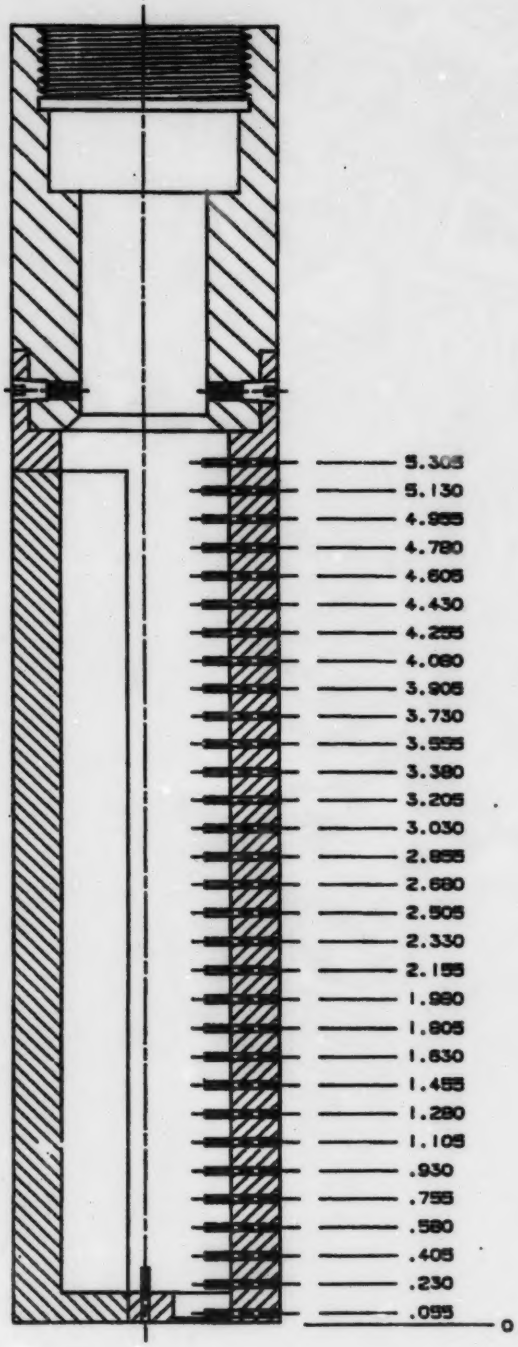
5.305
5.130
4.955
4.780
4.605
4.430
4.255
4.080
3.905
3.730
3.555
3.380
3.205
3.030
2.855
2.680
2.505
2.330
2.155
1.980
1.805
1.630
1.455
1.280
1.105
.930
.755
.580
.405
.230
.055
0

FIGURE 37 - Pressure taps positionning, afterbody surface pressure model, dimensions in inches

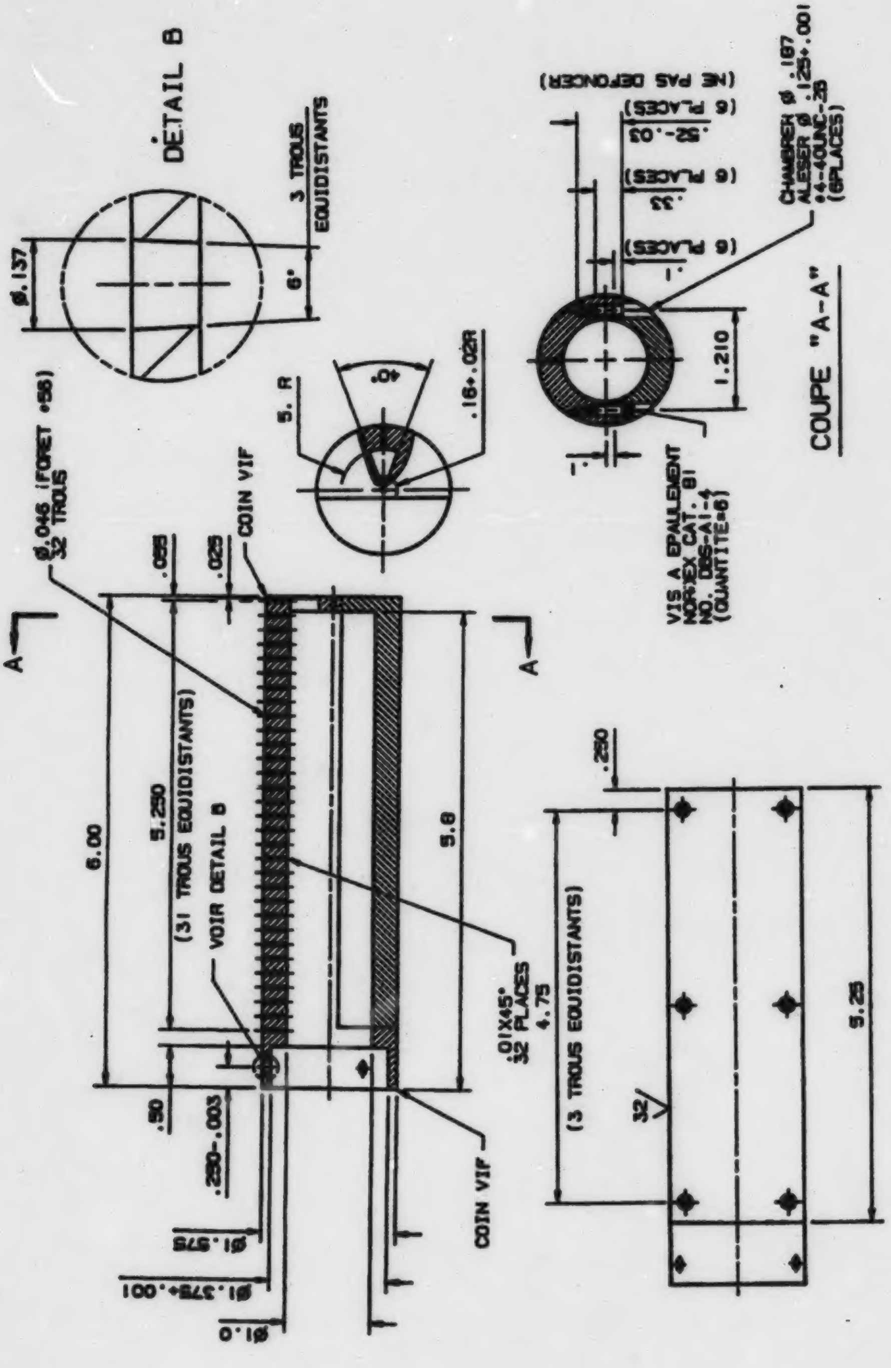
A
A
6.00
5.250
(31 TROUS EQUIDISTANTS)
VOIR DETAIL B
5.8
.50
.250-.003
Ø1.375
Ø1.375+.001
Ø1.0
COIN VIF
COIN VIF
.065
.025
Ø.046 (FORET #56)
32 TROUS
.01X45°
32 PLACES
4.75
(3 TROUS EQUIDISTANTS)
32
.250
5.25
5. R
40°
.16+.02R
Ø.137
6°
3 TROUS
EQUIDISTANTS
DETAIL B
VIS A EPAULEMENT
NORTEX CAT. 81
NO. DBS-A1-4
(QUANTITE=6)
1.210
.1
.1
(6 PLACES)
.33
(6 PLACES)
.52-.03
(6 PLACES)
(NE PAS DEFONCER)
CHAMBRER Ø .187
ALESER Ø .125+.001
#4-40UNC-2B
(6PLACES)
COUPE "A-A"

FIGURE 38 - Afterbody surface pressure model, dimensions in inches

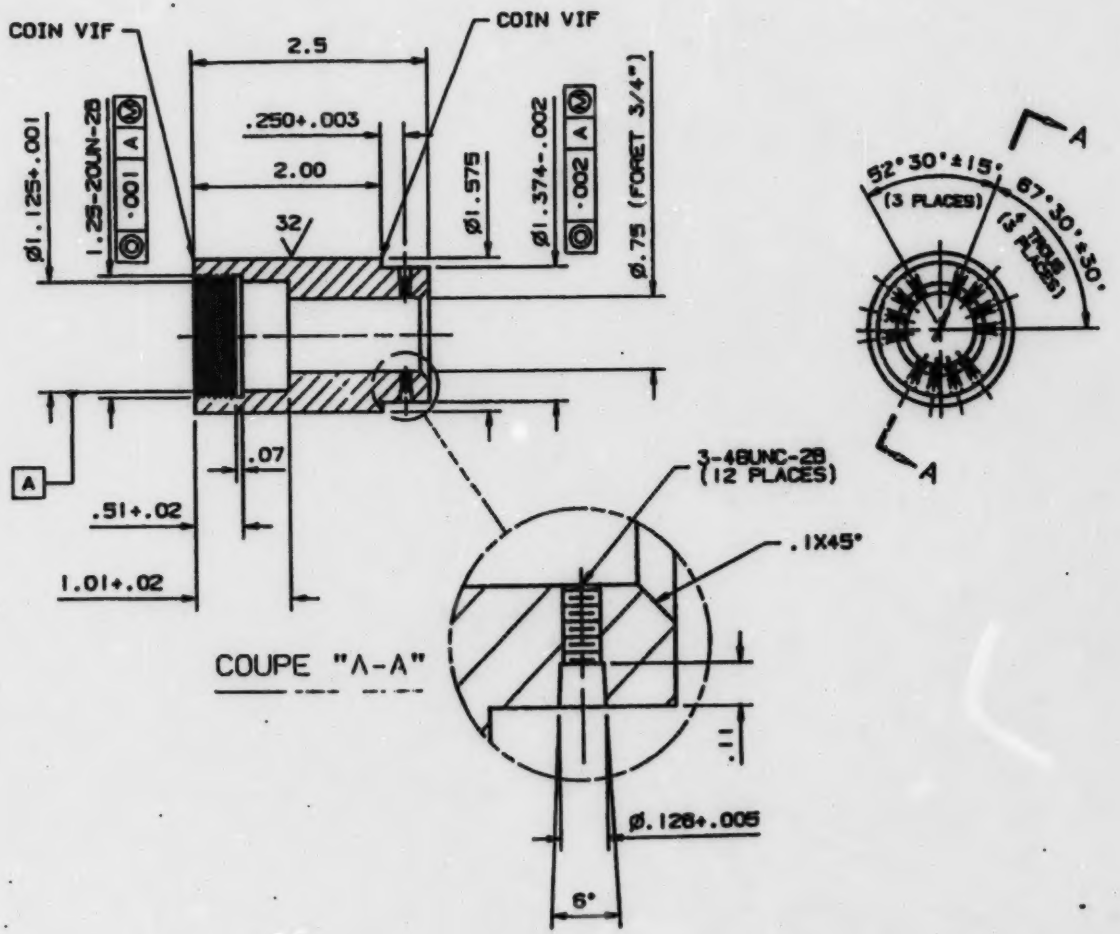
COIN VIF
COIN VIF
2.5
.250+.003
2.00
32
Ø1.125+.001
1.25-20UN-2B
◎ .001 A Ⓜ
Ø1.575
Ø1.374-.002
◎ .002 A Ⓜ
Ø.75 (FORET 3/4")
A
.07
.51+.02
1.01+.02
COUPE "A-A"
3-48UNC-2B
(12 PLACES)
.1X45°
.11
Ø.128+.005
6°
52°30'±15'
(3 PLACES)
67°30'±30'
4 TROUS
(3 PLACES)
A
A

FIGURE 39 - Afterbody surface pressure model, anchorage dimensions in inches

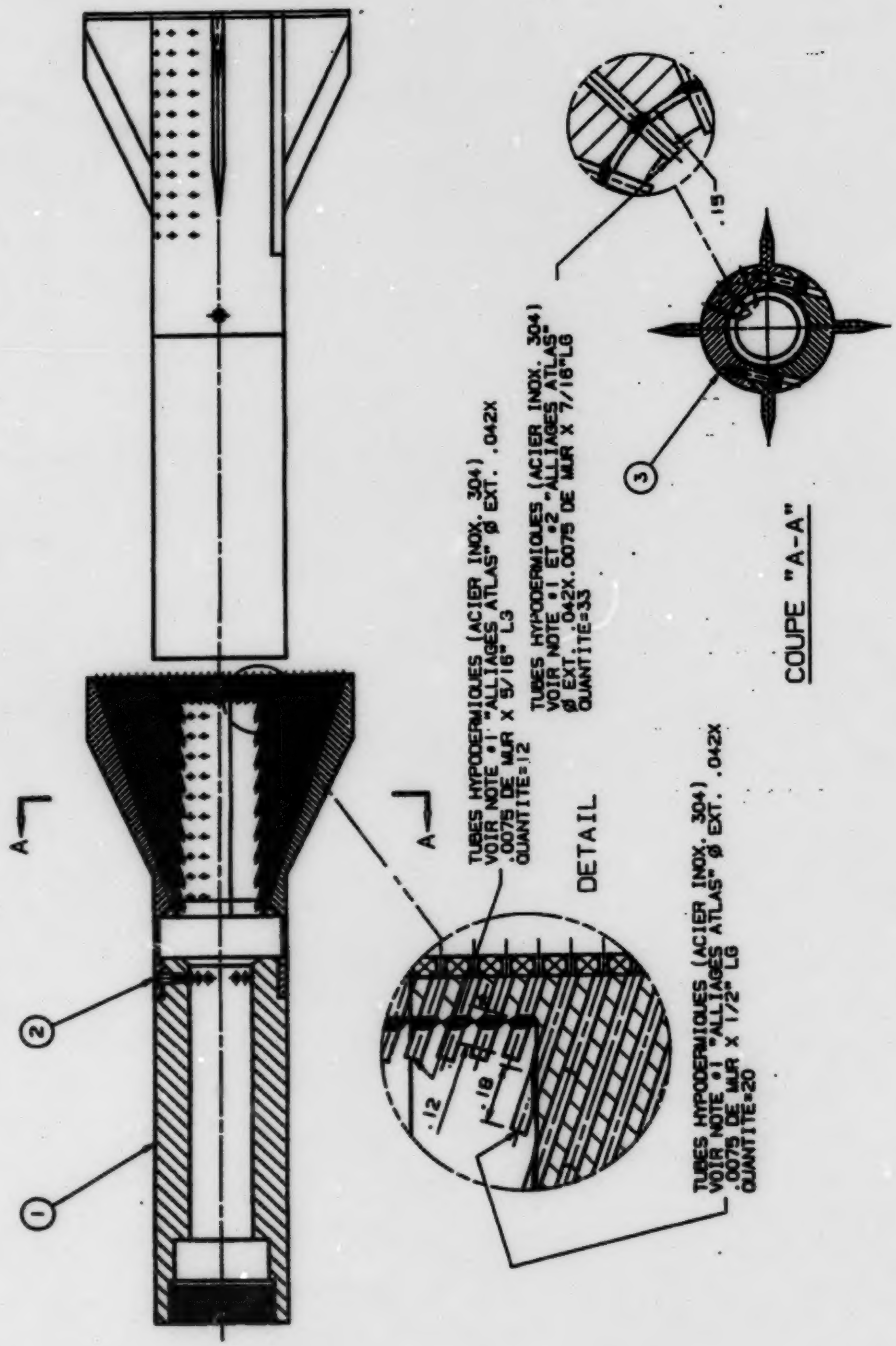
A
A
①
②
③
TUBES HYPODERMIQUES (ACIER INOX. 304)
VOIR NOTE #1 "ALLIAGES ATLAS" Ø EXT. .042X
.0075 DE MUR X 5/16" L3
QUANTITE=12
TUBES HYPODERMIQUES (ACIER INOX. 304)
VOIR NOTE #1 ET #2 "ALLIAGES ATLAS"
Ø EXT. .042X.0075 DE MUR X 7/16"LG
QUANTITE=33
TUBES HYPODERMIQUES (ACIER INOX. 304)
VOIR NOTE #1 "ALLIAGES ATLAS" Ø EXT. .042X
.0075 DE MUR X 1/2" LG
QUANTITE=20
DETAIL
.12
.18
.15
COUPE "A-A"

FIGURE 40 - Finned afterbody model, general arrangement

FIGURE 41 - Finned afterbody model, access cover removed

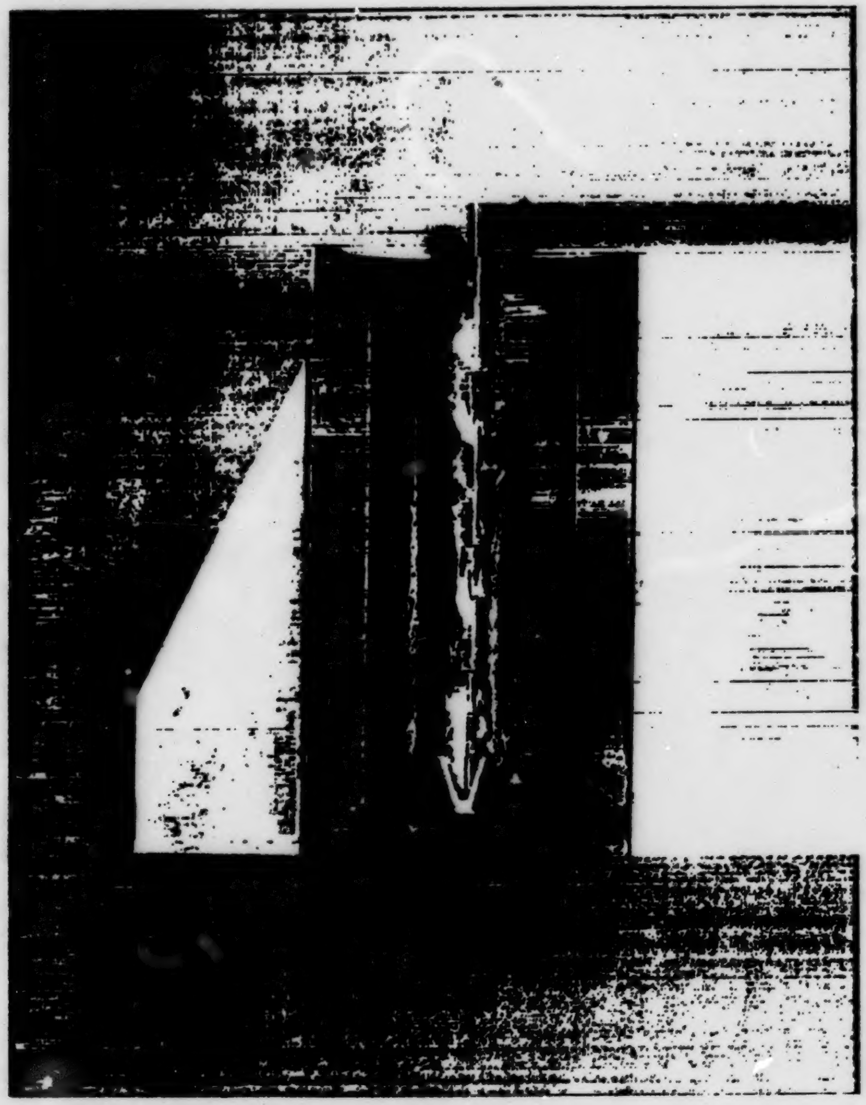

FIGURE 42 - Finned afterbody model, access cover containing the tubing from the pressure taps located on the model base and the fin trailing edge

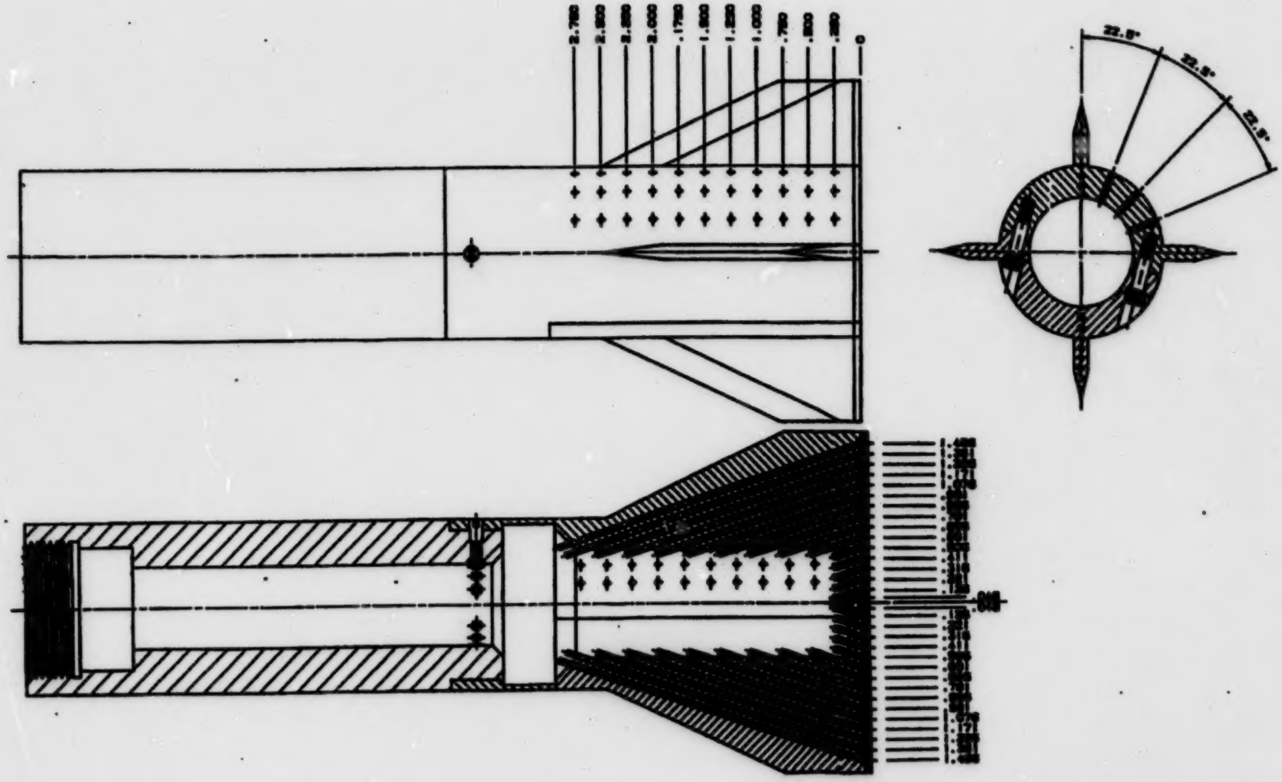
22.5°
22.5°
22.5°
0
.250
.500
.750
1.000
1.250
1.500
.1750
2.000
2.250
2.500
2.750

FIGURE 43 - Finned afterbody model, pressure taps positionning with dimensions in inches

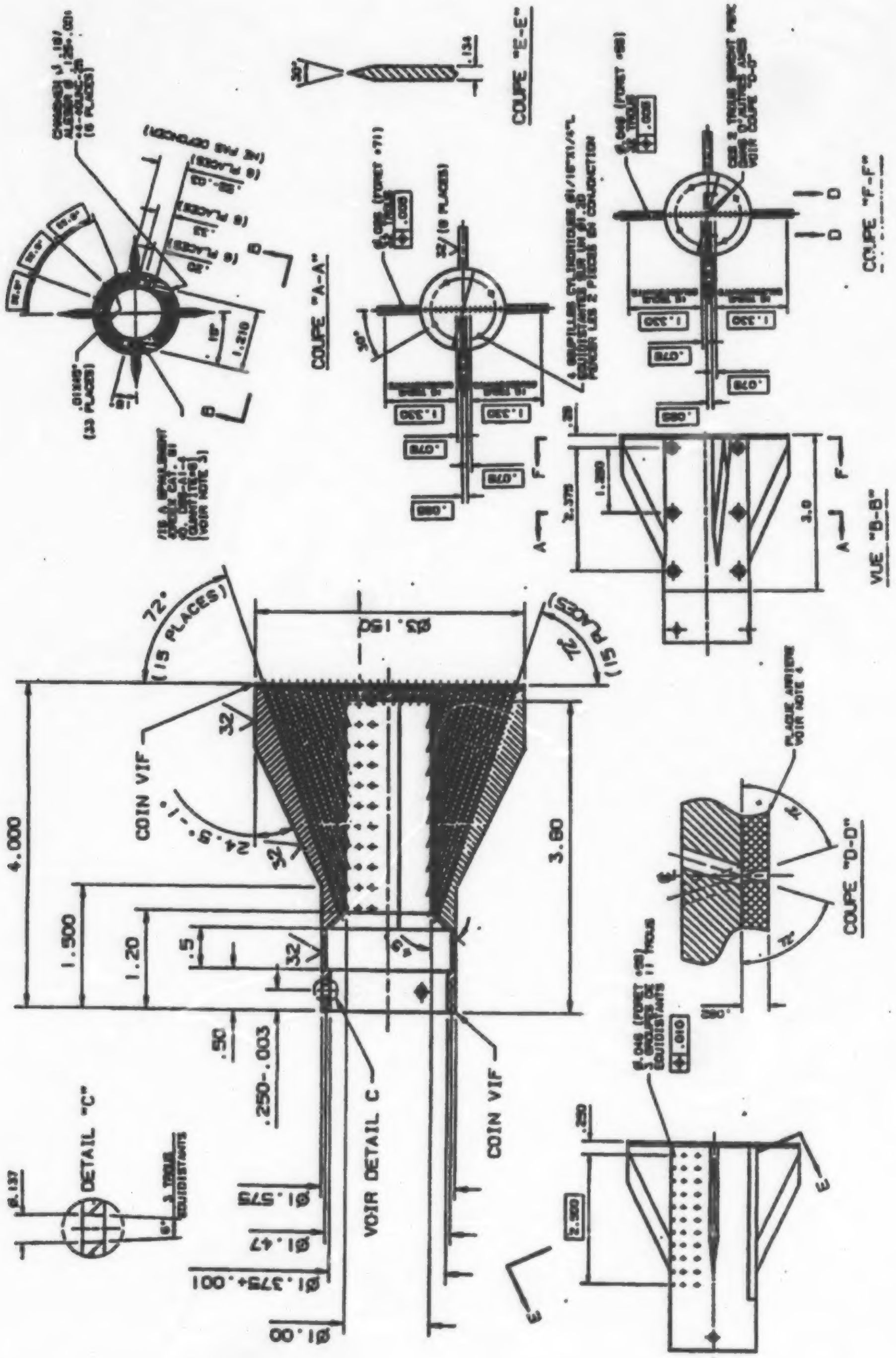
DETAIL "C"
VOIR DETAIL C
COIN VIF
COIN VIF
4.000
1.500
1.20
.5
3.80
.50
.250-.003
Ø1.575
Ø1.47
Ø1.375+.001
Ø1.00
Ø3.150
72° (15 PLACES)
72° (15 PLACES)
24.5°
32
COUPE "A-A"
COUPE "E-E"
COUPE "F-F"
COUPE "D-D"
VUE "B-B"
1.330
.078
.080
1.210
2.375
1.280
3.0
2.500
.134
30°

FIGURE 44 - Finned afterbody model, tail dimensions in inches

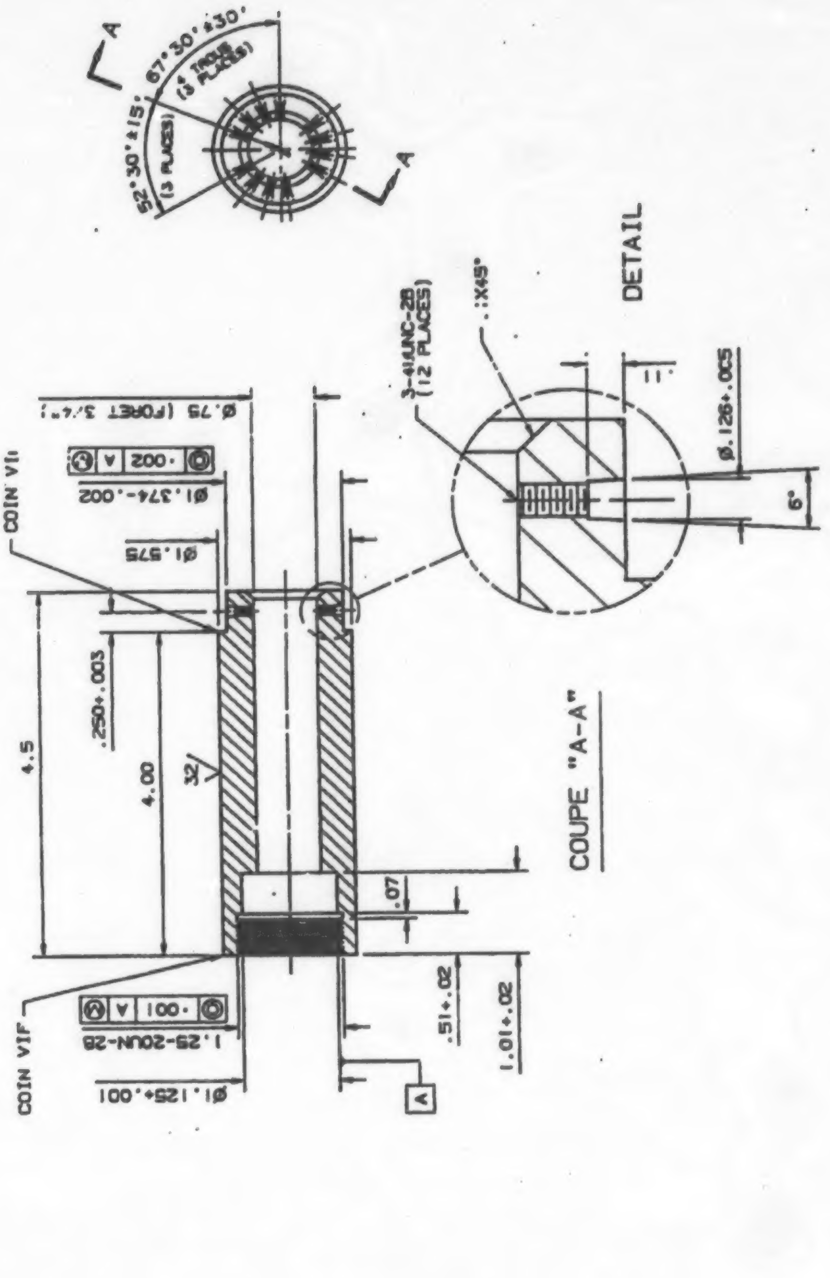
A
52°30'±15'
(3 PLACES)
67°30'±30'
TROUS
(3 PLACES)
A
DETAIL
3-48UNC-2B
(12 PLACES)
.1X45°
.11
Ø.126+.005
6°
Ø.75 (FORET 3/4")
Ø1.374-.002
.002 A
COIN VII
Ø1.575
4.5
.250+.003
4.00
32
.07
COUPE "A-A"
COIN VIF
Ø1.125+.001
1.25-20UN-2B
.001 A
.51+.02
1.01+.02
A

FIGURE 45 - Finned afterbody model, anchorage dimensions in inches

3.0 DREV TRISONIC FACILITY - DESCRIPTION

The DREV trisonic facility (Figs. 46 and 47), is an intermittent indraft type with a 0.6 m x 0.6 m working test section. During a run, the air flows from a flexible air reservoir (air bag 935 m^3), which is prior to the test inflated with dry air to slightly above atmospheric pressure, through a manifold section, a settling chamber fitted with proper honey-combs and screens (56% open area vs total area), a convergent, the nozzles section, the test section, the diffuser and butterfly valve used to initiate and shut-down the flow. Finally air flow exhausts into a vacuum vessel (889 m^3).

The use of dry air is necessary because humid atmospheric air would result into dense fog, water drops and ice pellets in test section at high Mach numbers, introducing important errors in measurements. The inlet air, which is normally at ambient temperature in the air bag, has been previously dried to a nominal dew point of -40° C through the use of an electrically heated Silica-Gel air dryer and fan system.

The supersonic regimes, which has a duration of approximately 7 s (about 5 s are usable), is obtained by separate sets of nozzle blocks (two dimensional) that are used for each of the supersonic test Mach numbers, (Mach 2.0 as the present test series is concerned).

The operation of the wind tunnel is controlled by means of an HP-375 data system processor that performs the following duties:

- opening of the butterfly valve to start the flow,
- pitching of the model through the chosen incidence angles (usually from -5 deg to +15 deg with standard sting),
- shut-down butterfly valve at the end of a run,
- automatic shut-down of air flow in case of an emergency (for example if the balance is overloaded),
- automatic sting return to zero incidence in case of balance overloads and before to flow shut-down in order to avoid stopping shock waves and associated loads to damage the balance,
- and finally acquisition and processing of data.

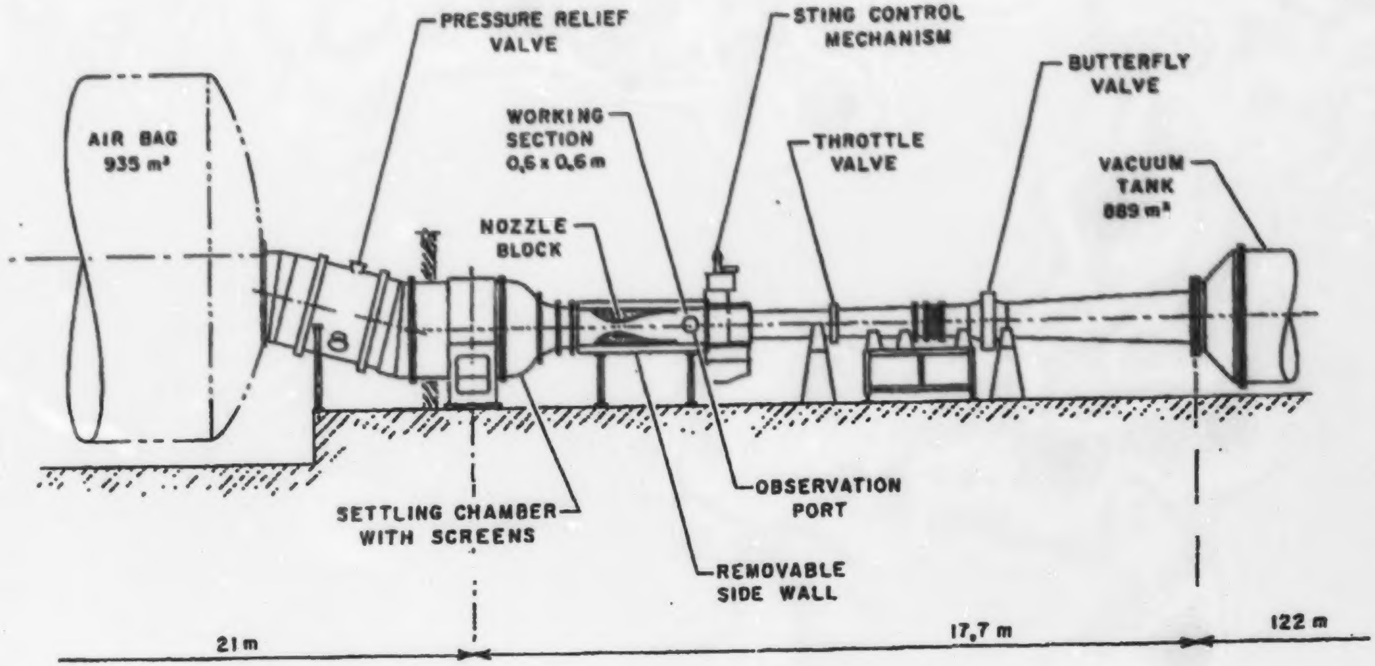
AIR BAG
935 m³
PRESSURE RELIEF
VALVE
WORKING
SECTION
0,6 x 0,6 m
NOZZLE
BLOCK
STING CONTROL
MECHANISM
THROTTLE
VALVE
BUTTERFLY
VALVE
VACUUM
TANK
889 m³
SETTLING CHAMBER
WITH SCREENS
OBSERVATION
PORT
REMOVABLE
SIDE WALL
21 m
17,7 m
122 m

FIGURE 46 - DREV 0.6-m x 0.6-m trisonic wind tunnel

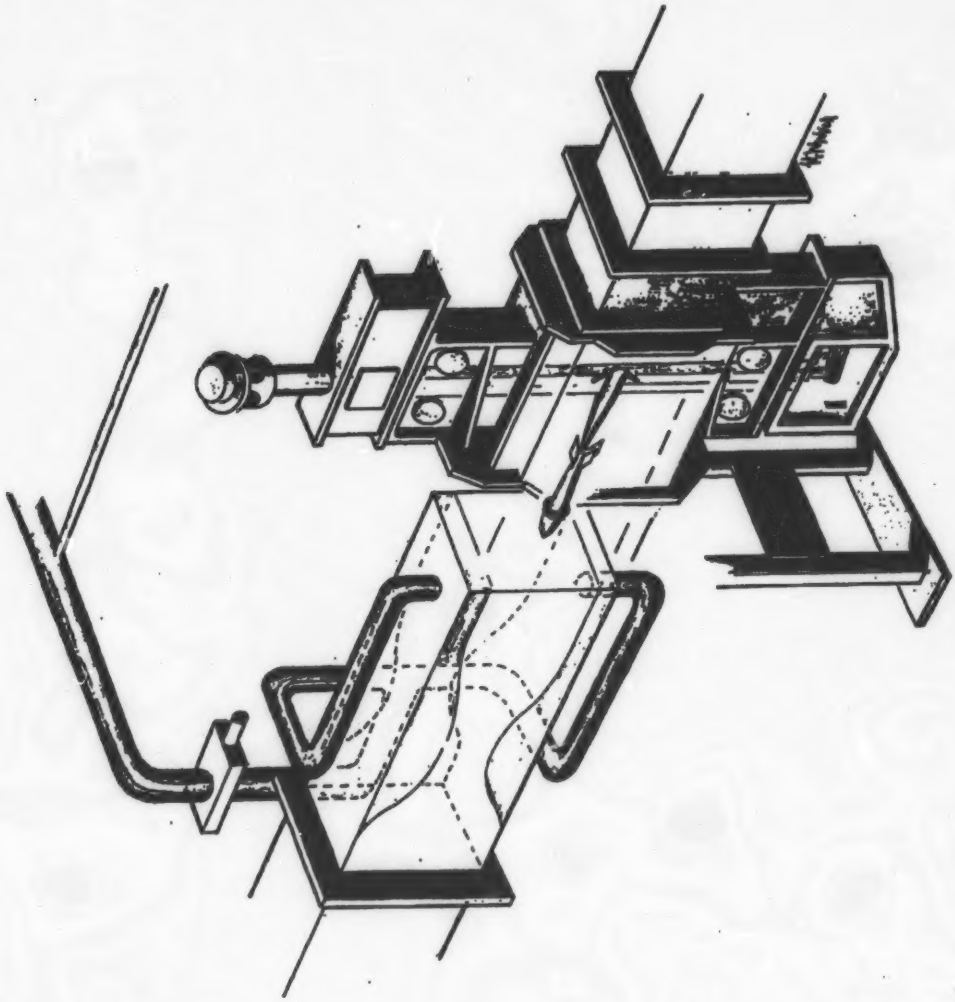

FIGURE 47 - Exploded view of DREV 0.6 m x 0.6 m tunnel test section

The subsonic flow which has a duration of about 5 s (about 4 s are usable), is produced and controlled with the combined use of a special set of two dimensional nozzles (which are much flatter than supersonic ones) and a variable throttle valve which is located downstream of the working section. When transonic flow is required, dedicated test section walls are installed in replacement to the standard ones used for supersonic and subsonic tests. The transonic walls, which bear aspiration holes drilled at angle against the flow direction, are utilized in conjunction with proper manifold system and valves to obtain a suction through the walls that is uniform but variable in intensity. This system, by allowing the aspiration of the lateral flow components that occur after oblique shock waves, avoids shock reflection on test section walls. Otherwise, shock waves, which are almost normal at transonic regime, would reflect back on the model and introduce measurements errors.

Because the DREV facility is an indraft tunnel drawing air into an evacuated tank from an atmospheric pressure reservoir, the Reynolds number drops to very low values at high Mach numbers. The effect of Reynolds number is often not very well known in most of projected experiments. Reynolds numbers (per metre of model length) for each Mach number in the test section and Reynolds number that would be obtained in flight at these Mach numbers under standard sea level conditions are listed in Table I. This data is also presented in graphical form in Fig. 48. If the flow is not purposely tripped in order to produce a realistic boundary layer velocity profile and no means are available to characterize it, induced errors in aerodynamic coefficients could intervene. It can be observed that test conditions would often give a laminar boundary layer around the model in the tunnel while predominant turbulent boundary layers are present for the case of a similar projectile in flight at sea level. This means a farther back transition zone in the tunnel than in atmospheric flight conditions.

TABLE I

Comparison Between Tunnel and Free-Flight Unit Reynolds Numbers

* With Standard Sea Level Conditions in Dry Air Reservoir

** Standard Sea Level Conditions

Mach No.	Re/x (Tunnel)*	Re/x (Free Flight)**
0.23	5.1×10^6/metre	5.3×10^6/metre
0.50	10.2	11.4
0.70	13.0	16.0
0.80	14.0	18.3
1.03	15.3	23.6
1.17	15.6	26.8
1.28	15.6	29.3
1.35	15.5	30.9
1.50	15.2	34.3
2.0	12.8	45.7
2.5	10.1	57.2
3.0	7.8	68.6
3.5	6.0	80.0
4.0	4.7	91.5

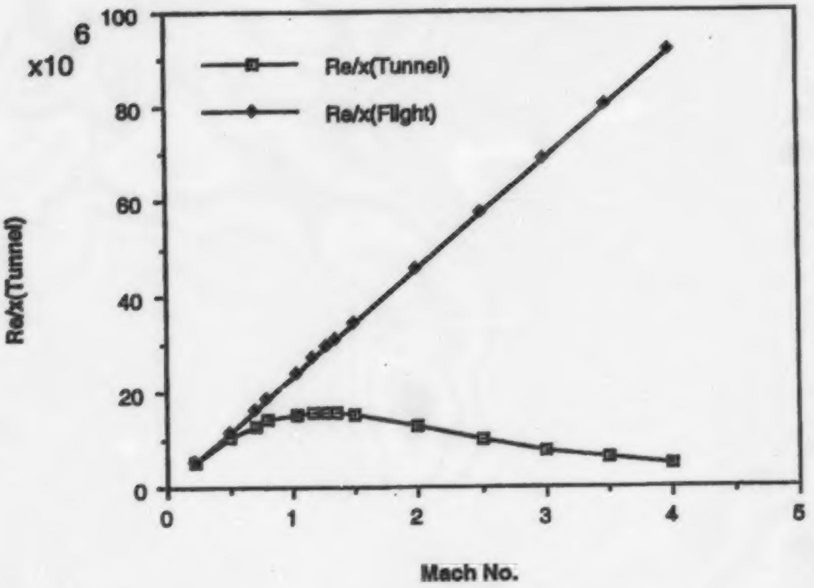

FIGURE 48 - DREV tunnel and free-flight Reynolds number (per metre) as a function of Mach number

4.0 BOUNDARY LAYER CHARACTERIZATION - EXPERIMENTAL METHODOLOGY AND DESCRIPTION OF APPARATUS

The primordial interest of present wind tunnel test series was to produce data on the pressure distribution over the surface of afterbody models of generic projectile configurations. It was assumed that experimental conditions providing a similarity in the velocity profile and in the relative thickness of the boundary layer approaching the model blunt base should result into pressure distribution rather similar to that of a projectile in free-flight (as per Ref. 11 mainly and associated Refs. 12 to 35).

The resulting base/afterbody pressure distribution of a projectile is therefore expected to be directly affected by the approaching boundary layer velocity profile regardless of being natural or artificially produced. If the flow around a test model could be purposely tripped and/or the boundary layer aspired in order to alter boundary layer parameters, it should be possible to observe some repeatable changes in the pressure measurements.

A preliminary boundary layer characterization exploratory experiment was performed in order to find the flow tripping and the aspiration conditions to produce a boundary layer velocity profile that would make possible the comparison of results on pressure distribution with those from the ISL wind tunnel facility. The approach then adopted can be summarized in two statements:

a- Firstly, the base/afterbody pressure distribution data from the present test series had to be compatible with basic data and flow conditions already available, in order to make possible comparisons and analysis. But, the following problems had however to be solved:

- Because the DREV facility is an indraft tunnel, the Reynolds numbers drop to very low values at high Mach numbers. The Reynolds numbers obtained in the DREV facility were about 3.6 times inferior to those encountered in free flight range tests. Also results from ISL were obtained in flow conditions featuring Reynolds numbers about 20 times larger. There was a challenge to modify the boundary layer velocity profile in such a manner to have a same basis of comparison. It was then decided to investigate the boundary layer and try to find the specific combinations of transition strip collars/aspiration intensities to produce a turbulent approaching boundary layers having a thickness of $Y/R \approx 1.4$ at Mach 2.0.

b - Secondly, the boundary layer characteristics had to be known in order to serve as inputs to CFD programs which have the potential to simulate extrapolated conditions.

The boundary layer characteristics measured or calculated from experimental data were:

1 - $\delta \equiv$ Boundary layer total thickness
2 - $\delta_1 \equiv$ Displacement thickness, (conditions of compressible flow and cylindrical body)

3 - $\delta_2 \equiv$ Momentum thickness, (conditions of compressible flow and cylindrical body)

4 - $H \equiv$ Form parameter

5 - Value of " n " in $\frac{U}{U_\infty} = \left(\frac{Y}{\delta} \right)^{\frac{1}{n}}$
if $n \approx 4$, laminar boundary layer,
if $n \approx 7$, turbulent boundary layer.

More details are given about these characterization parameters in Refs. 35, 39 and Chapter 7.0.

The specially designed afterbody model dedicated to boundary layer characterization (designed at DREV) is described in Section 2.1 (see Figs. 23 to 27 while Figs. 7 to 22 present the upstream-sting system to hold it). Two different types of total pressure tubes were used in conjunction with this apparatus. For the boundary layer exploration from the model surface to an height " Y " of 13 mm over the model surface, a flat (duck beak) probe (Figs. 27, 49 and 50) was used due to its inherent capacity to approach its centreline very close to the model surface. For the values of " Y " over 13 mm, a cylindrical probe (with conical inlet) was a better choice (Figs. 26, 51 and 52), its recovery coefficient being less dependent on the flow angularity (i.e. unsteady flow angularities induced by the air flow turbulence). Also, a pressure tap on the model surface was located just under the tip of the pitot tube (Fig. 53). Values of " Y " used in the data analysis (Appendix D - Boundary layer - Summary of results) correspond to the distance apart from the model cylindrical surface to the probe centreline.

Although there were several longitudinal positions available for the pitot probe, only the second one (from upstream to downstream) was used. During these tests, the probe tip was set at various heights in a transverse plane located 70 mm from the model base (which corresponded to 1.75 D or nominal base diameter from astern). Vertical adjustment of the probe from the model surface was made with the aid of semi-circular gauge blocks having the appropriate thicknesses (Fig. 28). The lateral alignment (in yaw) was achieved with another gauge block specially devised for that purpose (Fig. 29).

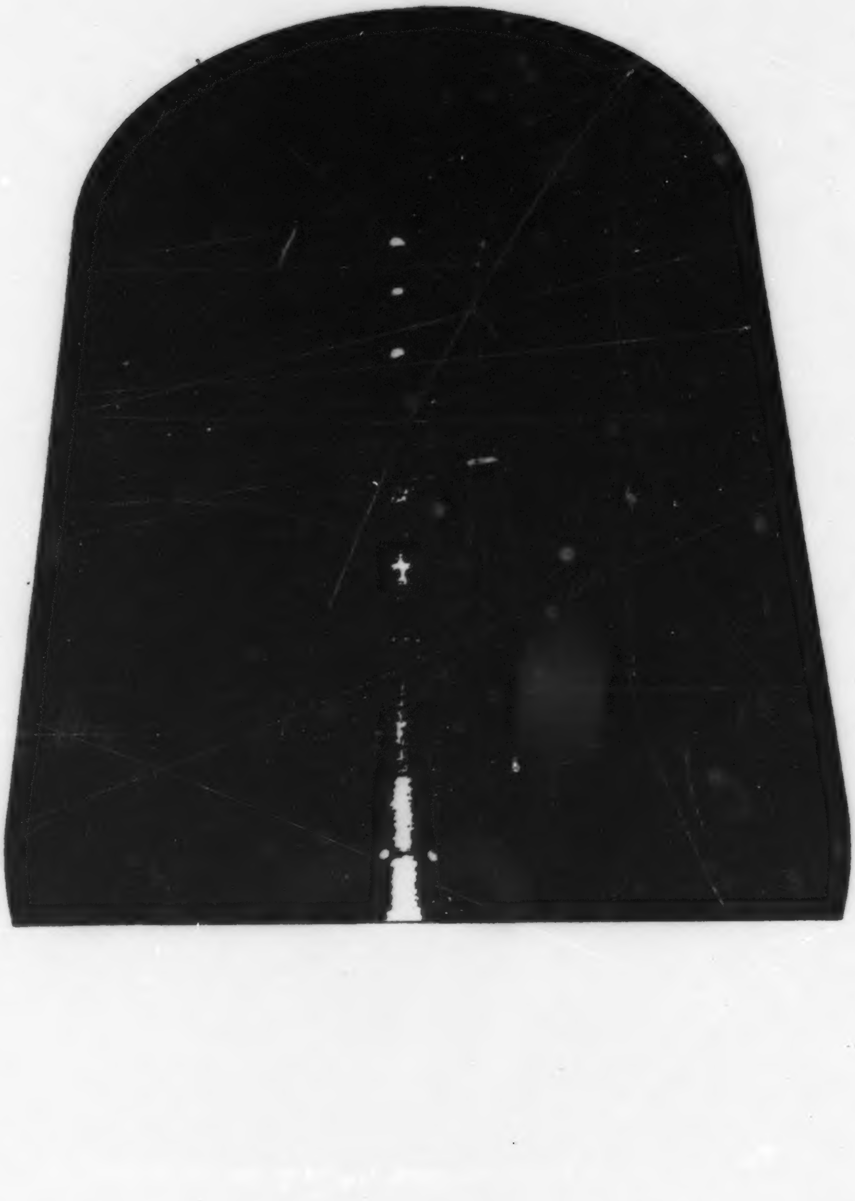

FIGURE 49 - Flat (duck beak) total pressure probe used for boundary layer exploration from surface to 13 mm

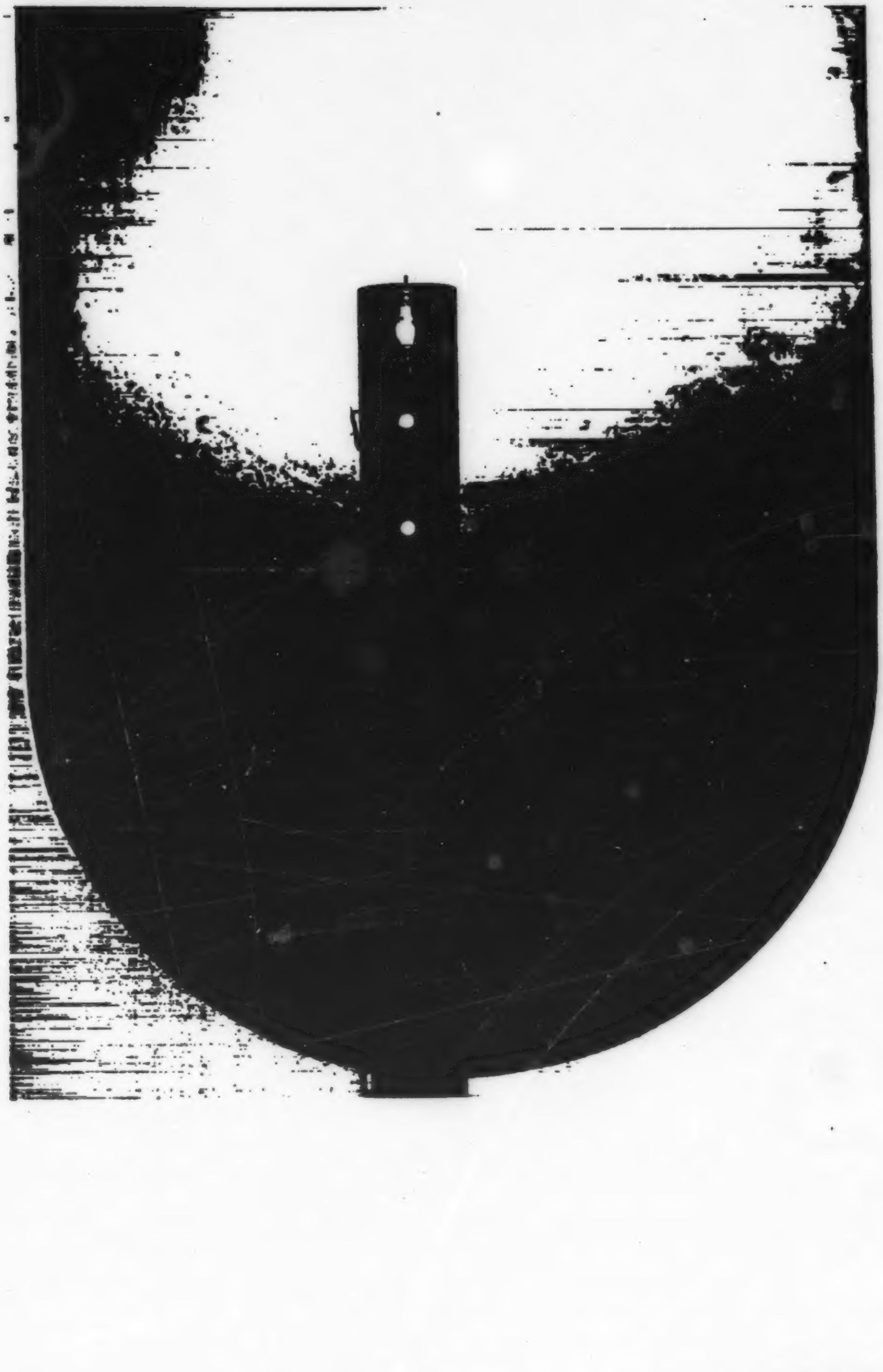

FIGURE 50 - Flat (duck beak) total pressure probe while tangent to model surface

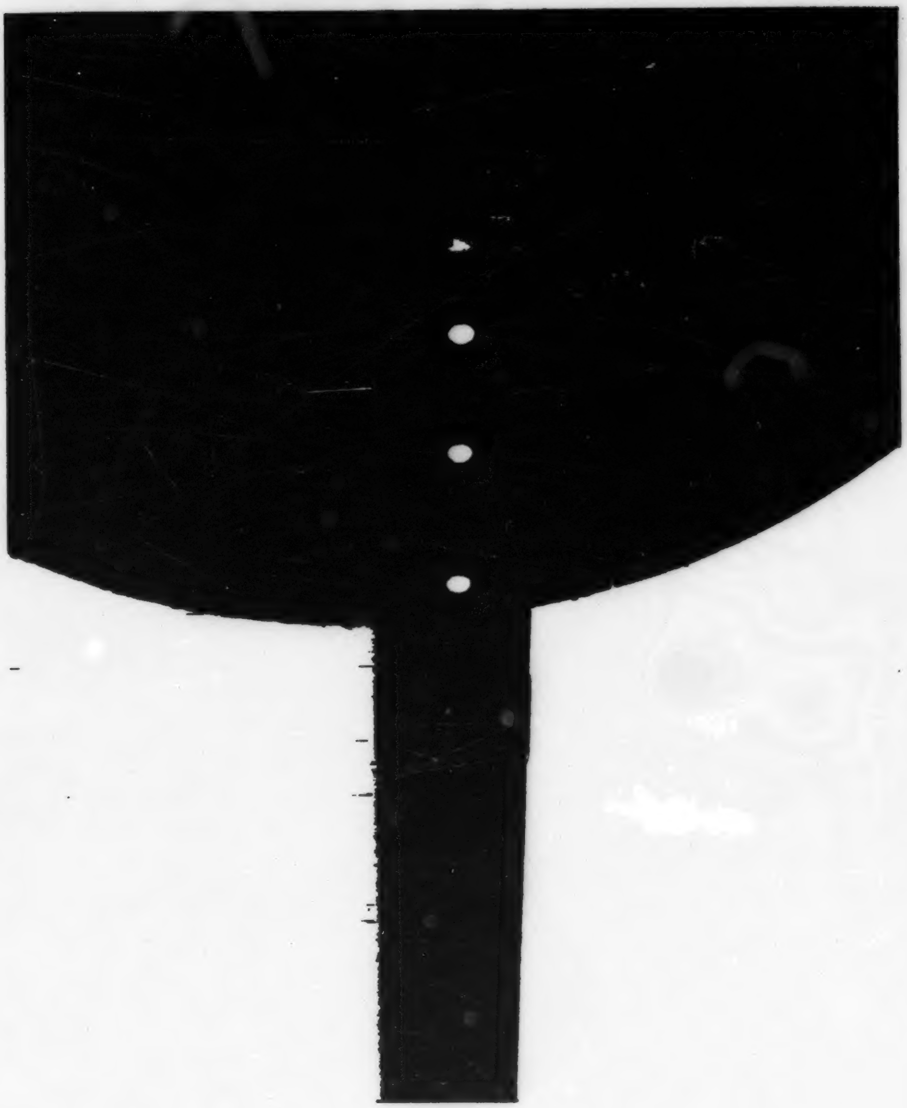

FIGURE 51 - Cylindrical total pressure probe used to explore boundary later over 13 mm from model surface

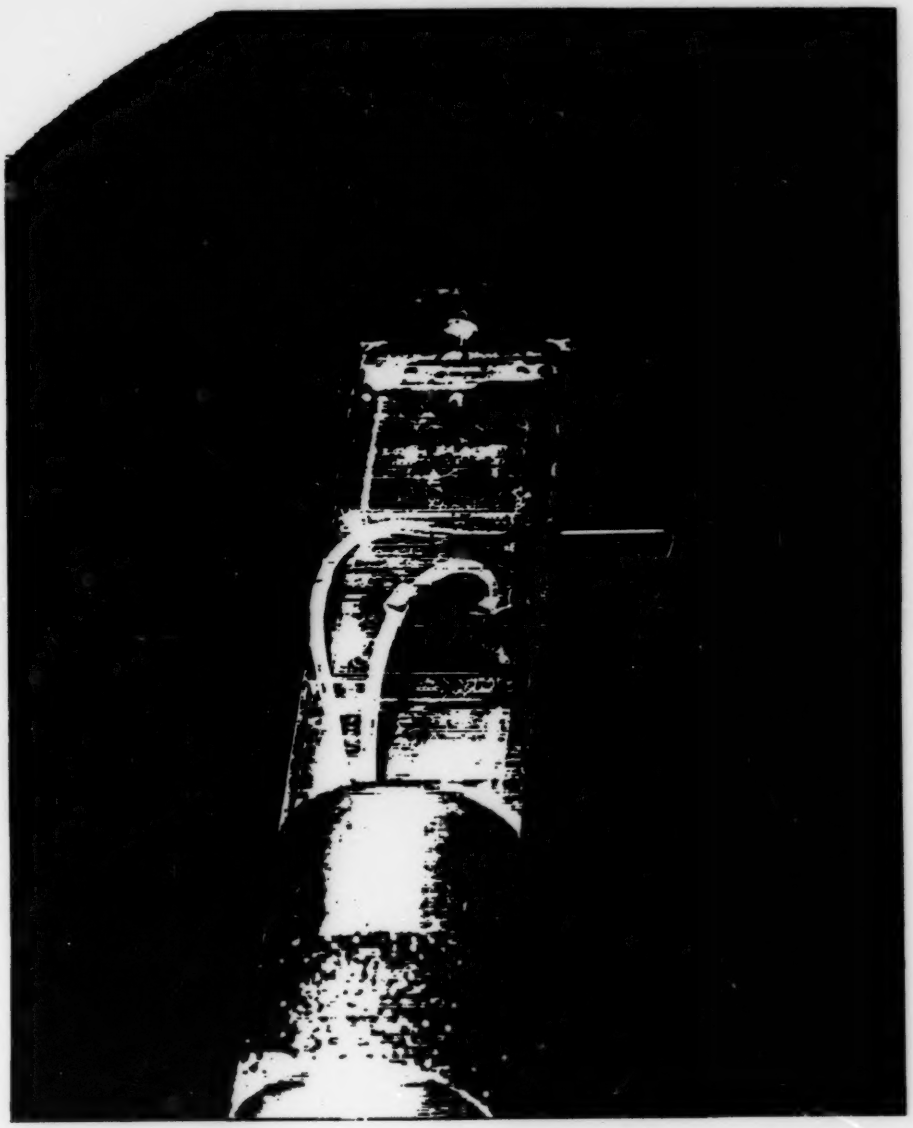

FIGURE 52 - Cylindrical pitot probe with conical inlet, afterbody model with access cover removed

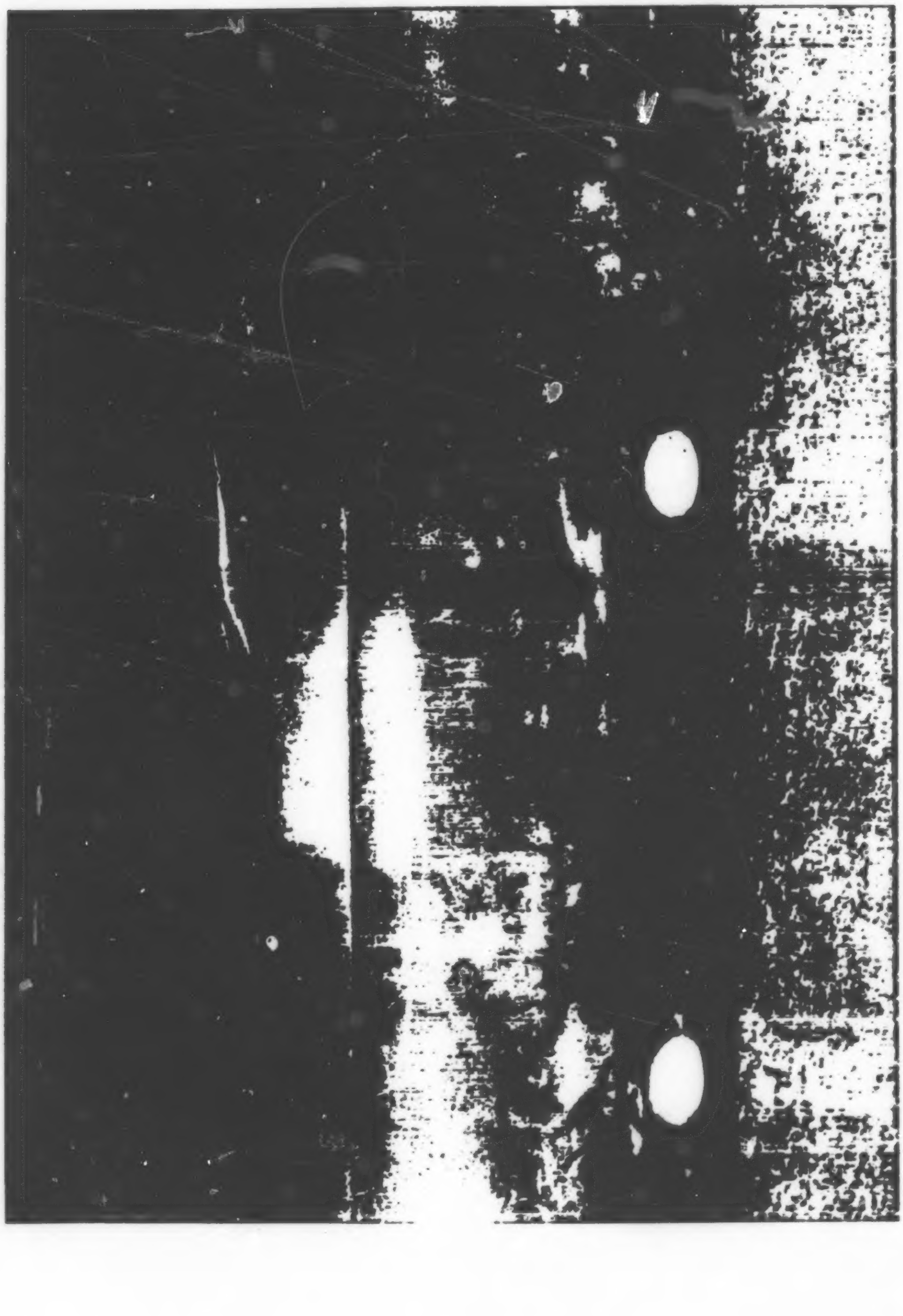

FIGURE 53 - Duck beak pitot tube, surface static pressure tap in a same plane than the probe tip

The procedure sequence that was adopted to perform the boundary layer characterization tests at Mach 2.0 can be stated as follows:

1- A proper alignment of the upstream-sting with respect to flow is achieved as per the procedure described in the Appendix B. The model used for this procedure is the base pressure exploration model described in Section 2.2. See Chapter 9.0 for treatment of data.

2- A first estimation of boundary layer condition and thickness is realized as per the procedure described in Appendix C.

3- Finally, the boundary layer characterization tests are made at Mach 2.0 with the use of the " boundary layer exploration afterbody model ". After several cycles of trials, the tests conditions and related boundary layer with its velocity profile is adopted. It is presented in Appendix D. Chapter 7.0 gives equations and algorithms used for the data reduction.

Knowing the potential influence of boundary layer, all pressure tests were made with settings capable to approach, to some extent, the boundary layer characteristics encountered for similar test performed in the ISL facility (Refs. 3, 4 and 6) with the same configurations of afterbody models (See Appendix D). These settings consisted in:

1- The length adjusting anchorage with aspiration holes (Figs. 20, 50 and 60) was used alone (and not in conjunction with the main body section dedicated to aspiration),

2- Aspiration valve was set at 90 deg, i.e. full open,

3- A transition strip was used, and made of no: 100 grit sand paper, 25.4 mm large collar and located at 4D from the model base.

The boundary layer characteristics then obtained and based on measurements presented in Appendix D are listed below:

$\delta = 0.98998 \approx 19.8$ mm, boundary layer total thickness $\approx Y/R$ value where $U/U_\infty = 0.99$, to be noted that from experimental data it can be observed that $Y/R = 1.426$ for $U/U_\infty = 1.000$

$\delta_1 = 6.3293$ mm, displacement thickness, compressible flow, cylindrical body,

$\delta_2 = 2.1341$ mm, momentum thickness, compressible flow, cylindrical body,

$H = \frac{\delta_1}{\delta_2} = 2.9658$, Form parameter,

$\frac{U}{U_\infty} = \left(\frac{Y}{\delta} \right)^{\frac{1}{n}}$ where the value of " n" was = 6.97

An electronically scanned pressure sensor module was used to measure the static pressure from the model unique pressure tap located on the model and the total pressure from pitot tube (used to measured the velocity profile). The module gave signals proportional to the difference between the pressures from the model single pressure tap (surface static pressure), the pitot probe (total pressure inside model boundary layer) and a pressure of reference.

These pressure modules were " PRESSURE SYSTEMS INCORPORATED " models ESP-32SL ± 5 psid. Fig. 54 and Table II present their characteristics. These pressure measurements were displayed in table form for each 0.1 sec of time interval and between a time frame of approximately 3.5 to 6.0 sec with respect to the butterfly valve opening. Their averages corresponded to the time interval where pressure measurements were stabilized in the test section during a run. Section 9.1 presents examples of data results tables.

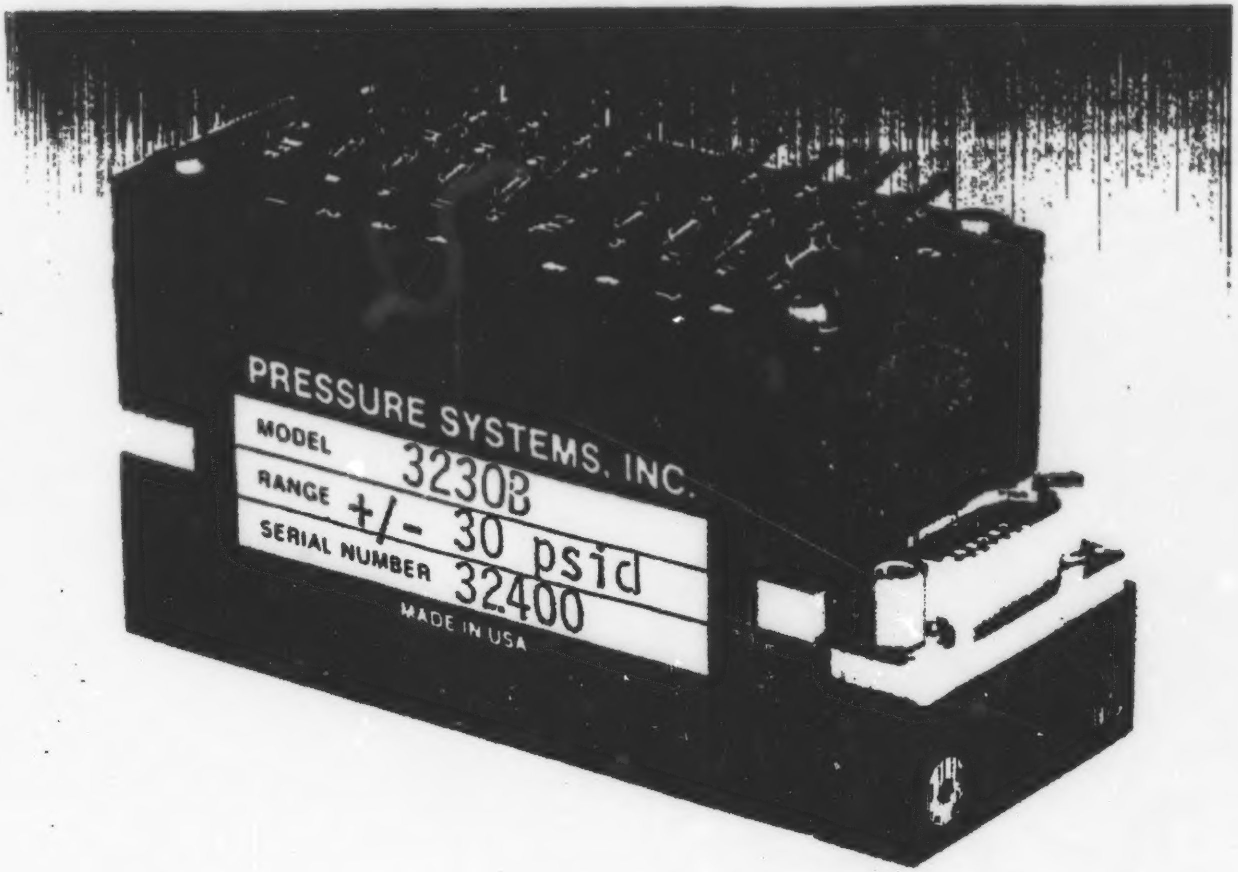
PRESSURE SYSTEMS, INC.
MODEL 3230B
RANGE +/- 30 psid
SERIAL NUMBER 32400
MADE IN USA

FIGURE 54 - Pressure measurement module (± 5 psid) used for boundary layer characterization

TABLE II
SPECIFICATIONS

Number of Pressure Inputs	32
Pressure Span	+5, ±5, +15, ±15, +30, ±30, +45, ±45, 100 psid unidirectional or bidirectional differential
Over Pressure	300%, 5-45 psid; 150%, 100 psid
Max. Reference Pressure	30 psig
Static Error Band[1]	±0.15% FS Worst Case
Thermal Sensitivity Shift	±.05% FS/°F Worst Case
Thermal Zero Shift	±.05% FS/°F Worst Case
Calibration Valve	Controlled by two 100 psi control pressures, two position
Pressure Port Selection	Digital, 5 bit binary
Scan Rate	Up to 20,000 readings/sec.
Full Scale Output	±5 VDC Nominal
Power Requirements	+5 @ 50 ma max. +12 @ 80 ma max. −12 @ 35 ma max.
Temperature Range	0–175°F
Media: Measurement Ports Reference Port	Non-corrosive gases up to 100% non-condensing humidity Dry, non-corrosive gases
Acceleration Response	Perpendicular ±0.008% FS/G, worst case Transverse ±0.008% FS/G, worst case
Ouput Connector	15 pin connector, 12 pins used sub-miniature Cannon connector, part number MDM-15SSB
Size	1" × 2.5" × 1.45" (2.54 × 6.35 × 3.68 cm)
Weight	5 oz.

[1] Includes hysteresis, repeatability and non-linearity.

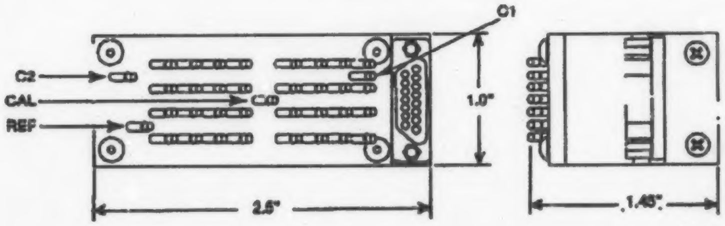

PRESSURE SYSTEMS INCORPORATED

In order to avoid a saturation of the ± 5 psid pressure module that was connected to both the pitot probe and the unique pressure tap located underneath, the setting value of the reference pressure had to be adjusted by trial and error. It finally was adjusted somewhere between the test section static pressure (Mach 2.0 ≈ 126 MBARS) and the dynamic pressure (Mach 2.0 ≈ 352 MBARS).

In order to reduce to a minimum the total length of tubing and consequently induced time lag, the module was located inside the upstream sting stream-lining (Figs. 7 and 19). The total length of " TYGON " tubing running between the pressure module and model unique pressure tap or the pitot tube was approximately 40.0 in. Preliminary testing had shown that no data reading time lag problem was identified for this arrangement. A major potential problem would have been to have a time lag so long that the pressure readings could not have stabilized during the run time period where conditions are constant in the test section.

The test section static reference pressure was the average pressure from wall taps no:7 and 8 ($P_\infty \approx P_V$) which corresponded to the tunnel wall conditions at the location of the afterbody model. The pressure module reference pressure was obtained from a constant pressure reservoir connected to the module reference pressure port. Before a test run, it was adjusted manually with the use of a mercury column barometer. During a test run, an appropriate manifold system connected the constant pressure reservoir to a Rosemont absolute pressure sensor which measured the pressure of reference at each pressure reading for data processing.

5.0 BASE PRESSURE DISTRIBUTION - EXPERIMENTAL METHODOLOGY AND DESCRIPTION OF APPARATUS

The base pressure distribution tests were intended to evaluate the dependance of the base pressure on the thickness and characteristics of the approaching boundary layer. Tests were made at Mach 2.0 in conjunction with the upstream sting described in Section 2.1 and with the flat base with/without fins pressure exploration models (Section 2.2). The Appendix A gives a complete summary of the test runs that were performed.

The upstream sting was aligned as per the procedure described in Appendix B which presents examples of alignment test results in graphical form. A good alignment produced symmetrical radial base pressure distribution. As indicated in Appendix A, the resultant alignment parameters were 0.00 deg of incidence in yaw, and +0.05 deg in pitch. This light longitudinal assymmetry of the flow in the test section had already been identified long time before and, it is believed, must be due to the flow inertial effects caused by the convergent section running at angle between the dry air reservoir (air bag) and the settling chamber.

Each of the four test models bore 32 pressure taps located at various positions of interest. They were all tested with no roll angle, except for Model no. 4 dedicated specifically to a between fins pressure survey that was indexed at 45 deg in order to avoid its between fins pressure taps to be directly influenced by the wake that was left from the wing support trailing edge. The test models are listed below with related figure numbers:

Model no. 2 - BASE PRESSURE EXPLORATION MODEL

Finless model (Figs 30 to 34 of Chapter 2.0, Figs 2 and 3 and also a close view of the base pressure taps is presented in Fig. 55.

Model no. 3 - AFTERBODY SURFACE PRESSURE MODEL

Finless model (Figs 35 to 39 of Chapter 2.0 and Fig. 56)

Model no. 4- FINNED AFTERBODY MODEL, BETWEEN FINS PRESSURE SURVEY

Finned model of DREV-ISL Cone/Cylinder configuration of reference (Figs 40 to 45 of Chapter 2.0 and Fig. 57)

Model no. 5- FINNED AFTERBODY MODEL, FINS AND BASE PRESSURE SURVEY

(Figs 40 to 45 of Chapter 2.0 and Figs 58 and 59).

All pressure tests in present tunnel run series were made with settings to produced the boundary layer characteristics presented in Chapter 5.0 and Appendix D. The transition strip can be seen in Fig. 57 in conjunction with the finned model. A close view of the length adjusting anchorage is presented in Fig. 60.

An electronically scanned pressure sensor module was utilized to measure static pressure from the models 32 pressure taps at a time. This module was still located inside the upstream sting stream-lining and its connection arrangement was similar to that used in the boundary layer characterization tests described in Chapter 4.0. The module was of a type ESP32 SL ±1 psid and connected to the model pressure taps. It can be seen in Fig. 54 and its characteristics are presented in Table II.

These pressure measurements were displayed in table form for each 0.1 sec of time interval and between a time frame of approximately 3.5 to 6.0 sec with respect to butterfly valve opening. Data results averaged values were related to the time interval where pressure measurements were stabilized in the test section during test runs. The beginning and the end of this time interval was determined manually by the operator for each run since it varied more than for the usual tests that are made with the standard sting. This is because of the long tubing between the pressure tap and the pressure module that increased the time necessary to evacuate the air inside the tubing and pressure sensor. Depending on the pressure variations to be measured, the time needed to obtain stabilized measurements was affected. Section 9.2 presents examples of data results tables and graphical layouts.

FIGURE 55 - Base pressure exploration module to be used in conjunction with the upstream sting

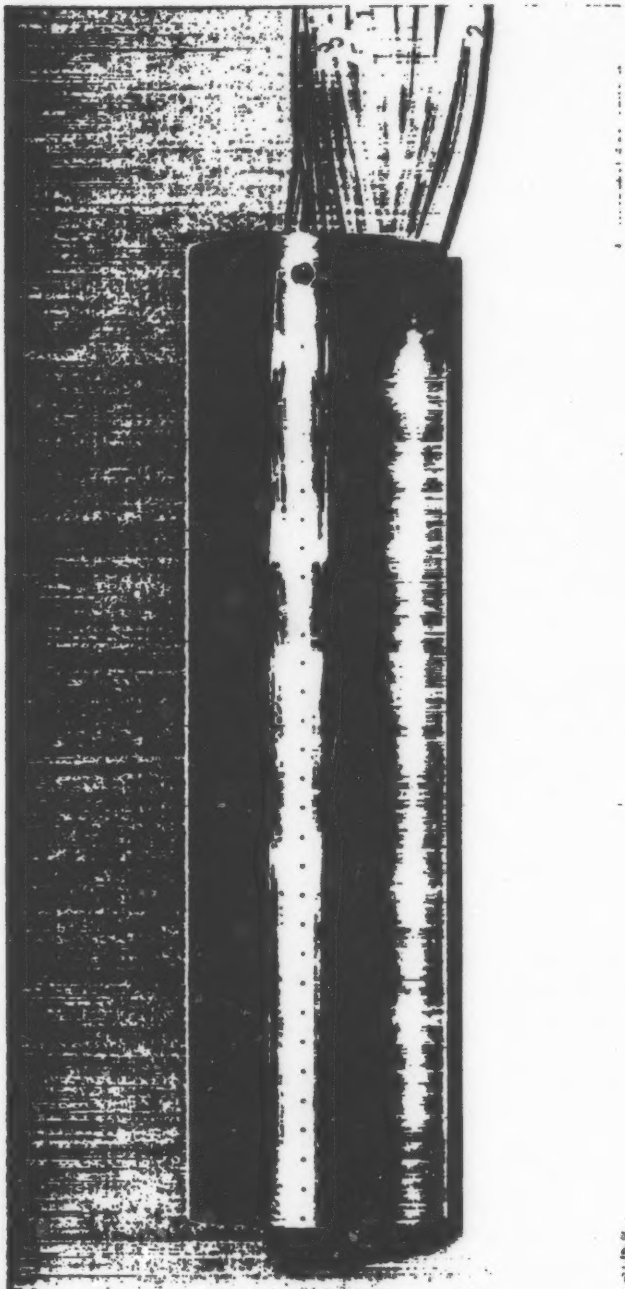

FIGURE 56 - Afterbody surface pressure exploration module to be used in conjunction with the upstream sting

FIGURE 57 - Afterbody model with fins dedicated to between fins pressure survey, in test section while assembled on the upstream sting

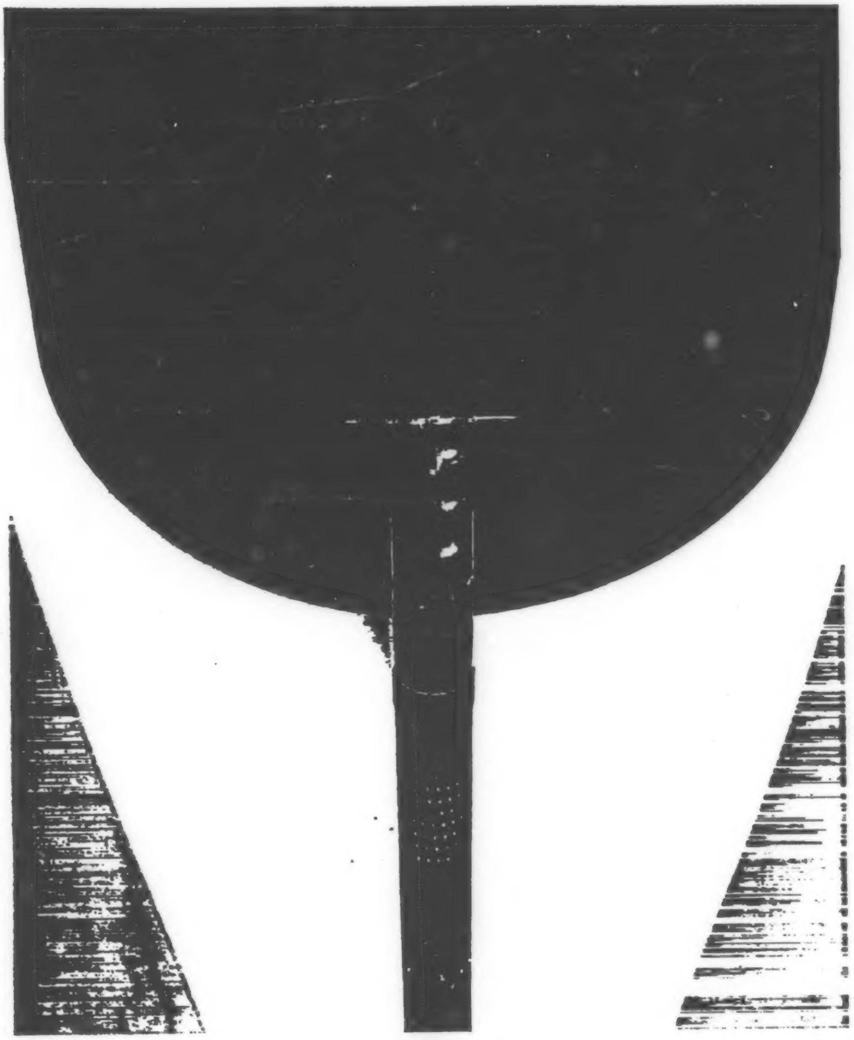

FIGURE 58 - Afterbody model dedicated to fins trailing edge and base pressure survey, shown assembled on the upstream sting. Note aspiration holes and transition strip sand paper collar

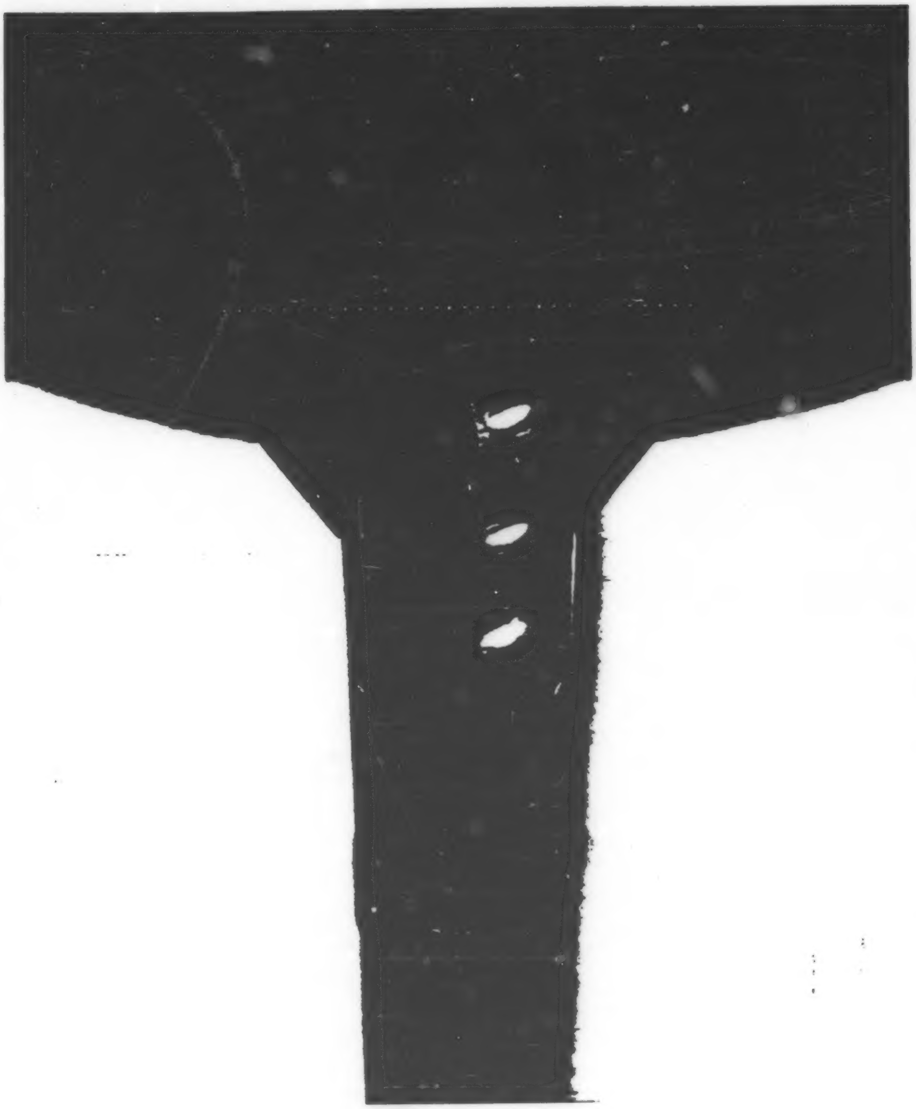

FIGURE 59 - Close view of pressure taps positionning on base and fin trailing edges

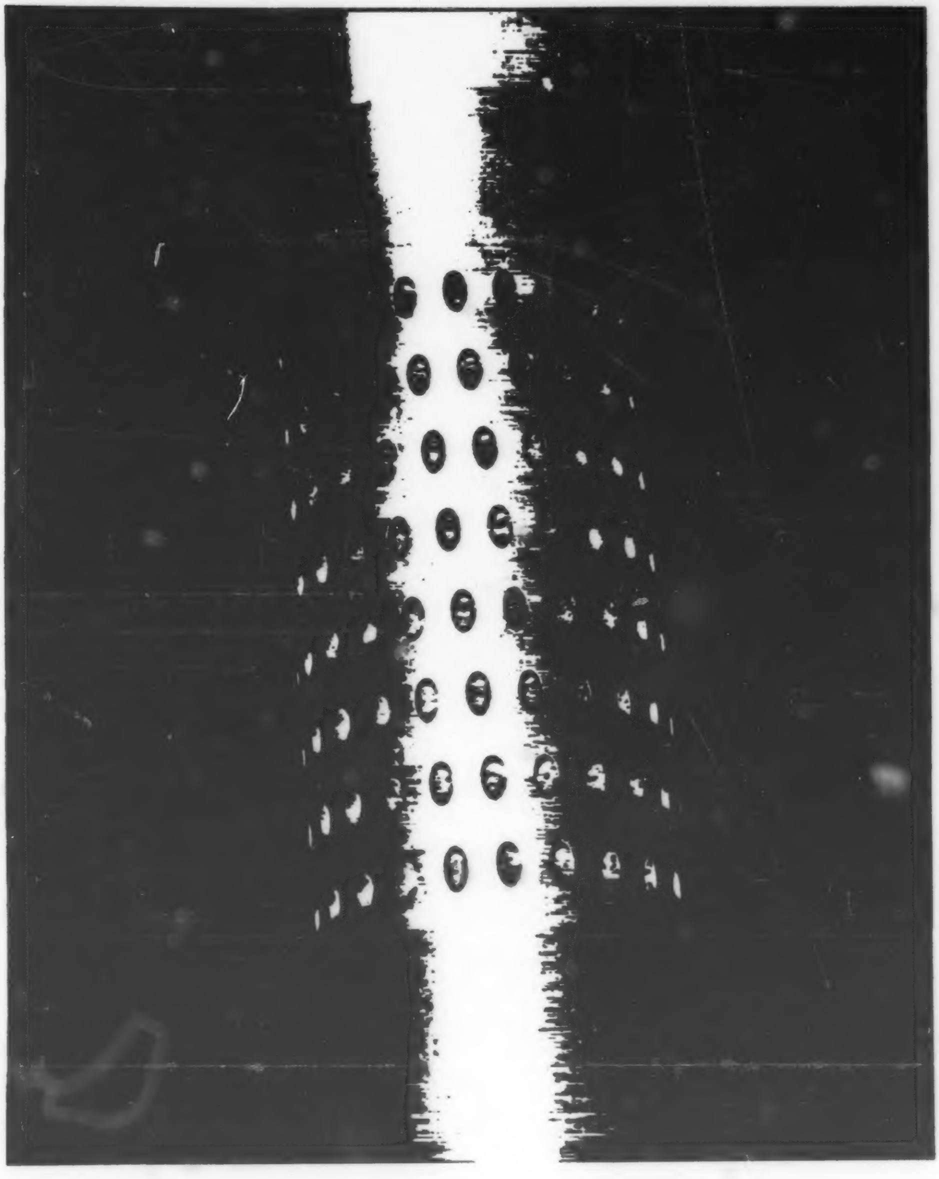

FIGURE 60 - Close view of astern aspiration holes section used for pressure survey tests. Note low pitch helix angle of aspiration holes in order to avoid a flow strip to pass over sting surface without to encounter at least one aspiration hole

The test and data acquisition procedure was much similar to the one used for the boundary layer characterization tests, i.e. The test section static reference pressure was the average from wall taps no: 7 and 8 corresponding to flow conditions at the location of the model base/afterbody. The pressure module utilized was more sensitive than the one used for the boundary layer measurement tests. Its reference pressure had to be adjusted by trial and error in order to avoid a sensor saturation that would have resulted into erroneous readings and also to not exceed the 300% overpressure that can be sustained by the pressure module. The values that had to be utilized were dependent on the test being done but resembled those utilized for static pressure measurement in the boundary layer characterization tests.

Because the DREV facility is an indraft tunnel drawing air into an evacuated tank from an atmospheric pressure reservoir, the Reynolds number drops to very low values at high Mach numbers. Although special precautions were taken in order to artificially modify the boundary layer velocity profile around the afterbody model, it remained that fundamentally, the ratio between inertial and viscous forces corresponded to low Reynolds numbers.

For the particular flow conditions encountered in the DREV 0.6-m x 0.6-m indraft wind tunnel and at test Mach numbers, Reynolds numbers were as it follows:

COMPLETE ISL CONE/CYLINDER IN TEST SECTION

MACH NUMBER	R_{∞_D}	R_{∞_L}	R_{CF}
2.0	5.12×10^5	3.07×10^6	1.33×10^5

COMPLETE ISL CONE/CYLINDER IN FREE FLIGHT

MACH NUMBER	R_{∞_D}	R_{∞_L}	R_{CF}
2.0	1.83×10^6	1.10×10^7	4.73×10^5

Those figures are given as an indication only and considered barely supercritical by Ref. 36 as wind tunnel test conditions may be concerned. Figure 61 (Ref. 37) gives laminar to turbulent transition Reynolds numbers as a function of Mach number for few configurations of reference and as per these figures, tunnel Reynolds numbers would have been subcritical.

It must be noted that finless projectiles are often spin-stabilized. It is not known to which extent the data results from static tests could be applicable to the aerodynamics of spinning projectiles. In a first time, it could be said that because barrel rifle angles used are rather small, the lateral tangential velocity component due to spin represents a little contribution relatively to the total air flow velocity due to projectile forward movement. By then, the pressure measurement data from present wind tunnel experiment and that on laminar to turbulent Reynolds number of Fig. 61 related to static conditions could possibly be used as a first approximation to cases of spinning projectiles.

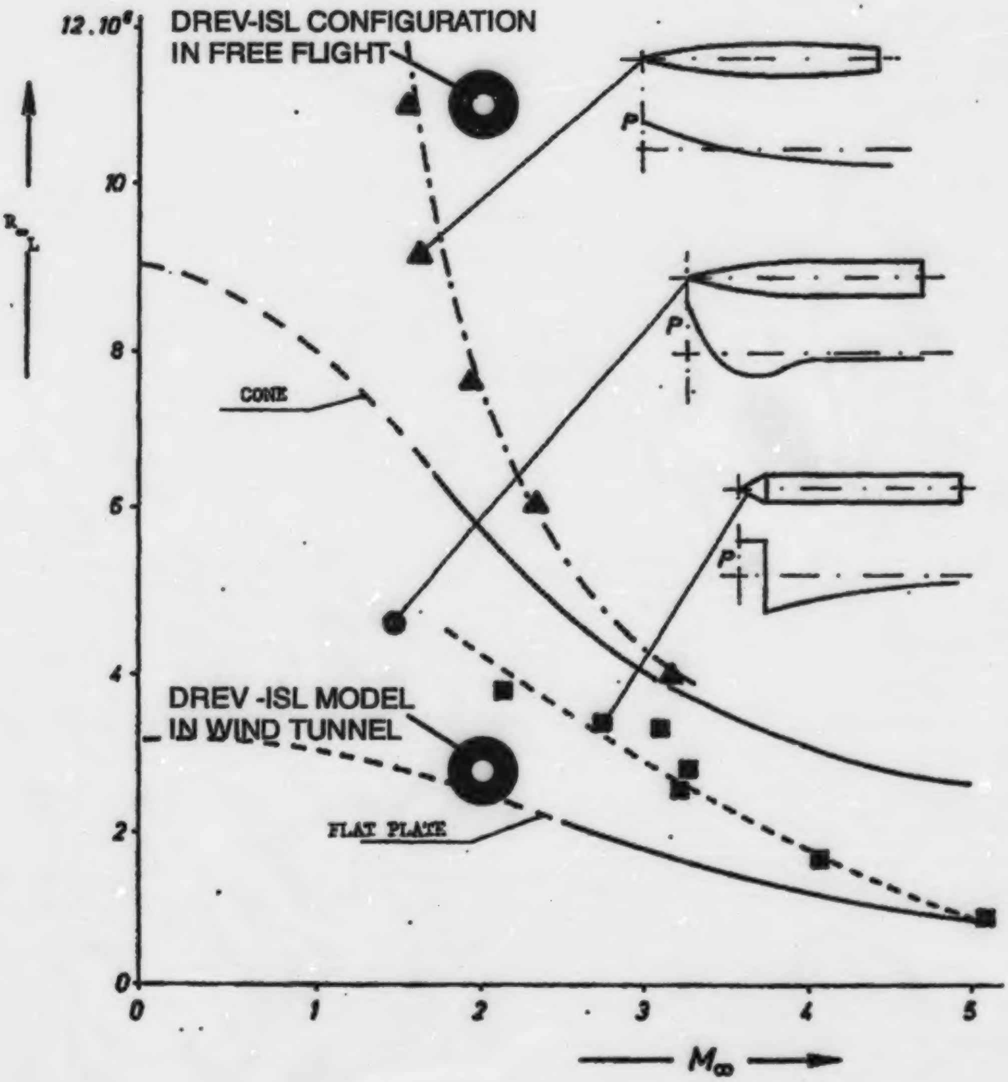

FIGURE 61 - Laminar to turbulent Reynolds number as a function of Mach number and configurations of reference

6.0 DATA ACQUISITION SYSTEM

While performing wind tunnel tests, the calibration of the various instruments that are used can be a matter of questioning. It has not been rare in the past to reprocess recorded digitized analogic signals from a wind tunnel test run series while using different values of calibration parameters or matrices.

The use of a balance to perform force measurement tests implies calibrations and data reductions which are rather complex. These are usually adaptable processes that can be made in various ways. In the present test series there were no force tests but only pressure measurements. The calibration of the pressure modules were made by the automatic calibrator and data reduction by the controller. Since the reduced pressure measurements were the only data recorded, it would not be possible to reprocess the data with new values of calibration parameters but only with some different values of the pressures of reference.

Individual pressure sensors had non-linear calibration curves based on three points used to generate second order polynomials. Since the calibration pressure values for each of the three points were determined by adjusting manually three calibrator valve handles, the calibration curves were directly affected. Some tests conditions corresponded to a very low percentage of sensor nominal capacities, and depending on how calibration set points were chosen, the sensor non- linearities encountered in these conditions may not have been well reproduced by the calibration curves. In the case of divergence of opinion regarding the pressure module calibration, there would be no other alternative than to make new tests.

Since the test section static pressure was measured with absolute pressure sensors whose analogic output data was recorded, it would be possible to reprocess test run data with new values of calibration parameters. For example, the test section static pressure, Mach number and dynamic pressure could be recalculated. These new values of test conditions would affect the data reduction of surface pressure and boundary layer measurements that could be reprocessed.

6.1 Boundary Layer Characterization Tests

For tests dedicated to boundary layer velocity profile measurements, the " PRESSURE SYSTEM INCORPORATED " modules and control systems used at DREV perform automatically a new calibration for each pressure tap transducer (total of 32) before a wind tunnel run (although only 2 ports were used).

The controller was : PSI, DACU 780B-D
Part no: 7802 - 01

The calibrator was : PSI, CALIBRATION UNIT 780 B
Part no: 7803-03-04-05
with interface IEEE488
Ranges: 8 psid or 23 psia
15 psid or 30 psia
30 psid or 45 psia

P_∞, M (Test section Mach number) and Q were based on test section wall taps no: 7 and 8 (manifolded together) measurements from ROSEMOUNT 1301A/317, calibrated 11/06/1991.

6.2 Base Pressure Distribution Tests

These tests used the same system described in Section 6.1 and that were utilized for the boundary characterization tests.

7.0 TREATMENT OF DATA - BOUNDARY LAYER CHARACTERIZATION IN A COMPRESSIBLE FLOW

Boundary layer characterization experiments are a novelty at DREV and the specific approach that was adapted to the flow conditions in tunnel test section and to the instrumentation and sensors available is still under improvement. The development of equations that are to be used for reduction of pitot tube pressure measurement data, including the assumptions that were made, are presented in this section.

7.1 Velocity Ratio Profiles as a Function of Mach Number Inside Boundary Layer

Among all flow conditions parameters indicated in Fig. 62, the following parameters can be known by direct measurements assuming a uniform (for longitudinal and lateral distribution) and constant static pressure: P_∞, P_{t_∞}, M_∞, T_∞, U_∞, ρ_∞, P_1, P_2, P_{t_2}.

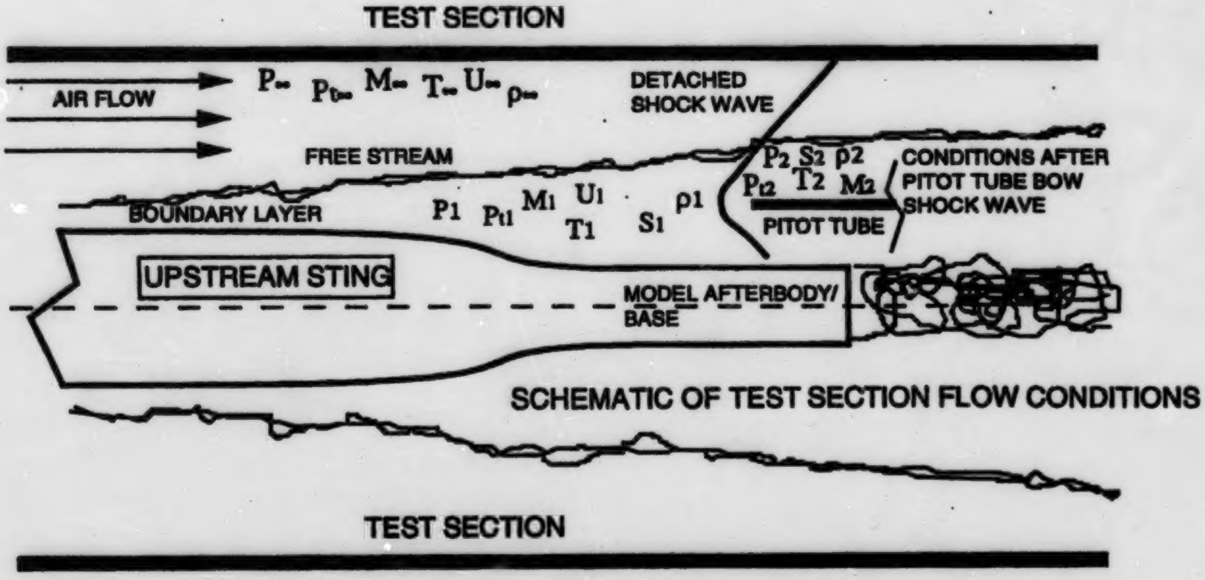
TEST SECTION
AIR FLOW
P_∞ $P_{t\infty}$ M_∞ T_∞ U_∞ ρ_∞
DETACHED SHOCK WAVE
FREE STREAM
P_2 S_2 ρ_2
P_{t2} T_2 M_2
CONDITIONS AFTER PITOT TUBE BOW SHOCK WAVE
BOUNDARY LAYER
P_1 P_{t1} M_1 U_1 T_1 S_1 ρ_1
PITOT TUBE
UPSTREAM STING
MODEL AFTERBODY/ BASE
SCHEMATIC OF TEST SECTION FLOW CONDITIONS
TEST SECTION

Figure 62 - Identification of three levels of flow parameters: Free stream, inside boundary layer and after pitot probe bow shock wave

Free stream and inside boundary layer velocities can be expressed as a function of respective Mach numbers and temperatures:

$$U_1 = M_1 \sqrt{\gamma g_c R\, T_1} \qquad (1)$$

$$U_\infty = M_\infty \sqrt{\gamma g_c R\, T_\infty} \qquad (2)$$

$$\frac{U_1}{U_\infty} = \frac{M_1}{M_\infty} \sqrt{\frac{T_1}{T_\infty}} \qquad (3)$$

Temperature and velocity gradients internal to the boundary layer provide heat conduction and viscous dissipation that render the boundary layer flow process internally irreversible. In default of having a reliable instrumentation to measure the flow temperature at different level inside the boundary layer, this temperature had to be calculated by assuming an isentropic process. It is believed that irreversibility that occurred inside the boundary layer for that particular test was negligible compare to the one imputable to pitot tube bow shock wave. Relationship between air flow temperatures and Mach numbers assuming constant stagnation temperature and a perfect gas can be expressed as follows:

$$T_\infty \left(1 + \frac{\gamma-1}{2} M_\infty{}^2\right) = T_1 \left(1 + \frac{\gamma-1}{2} M_1{}^2\right)$$

By substitution in (3)

$$\frac{U_1}{U_\infty} = \frac{M_1}{M_\infty} \sqrt{\frac{1 + \frac{\gamma-1}{2} M_\infty{}^2}{1 + \frac{\gamma-1}{2} M_1{}^2}} \qquad (4)$$

In the data reduction programme, M_1 is calculated from the pitot probe total pressure measurements by using a convergent iteration algorithm to the solve equation (7) which is demonstrated in section 7.2. Afterwards, equation (4) is used to determine the boundary layer velocity ratios at various levels from the model surface in subsonic or supersonic regime.

7.2 Relationship Between Mach Number and the Pitot Probe Total Pressure Measurement at Supersonic Regime Inside Boundary Layer

Although the boundary layer velocity profiles to be measured in this experiment are mostly supersonic over its whole thickness, subsonic and supersonic regimes are taken into account by the inclusion of two equations (to be solved) in the data reduction algorithm: one for the subsonic regimes encountered at low levels close to the model surface and the other one for the supersonic regimes at higher levels. This section presents a demonstration and explanations of the equation used to convert the total pressure measurements into Mach numbers at high level (far from model surface) inside the boundary layer where supersonic regimes supervened.

To make data insensitive to test section static pressure variations induced by atmospheric pressure fluctuations, the total pressure measurements are non-dimensionalized with respect to P_∞ :

$$\frac{P_{t_2}}{P_\infty} = \frac{\text{Pitot tube total pressure}}{\text{Test section static pressure}} = \text{Measured data}$$

Assuming a uniform and constant static pressure (longitudinal and lateral distribution) :

$$P_1 = P_\infty$$

In supersonic regime, the pressure P_{t_2} is the total pressure behind the normal shock and which is recreated by the pitot tube. It can be calculated as follows: the total pressure P_{t_1} of the flow upstream of the shock can be calculated from M_1:

$$\frac{P_\infty}{P_{t_1}} = \left(1 + \frac{\gamma-1}{2} M_1{}^2\right)^{\frac{-\gamma}{\gamma-1}} \qquad (5)$$

(for a calorically ideal gas at constant entropy)

The ratio of stagnation pressures across a normal shock can be calculated with the following equation:

$$\frac{P_{t_2}}{P_{t_1}} = \left[\frac{(\gamma + 1)\, M_1{}^2}{2 + (\gamma-1)\, M_1{}^2}\right]^{\frac{\gamma}{(\gamma - 1)}} \bullet \left[\frac{2\gamma M_1{}^2 - (\gamma-1)}{\gamma + 1}\right]^{\frac{-1}{(\gamma - 1)}} \qquad (6)$$

The total pressure behind the normal shock is therefore obtained from (5) and (6):

SUPERSONIC REGIME

$$\frac{P_{t_2}}{P_\infty} = \frac{P_{t_2}}{P_1} \bullet \frac{P_{t_1}}{P_\infty} = \frac{(\gamma+1)\, M_1{}^2}{2} \bullet \left[\frac{M_1{}^2 \bullet (\gamma+1)^2}{4\gamma M_1{}^2 - 2\,(\gamma-1)}\right]^{\frac{1}{\gamma-1}} \qquad (7)$$

Where the value of M_1 (Mach number inside boundary layer) has to be solved by iteration through the use of a convergent algorithm and where the value of $\frac{P_{t_2}}{P_\infty}$ = known measured data. The equation (7) is similar to an equation given in a paper of W. Wuest (Ref. 38), presenting the various methods of flow pressure measurements in general experimental aerodynamics.

7.3 Relationship Between Mach Number and Pitot Probe Total Pressure Measurement at Subsonic Regime Inside Boundary Layer

This section presents the development of the equation used to convert total pressure measurements into Mach numbers at low levels inside the boundary layer where subsonic regimes occurred.

$$\frac{P_{t_2}}{P_\infty} = \frac{\text{Pitot tube total pressure}}{\text{Test section static pressure}} = \text{Measured data}$$

In reference to Fig. 62, the following assumptions are made:

$$M_1 = M_2$$

$$P_1 = P_\infty$$

$$P_{t_1} = P_{t_2}$$

Then from equation (5)

$$\frac{P_{t_2}}{P_\infty} = \left(1 + \frac{\gamma-1}{2} M_1{}^2\right)^{\frac{\gamma}{\gamma-1}}$$

Solving for M_1 the following relationship is obtained:

SUBSONIC REGIME

$$M_1 = \sqrt[2]{\frac{2}{\gamma-1} \cdot \left[\left(\frac{P_{t_2}}{P_\infty}\right)^{\frac{\gamma-1}{\gamma}} - 1\right]}$$

7.4 Algorithm Used to Calculate the Boundary Layer Velocity Ratio Profile

The following algorithm was used to process the boundary layer total pressure measurements data obtained with pitot tubes. The symbol " * " preceding a variable indicates that this variable is displayed in tabulated data:

* $Y \equiv$ Radial distance from model surface

Note: The true pitot tube total pressure of each pressure measurement is obtained by using the following equation:

$$P_{pitot_i} = \underset{\text{(as read)}}{P_{pitot}} + \underset{\text{(as read)}}{P_{ref}}$$

* $P_\infty = P_{s_i} = P_{\text{average from wall taps no: 7 and 8}}$

* $RP_{pitot_i} = \frac{P_{pitot_i}}{P_\infty}$ Reduced total pressure from pitot tube measurements at the i^th^ reading

* $\overline{RP_{pitot}} = \frac{P_{t_2}}{P_\infty} = \frac{1}{n}\sum_{i=1}^{n} \frac{P_{pitot_{i\,true}}}{P_\infty}$ Average total pressure frcm pitot tube measurements for all readings between 3.5 and 6.0 sec. run time

$$* \; R_{P_{mstat_i}} = \frac{P_{mstat_i}}{P_\infty} = \frac{\left(P_{mstat_{i\,\text{as read}}} - P_{i\,\text{ref as read}}\right)}{P_\infty}$$

Model surface static pressure ratio at the ith reading

$$* \; \overline{R_{P_{mstat}}} = \frac{1}{n}\sum_{i=1}^{n} \frac{P_{mstat_i}}{P_\infty}$$

$$M_i = \sqrt[2]{\frac{2}{\gamma-1} \cdot \left[\left(\frac{P_{t_i}}{P_{s_i}}\right)^{\frac{\gamma-1}{\gamma}} - 1\right]}$$

$$Q_i = \frac{\gamma}{2} \cdot M_i^2 \cdot P_{s_i}$$

$* \; \overline{M} = M_\infty = \frac{1}{n}\sum_{i=1}^{n} M_i$ between 3.5 to 6.0 sec. run time

$P_T = \frac{1}{n}\sum_{i=1}^{n} P_{t_i}$ between 3.5 to 6.0 sec. run time

$* \; \overline{Q} = \frac{1}{n}\sum_{i=1}^{n} Q_i$ between 3.5 to 6.0 sec. run time

$$T_a = 273.15 + t_c$$

$M_a = M_\infty$

$$T_\infty \approx T_v = T_a \left(1 + \frac{\gamma-1}{2} \cdot M_a{}^2\right)^{-1}$$

$$* \text{ REY/M} = \frac{\rho \bullet V}{\mu}$$

$$\text{Where } \rho = \frac{P_T}{R \bullet T_a} \left(\frac{T_v}{T_a}\right)^{\frac{1}{\gamma-1}} = \frac{P_T}{287.05\ T_a} \times \left(\frac{T_v}{T_a}\right)^{2.5}$$

$$\mu = 1.458 \times 10^{-6} \times \frac{T_v{}^{1.5}}{T_v + 110.4}\ \mathrm{N} \cdot \mathrm{s/m}^2$$

$$V = 20.05\ M_\infty\ (T_v)^{1/2}$$

$$M_M = \sqrt[2]{\frac{2}{\gamma-1} \cdot \left[\left(\frac{P_{t_2}}{P_\infty}\right)^{\frac{\gamma-1}{\gamma}} - 1\right]}$$

If $M_M \leq 1$, then $M_1 = M_M$

If $M_M > 1$,

then continue by iteration, a solution value for M_1 is calculated in the following equation:

$$\overline{RP_{pitot}} = \frac{(\gamma+1)\, M_1{}^2}{2} \bullet \left[\frac{M_1{}^2 \bullet (\gamma+1)^2}{4\gamma M_1{}^2 - 2\,(\gamma-1)}\right]^{\frac{1}{\gamma-1}}$$

$* \ M_1 = M_1$

$$* \frac{U_1}{U_\infty} = \frac{M_1}{M_\infty} \sqrt[2]{\frac{1 + \frac{\gamma - 1}{2} M_\infty^2}{1 + \frac{\gamma - 1}{2} M_1^2}}$$

Those two values of $\overline{{}^{R}P_{pitot}} = \frac{P_{t_2}}{P_\infty}$ and $\frac{U_1}{U_\infty}$ are to be tabulated for distance " Y " value explored in order to determine the velocity ratio profile.

7.5 Equations to Characterize the Boundary Layer

Tests were made first without boundary layer aspiration on the sting and thereafter with different aspiration intensities that were gradually increased and also with various transition strips up to obtaining a boundary layer with specified characteristics (see Section 4.0 and Appendix C). In order to characterized the boundary layer then obtained around the upstream-sting model afterbody, the following equations were used (the symbol " * " preceding a variable indicates that this variable is displayed in tabulated data):

$* \delta =$ Boundary layer total thickness = value of " Y " where U/U_∞ is equal to 0.99

$$* C_r^2 = \frac{M_\infty^2}{\frac{2}{\gamma - 1} + M_\infty^2} \equiv \text{Crocco number}$$

$$* \delta_1 = \int_0^{\delta} \left(1 - \frac{\rho_1}{\rho_\infty} \cdot \frac{U}{U_\infty}\right) \cdot \left(1 + \frac{Y}{R}\right) dy \equiv \quad (8)$$

Displacement
thickness,
compressible
flow, cylindrical
body,
See Ref. 39

$$* \delta_2 = \int_0^{\delta} \frac{\rho_1}{\rho_\infty} \cdot \frac{U}{U_\infty} \cdot \left(1 - \frac{U}{U_\infty}\right) \cdot \left(1 + \frac{Y}{R}\right) dy \equiv \quad (9)$$

Momentum
thickness,
compressible
flow, cylindrical
body,
See Ref. 39

Where:

$$\frac{\rho_1}{\rho_\infty} = \frac{1 - C_r^2}{1 - C_r^2 \left(\frac{U}{U_\infty}\right)^2}$$

$$* H = \frac{\delta_1}{\delta_2} \equiv \text{Form parameter}$$

The velocity ratio profile is expressed under the form of the following equation:

$$\frac{U}{U_\infty} = \left(\frac{Y}{\delta} \right)^{\frac{1}{n}}$$

where the value of " n " is determined by using the methodology described in Section 7.7.

The factor: $\left(1 + \frac{Y}{R}\right)$ in equations (8) and (9), takes into account the cylindrical flow where the velocity " U " at a distance " y " from the wall is associated with the volume flow which passes through a strip of width " dy ". This volume is larger by a factor: $\left(1 + \frac{Y}{R}\right)$ than that which would passe through a flat area having a width of $2\pi R$ (Ref. 39).

7.6 Algorithms Used to Determined Boundary Layer Thickness and the Velocity Profile Power Law Exponent

The boundary layer thickness " δ " is defined as the value of " Y " (vertical distance over model surface) where the velocity ratio $\frac{U}{U_\infty}$ = 0.99 (some other authors define boundary layer upper limit where $\frac{U}{U_\infty}$ = 0.95). The physical reason of such a concept is because theoretically $\frac{U}{U_\infty}$ = 1.00 where $Y = \infty$.

As mentioned over, a useful relation under the form of:

$$\frac{U}{U_\infty} = \left(\frac{y}{\delta} \right)^{\frac{1}{n}}$$

to express the velocity ratio vertical distribution within the boundary layer, and known as the power law, is generally utilized in theoretical and experimental aerodynamics.

An important distinction must be made here. It is that the concept of boundary layer thickness of $\delta = Y$ where $\frac{U}{U_\infty} = 0.99$ is not completely correlated to the power law to represent the velocity distribution mentioned over. It is to be remarked that when $Y = \delta$, the power law would give $\frac{U}{U_\infty} = 1.00$ but never 0.99. The power law is not an asymptotic relation and for values of $\frac{Y}{\delta} \geq 1.0$, it gives velocity ratios $\frac{U}{U_\infty} \geq 1.0$. Because of this behavior, the power law is invalid for " Y " values superior to " δ ".

The variables " n " and " δ " being dependant and because of the condition δ (0.99), there exist a variety of methods to approximate their values.

An easy approach to find simultaneous solution values for " n " and " δ " is by performing a linear best fit of the data converted in logarithmic form:

$$\mathrm{Ln}\frac{U}{U_\infty} = \frac{1}{n}\mathrm{Ln}Y - \frac{1}{n}\mathrm{Ln}\delta$$

$$'' \quad '' \; '' \quad ''$$

$$W = B \cdot Z + C$$

$$\text{Where: } n = \frac{1}{B} \quad \text{and } \delta = \mathrm{Ln}^{-1}(-nC)$$

It must be realized that experimental data points from the constant velocity profile located over the boundary layer upper limit (for values of Y larger than δ) introduce errors in this simultaneous solution for " n " and " δ ". It follows that best fit mentioned over must be performed with experimental data from within the boundary layer thickness " δ ". For that purpose, an interim approximated value of " δ " can be obtained by direct interpolation or by a best fit polynomial.

The algorithm that is programmed to find values of " n " and " δ " takes into account that δ (0.99) instead of δ (1.00) as advocated by the methodology described over. In a first step, an interim approximated value of the boundary layer thickness " δ'' " is to be calculated by a linear best fit of experimental data converted in a logarithmic form ($\mathrm{Ln}\frac{U}{U_\infty}$ vs LnY) and by elimination of data points related to uniform flow velocity profile (outside the boundary layer). DELTA is called the linear fit constant:

$$\delta'' = \mathrm{Ln}^{-1}(- n \cdot \mathrm{DELTA})$$

In a second step, a linear fit of data (in logarithmic form) is made to determine the value of " n " but utilizing " δ'' ":

$$\mathrm{Ln}\frac{U}{U_\infty} = \frac{1}{n}\,\mathrm{Ln}\left(\frac{Y}{\delta''}\right)$$

$$\text{where } \delta = \delta'' \cdot (0.99)^{n}$$

Values of " n " and " δ " are printed.

7.7 Algorithm Used to Calculate the Boundary Layer Displacement Thickness and Momentum Thickness

Once the boundary layer thickness and the value of the related power law exponent are calculated by one of the two equivalent methods described in Section 7.6, numerical integrations are made by using Simpson triplets non-symmetrical method. The following algorithm was programmed for that purposed:

$$C_r^2 = \frac{M_\infty^2}{\frac{2}{\gamma-1} + M_\infty^2}$$

$$\frac{\rho_1}{\rho_\infty} = \frac{1 - C_r^2}{1 - C_r^2\left(\frac{U}{U_\infty}\right)^2}$$

$$\Delta 1 = \left(1 - \frac{\rho_1}{\rho_\infty} \bullet \frac{U}{U_\infty}\right) \bullet \left(1 + \frac{Y}{R}\right)$$

$$\Delta 2 = \frac{\rho_1}{\rho_\infty} \bullet \frac{U}{U_\infty} \bullet \left(1 - \frac{U}{U_\infty}\right) \bullet \left(1 + \frac{Y}{R}\right)$$

Where values of " $\Delta 1$ " and " $\Delta 2$ " have to be calculated for each value of " Y ".

At this step in the programme, the parameters used to calculate the equations of Simpson triplets non-symmetrical method is built up. In order to get an integral from " 0 " to " δ ", the first row had to be initialized, i.e $U = 0$ for $Y = 0$, $\Delta 1 = 1.0$ for $Y = 0$,
$\Delta 2 = 0.0$ for $Y = 0$:

Y height over model surface at which measurements where made within the boundary layer	Δ1	Δ2
Y=0 = a1 i.e at the model surface	Δ1(a1) = 1.0	Δ2(a1) = 0.0
b1=Y= height of first measurement, since no measurement are to be made at the model surface	Δ1(b1) = value of Δ1 at Y= b1 multiplied by b1	Δ2(b1)= value of Δ2 at Y= b1 multiplied by b1
c1 = a2 = Y = height of second measurement (third point)	Δ1(c1) = Δ1(a2)= value of Δ1 at Y= c1 multiplied by c1	Δ2(c1) = Δ2(a2)
b2 = Y = height of third measurement	Δ1(b2) = value of Δ1 at Y= b2 multiplied by b1	Δ2(b2)
c2= Y = height of fourth measurement	Δ1(c2)	Δ2(c2)
ci= Y = height of ith measurement	Δ1(ci)	Δ2(ci)

For $Y = \delta$, then $U/U_\infty = 0.99$

Points are taken 3 by 3 at a time in a Simpson triplets non-symmetrical method. Thereafter, partial integral values are summed together. Borders of triplets had to be adjacent (c1 = a2) and the following equations are used:

$$\delta_1 = \int_0^\delta \Delta 1 dy = \sum_{i=1}^{n} \Delta 1(ai)\left[\frac{(ai - ci)^2}{6(ai - bi)} - \frac{(ai - ci)}{2}\right] - \dots$$

$$\dots - \Delta 1(bi)\left[\frac{(ci - ai)^3}{6(bi - ai)(bi - ci)}\right] + \Delta 1(ci)\left[\frac{(ai - ci)^2}{6(bi - ci)} - \frac{(ai - ci)}{2}\right]$$

$$\delta_2 = \int_0^{\delta} \Delta 2 dy = \sum_{i=1}^{n} \Delta 2(ai) \left[\frac{(ai - ci)^2}{6(ai - bi)} - \frac{(ai - ci)}{2} \right] - \ldots$$

$$\ldots - \Delta 2(bi) \left[\frac{(ci - ai)^3}{6(bi - ai)(bi - ci)} \right] + \Delta 2(ci) \left[\frac{(ai - ci)^2}{6(bi - ci)} - \frac{(ai - ci)}{2} \right]$$

As a cross-check, values for boundary layer displacement thickness and momentum thickness are to be compared with figures obtained by using simple trapezoidal integration methods (see Section 9.1 and Appendix D).

8.0 TREATMENT OF DATA - BASE PRESSURE DISTRIBUTION

The following equations were used to process wind tunnel data on:

- Base pressure distribution used for upstream sting alignment,
- base pressure exploration survey with respect to boundary layer characteristics

The symbol " * " preceding a variable indicates that this variable is displayed in tabulated data.

The true static pressure of each pressure tap was obtained by using the following equations:

$* \dfrac{P_{ij\ \mathrm{TRUE}}}{P_\infty} =$ Pressure ratio for the j^{th} pressure tap at the time of the i^{th} reading, displayed in tabulated data for each 0.1 sec. between 3.5 to 6.0 sec. run time.

The true static pressure of each pressure tap was obtained by using the following equation:

$$P_{ij} = P_{\mathrm{ith\ reading,\ TAP1...32j\ TRUE}} = \ldots$$

$$\ldots \underset{\text{(as read)}}{P_{\mathrm{TAP1...32j}}} + \underset{\text{(as read by absolute pressure sensor)}}{P_{\mathrm{ref}}}$$

The value of P_∞ was obtained from an absolute pressure sensor:

$$* P_\infty = P_{8_i} = P_{\mathrm{average\ from\ wall\ tap\ no:\ 7\ and\ 8,\ ith\ reading}}$$

$* \overline{R_{PRij}} = \sum_{i=1}^{n} \frac{P_{ij\ TRUE}}{P_\infty}$ Average pressure ratio for the j^{th} pressure tap for all readings between 3.5 and 6.0 sec run time

$$M_i = \left[\left(\left(\frac{P_{t_i}}{P_{s_i}}\right)^{\frac{\gamma-1}{\gamma}} -1\right)\frac{2}{\gamma-1}\right]^{1/2}$$

$$Q_i = \frac{\gamma}{2} \cdot M_i^2 \cdot P_{s_i}$$

$* \overline{M} = \frac{1}{n}\sum_{i=1}^{n} M_i$ between 3.5 to 6.0 sec. run time

$P_T = \frac{1}{n}\sum_{i=1}^{n} P_{t_i}$ = average air bag pressure (total pressure) between 3.5 to 6.0 sec. run time

$* \overline{Q} = \frac{1}{n}\sum_{i=1}^{n} Q_i$ between 3.5 to 6.0 sec. run time

$$T_a = 273.15 + t_c$$

$$T_v = T_a\left(1 + \frac{\gamma-1}{2} \cdot M_a^2\right)^{-1}$$

$$* \text{REY/M} = \frac{\rho \bullet V}{\mu}$$

Where $\rho = \frac{P_T}{R \bullet T_a}\left(\frac{T_v}{T_a}\right)^{\frac{1}{\gamma-1}} = \frac{P_T}{287.05\ T_a} \times \left(\frac{T_v}{T_a}\right)^{2.5}$

$$\mu = 1.458 \times 10^{-6} \times \frac{T_v^{1.5}}{T_v + 110.4}\ \text{N} \cdot \text{s/m}^2$$

$$V = 20.05\ M\ (T_v)^{1/2}$$

9.0 RESULTS

Typical result output formats are presented in this section. Complete data can be made available through the author upon request. A list of wind tunnel runs is presented in Appendix A that also gives the correspondence between the tunnel run numbers (i.e. R3843, etc...) and test conditions, the model configurations and summary of results.

9.1 Boundary Layer Characterization Tests

Boundary layer characterization tests results consisted of pressure ratios P/P_∞ from pitot tube and the unique model pressure tap (and their average values and standard deviations) displayed in table form for each 0.1 sec of time interval and between a time frame of approximately 3.5 to 6.0 sec with respect to butterfly valve opening. Their averages corresponded to the time interval where pressure measurements were stabilized in test section during a run. One table was produced for each individual run. Location of pitot probe inlet with respect to model base (X/D or x/d) was indicated although it was kept constant at 1.7486 D. Also, data tables bore the radial distance Y in inch and relative distance Y/R of the pitot inlet centreline from the model surface, the boundary layer velocity ratios U/U_∞ and corresponding Mach numbers encountered inside boundary layer (Mbl = Mach boundary layer).

An example of experimental data table layout is given in Figs 63 and 64 where are indicated headings describing experimental conditions. They consisted of the same parameters as for the case of the pressure distribution tests at the surface of the model base/afterbody (see section 9.2). Afterwards, δ, δ_1, δ_2, H and the value of " n " were calculated. The complete set of boundary layer data is presented in Appendix D.

9.2 Surface Pressure Distribution Tests

The base pressure distribution tests results consisted of pressure ratios P/P_∞ (associated to each pressure tap) displayed in table form for each 0.1 sec of time interval and between a time frame of approximately 3.5 to 6.0 sec with respect to butterfly valve opening. One table was produced for each individual run. Also, the average values of pressure ratios corresponding to each pressure tap were calculated, tabulated and plotted with respect to X/D, Y/D (or x/d, y/d). Their average value corresponds to the pressure averaged over the time interval where pressure measurements were stabilized.

One example of pressure tests table layout is given in Figs. 65 and 66. The heading of Fig. 65 displays the experimental conditions. M(mean) stands for Mean Mach number and was calculated between time interval where pressure measurements were stabilized. The test section static pressure was dependent on the Mean Mach number which affected the reduced values of pressure coefficients printed in table form. The pressure taps reference plane roll angle is indicated as MODEL INDEX. $P_\infty = P_V$ is indicated as P STAT.

Figures 67 to 71 present a typical example of the data graphical representation adopted. It is to be noted that the vertical and horizontal pressure taps data was plotted symmetrically, one over the other, in order to verify the upstream sting alignment with respect to the flow. Figure 68 shows a single line curve reproducing the one of Fig. 67, which indicates a perfect sting alignment. Figure 70 shows a double line curve making a " X ", indicating a small alignment error but still acceptable. Also, pertinent notes were added about transition strips, boundary layer aspiration valve settings and aspiration sections in use.

Figures 72 to 74 present typical examples of the data graphical representation adopted for tests with the afterbody surface pressure model and the finned afterbody model used for the between fins pressure survey, the fin trailing edges and base pressure survey.

For those special cases where a run had to be repeated, the two corresponding pressure ratios curves and sets of data points were presented on the same graph. A summary of results is given in Appendix E.

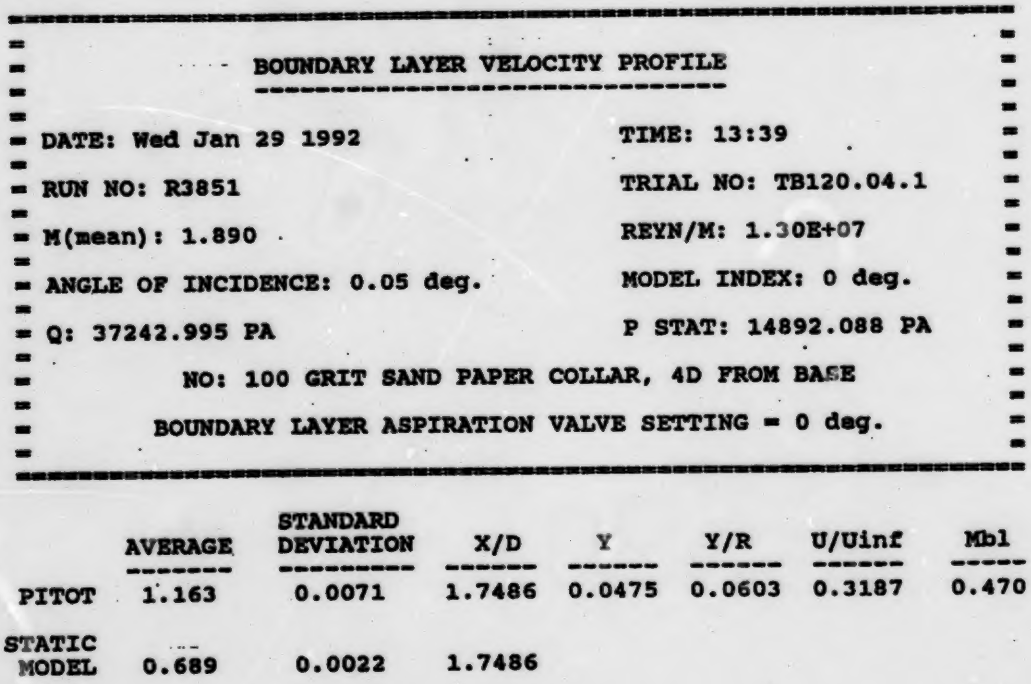

```
===========================================================================
=                                                                         =
=               BOUNDARY LAYER VELOCITY PROFILE                          =
=               -------------------------------                          =
=                                                                         =
= DATE: Wed Jan 29 1992                      TIME: 13:39                  =
=                                                                         =
= RUN NO: R3851                              TRIAL NO: TB120.04.1         =
=                                                                         =
= M(mean): 1.890                             REYN/M: 1.30E+07             =
=                                                                         =
= ANGLE OF INCIDENCE: 0.05 deg.              MODEL INDEX: 0 deg.          =
=                                                                         =
= Q: 37242.995 PA                            P STAT: 14892.088 PA         =
=                                                                         =
=          NO: 100 GRIT SAND PAPER COLLAR, 4D FROM BASE                   =
=                                                                         =
=       BOUNDARY LAYER ASPIRATION VALVE SETTING = 0 deg.                  =
=                                                                         =
===========================================================================

                      STANDARD
           AVERAGE    DEVIATION    X/D      Y        Y/R      U/Uinf    Mbl
           -------    ---------   ------  ------   ------   ------    -----
 PITOT      1.163      0.0071     1.7486  0.0475   0.0603   0.3187    0.470

STATIC
 MODEL      0.689      0.0022     1.7486
```

FIGURE 63 - Example of data table layout for boundary layer characterization tests (averages values)

RUN NO: R3851

PRESSURE RATIO (Pport/Pstat)

TIME	PORT1	PORT2
0.000	1.155	0.687
0.100	1.171	0.690
0.200	1.165	0.690
0.300	1.166	0.690
0.400	1.170	0.690
0.500	1.169	0.691
0.600	1.173	0.692
0.700	1.169	0.691
0.800	1.154	0.688
0.900	1.162	0.689
1.000	1.172	0.692
1.100	1.169	0.691
1.200	1.159	0.688
1.300	1.164	0.689
1.400	1.164	0.690
1.500	1.167	0.690
1.600	1.177	0.693
1.700	1.154	0.687
1.800	1.172	0.689
1.900	1.172	0.692
2.000	1.154	0.685
2.100	1.154	0.685
2.200	1.164	0.688
2.300	1.165	0.690
2.400	1.175	0.691
2.500	1.164	0.688
2.600	1.151	0.684
2.700	1.154	0.685
2.800	1.160	0.686
2.900	1.156	0.686
3.000	1.151	0.686
3.100	1.160	0.688
3.200	1.161	0.687
3.300	1.156	0.687
3.400	1.166	0.689
3.500	1.169	0.691
3.600	1.167	0.689
3.700	1.175	0.693
3.800	1.159	0.686
3.900	1.162	0.688
4.000	1.149	0.684
4.100	1.161	0.687
4.200	1.174	0.690
4.300	1.155	0.687
4.400	1.160	0.687
4.500	1.163	0.689
4.600	1.169	0.689
4.700	1.166	0.689
4.800	1.165	0.690
4.900	1.165	0.689
AVERAGE	1.163	0.689

FIGURE 64 - Example of data table layout for boundary layer characterization tests (measurements values)

```
-                                                                     -
-             AFTER BODY SURFACE PRESSURE MODEL                       -
-             ---------------------------------                       -
-                                                                     -
- DATE: Fri Feb 07 1992                    TIME: 14:51                -
-                                                                     -
- RUN NO: R3889                            TRIAL NO: P320.7           -
-                                                                     -
- M(mean): 2.002                           REYN/M: 1.20E+07           -
-                                                                     -
- ANGLE OF INCIDENCE: 0.05 deg.            MODEL INDEX: 0 deg.        -
-                                                                     -
- Q: 34953.976 PA                          P STAT: 12458.179 PA       -
-                                                                     -
-            NO: 100 GRIT SAND PAPER COLLAR, 4D FROM BASE             -
-        BOUNDARY LAYER ASPIRATION VALVE SETTING = 90 deg.            -
-              AFTERBODY ASPIRATION SECTION ONLY                      -

                               STANDARD
                  AVERAGE      DEVIATION        X/D
                  -------      ---------        ---
        TAP 1      0.655        0.0019
        TAP 2      0.978        0.0005         0.0349
        TAP 3      1.007        0.0003         0.1460
        TAP 4      1.008        0.0003         0.2571
        TAP 5      1.012        0.0003         0.3683
        TAP 6      1.009        0.0003         0.4794
        TAP 7      1.009        0.0003         0.5905
        TAP 8      1.007        0.0003         0.7016
        TAP 9      1.005        0.0003         0.8127
        TAP10      1.006        0.0002         0.9238
        TAP11      1.006        0.0002         1.0349
        TAP12      1.008        0.0002         1.1460
        TAP13      1.011        0.0002         1.2571
        TAP14      1.008        0.0002         1.3683
        TAP15      1.010        0.0002         1.4794
        TAP16      1.006        0.0002         1.5905
        TAP17      1.001        0.0002         1.7016
        TAP18      1.002        0.0002         1.8127
        TAP19      0.998        0.0002         1.9238
        TAP20      0.999        0.0002         2.0349
        TAP21      0.973        0.0018         2.1460
        TAP22      0.998        0.0002         2.2571
        TAP23      0.943        0.0033         2.3683
        TAP24      0.996        0.0002         2.4794
        TAP25      1.006        0.0002         2.5905
        TAP26      1.000        0.0002         2.7016
        TAP27      1.007        0.0003         2.8127
        TAP28      1.009        0.0003         2.9238
        TAP29      1.010        0.0003         3.0349
        TAP30      1.010        0.0003         3.1460
        TAP31      1.008        0.0003         3.2571
        TAP32      1.007        0.0004         3.3683
```

FIGURE 65 - Example of data table layout for pressure distribution tests (averages values)

```
                              RUN NO: R3889
                              -------------
                        PRESSURE RATIO (Ptap/Pstat)
                        ---------------------------
   TIME    TAP1    TAP2    TAP3    TAP4    TAP5    TAP6    TAP7    TAP8
  0.000   0.654   0.975   1.005   1.007   1.011   1.007   1.008   1.006
  0.100   0.654   0.977   1.006   1.008   1.012   1.008   1.008   1.006
  0.200   0.654   0.977   1.006   1.008   1.012   1.008   1.009   1.007
  0.300   0.654   0.978   1.007   1.008   1.013   1.009   1.009   1.007
  0.400   0.654   0.977   1.007   1.008   1.013   1.009   1.009   1.007
  0.500   0.654   0.978   1.007   1.009   1.013   1.009   1.009   1.007
  0.600   0.654   0.977   1.006   1.008   1.012   1.009   1.009   1.007
  0.700   0.654   0.977   1.006   1.008   1.012   1.009   1.009   1.007
  0.800   0.654   0.977   1.006   1.008   1.012   1.009   1.009   1.007
  0.900   0.655   0.978   1.006   1.008   1.012   1.009   1.009   1.007
  1.000   0.657   0.978   1.006   1.008   1.012   1.008   1.009   1.007
  1.100   0.658   0.978   1.007   1.008   1.013   1.009   1.009   1.007
  1.200   0.658   0.978   1.007   1.008   1.012   1.008   1.008   1.007
  1.300   0.658   0.977   1.007   1.008   1.012   1.009   1.009   1.007
  1.400   0.657   0.977   1.007   1.008   1.013   1.009   1.009   1.007
  1.500   0.654   0.977   1.007   1.009   1.013   1.009   1.010   1.008
  1.600   0.653   0.978   1.007   1.009   1.013   1.009   1.009   1.007
  1.700   0.654   0.977   1.007   1.008   1.012   1.009   1.009   1.007
  1.800   0.653   0.978   1.007   1.008   1.012   1.008   1.009   1.007
  1.900   0.655   0.979   1.007   1.008   1.012   1.009   1.009   1.007
  2.000   0.658   0.978   1.006   1.008   1.012   1.009   1.009   1.007
  2.100   0.658   0.978   1.007   1.008   1.013   1.009   1.009   1.007
  2.200   0.658   0.978   1.006   1.008   1.012   1.009   1.009   1.007
  2.300   0.656   0.978   1.007   1.008   1.013   1.009   1.009   1.007
  2.400   0.655   0.978   1.007   1.008   1.013   1.009   1.009   1.007
  2.500   0.655   0.978   1.007   1.008   1.012   1.009   1.009   1.007
  2.600   0.655   0.978   1.007   1.008   1.012   1.009   1.009   1.007
  2.700   0.654   0.977   1.007   1.009   1.013   1.009   1.009   1.007
  2.800   0.654   0.978   1.006   1.008   1.012   1.009   1.009   1.007
  2.900   0.653   0.978   1.007   1.009   1.013   1.009   1.009   1.007
  3.000   0.655   0.978   1.007   1.008   1.012   1.009   1.009   1.007
  3.100   0.655   0.978   1.006   1.008   1.012   1.009   1.009   1.007
  3.200   0.654   0.978   1.007   1.008   1.012   1.009   1.009   1.007
  3.300   0.653   0.978   1.007   1.008   1.012   1.009   1.009   1.007
  3.400   0.655   0.978   1.007   1.008   1.013   1.009   1.009   1.007
  3.500   0.655   0.978   1.007   1.008   1.013   1.009   1.009   1.007
  3.600   0.658   0.978   1.007   1.008   1.013   1.009   1.009   1.007
  3.700   0.659   0.978   1.007   1.009   1.013   1.009   1.009   1.007
  3.800   0.659   0.978   1.007   1.008   1.012   1.009   1.009   1.007
  3.900   0.658   0.978   1.006   1.008   1.012   1.009   1.009   1.007
  4.000   0.656   0.978   1.006   1.008   1.012   1.009   1.009   1.007
  4.100   0.655   0.977   1.006   1.008   1.012   1.009   1.009   1.007
  4.200   0.654   0.977   1.006   1.008   1.013   1.009   1.009   1.007
  4.300   0.655   0.978   1.006   1.008   1.013   1.009   1.009   1.007
  4.400   0.655   0.978   1.007   1.008   1.013   1.009   1.009   1.007
  4.500   0.652   0.978   1.007   1.008   1.012   1.009   1.009   1.007
  4.600   0.654   0.977   1.007   1.008   1.012   1.009   1.009   1.007
  4.700   0.656   0.978   1.006   1.008   1.012   1.008   1.008   1.006
  4.800   0.659   0.978   1.007   1.008   1.012   1.008   1.008   1.006
  4.900   0.657   0.978   1.006   1.008   1.012   1.008   1.008   1.007

AVERAGE   0.655   0.978   1.007   1.008   1.012   1.009   1.009   1.007
```

FIGURE 66 - Example of data table layout for pressure distribution tests (measurement values)

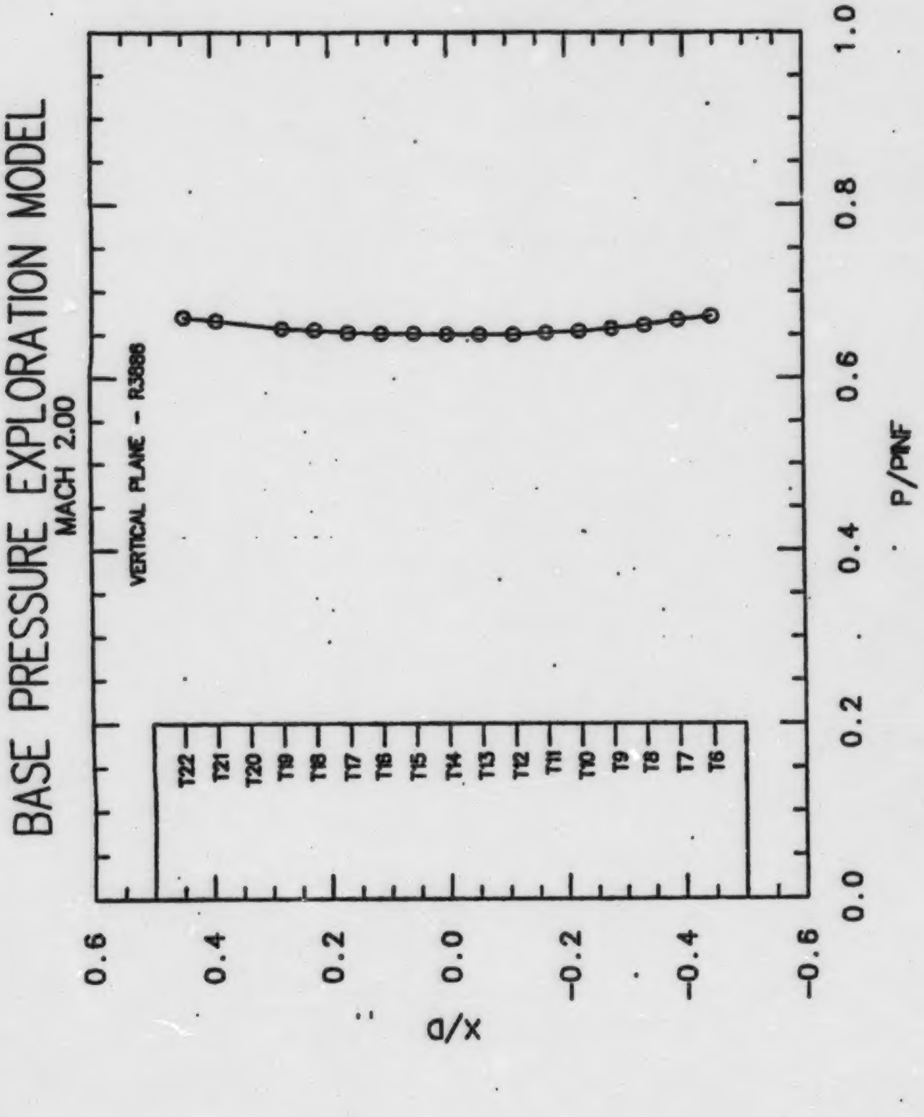

FIGURE 67 - Example of surface pressure ratio distribution graphical layout, Base Pressure Exploration Model

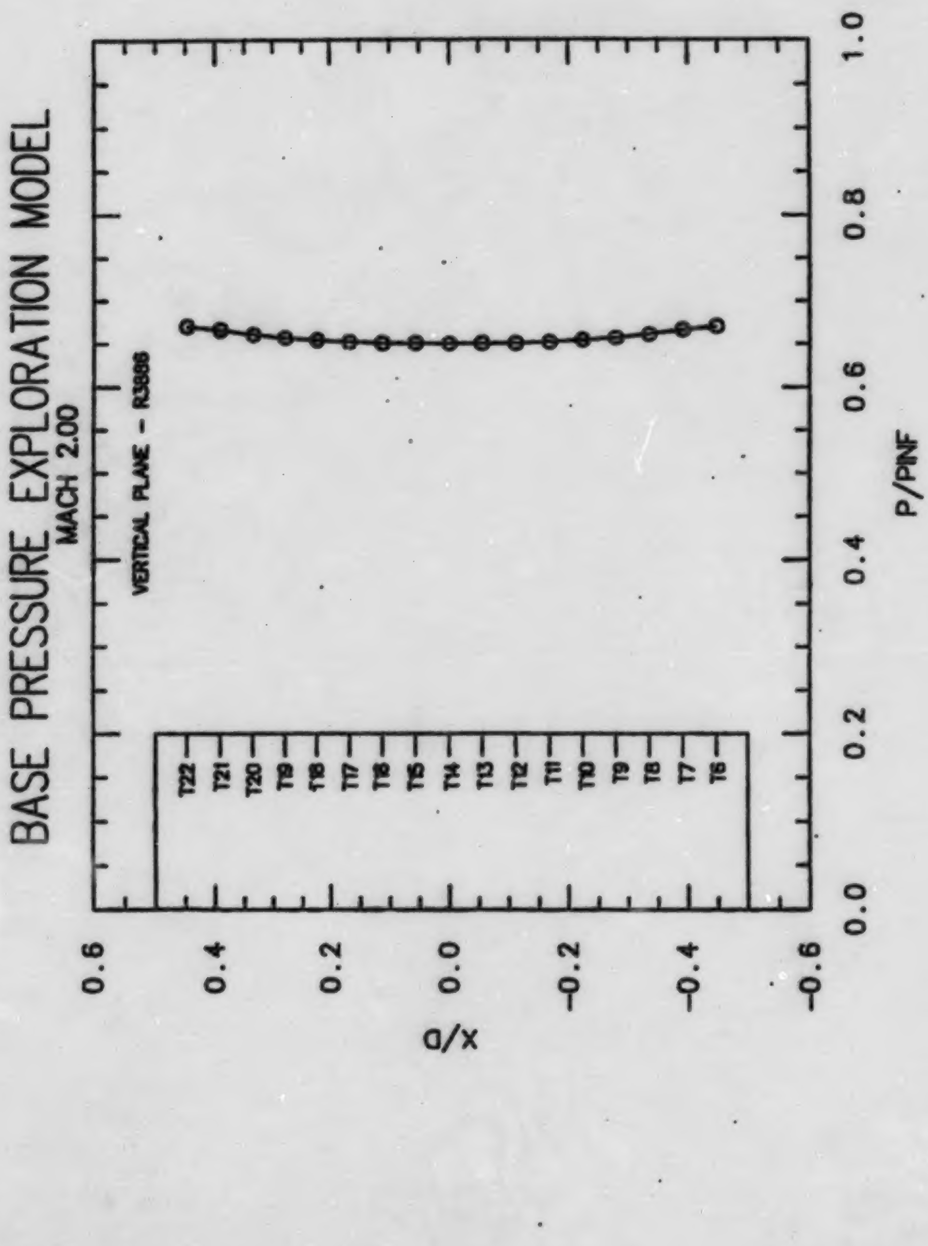

FIGURE 68 - Example of surface pressure ratio distribution graphical layout, Base Pressure Exploration Model, symmetrical plot to verify upstream sting alignment

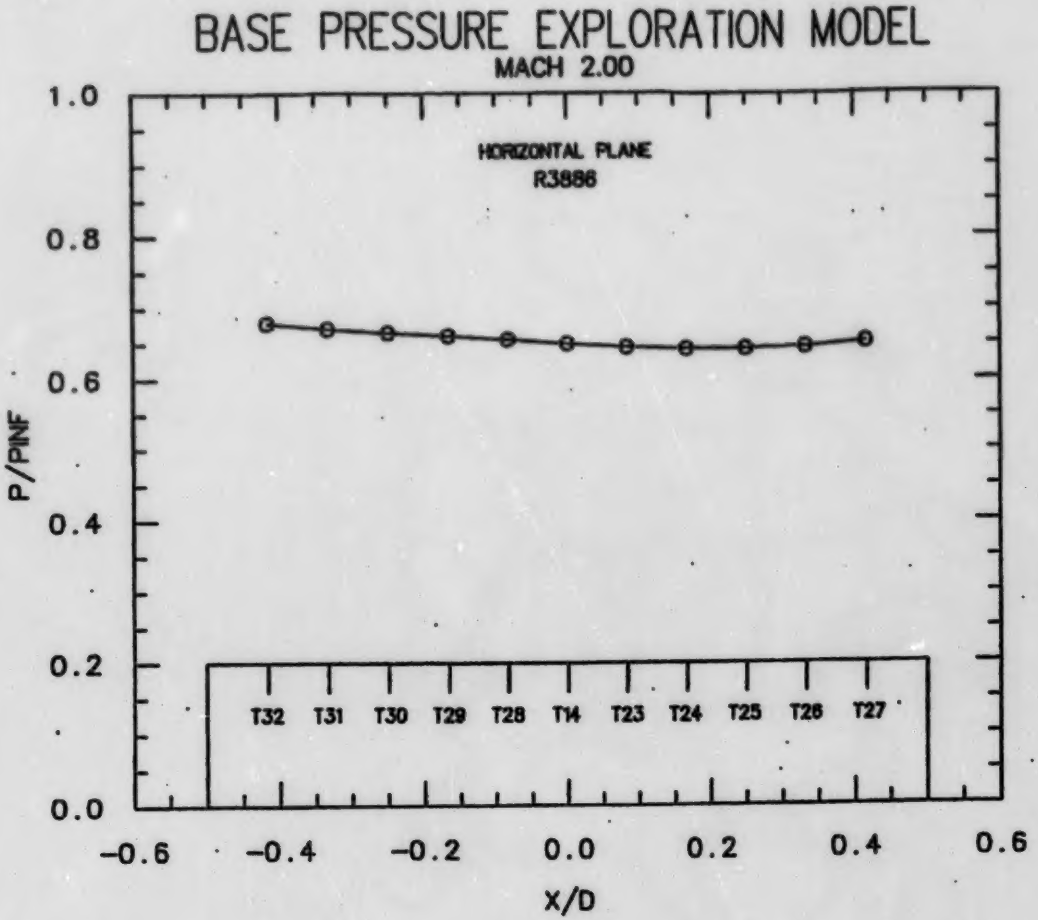

FIGURE 69 - Example of surface pressure ratio distribution graphical layout, Base Pressure Exploration Model

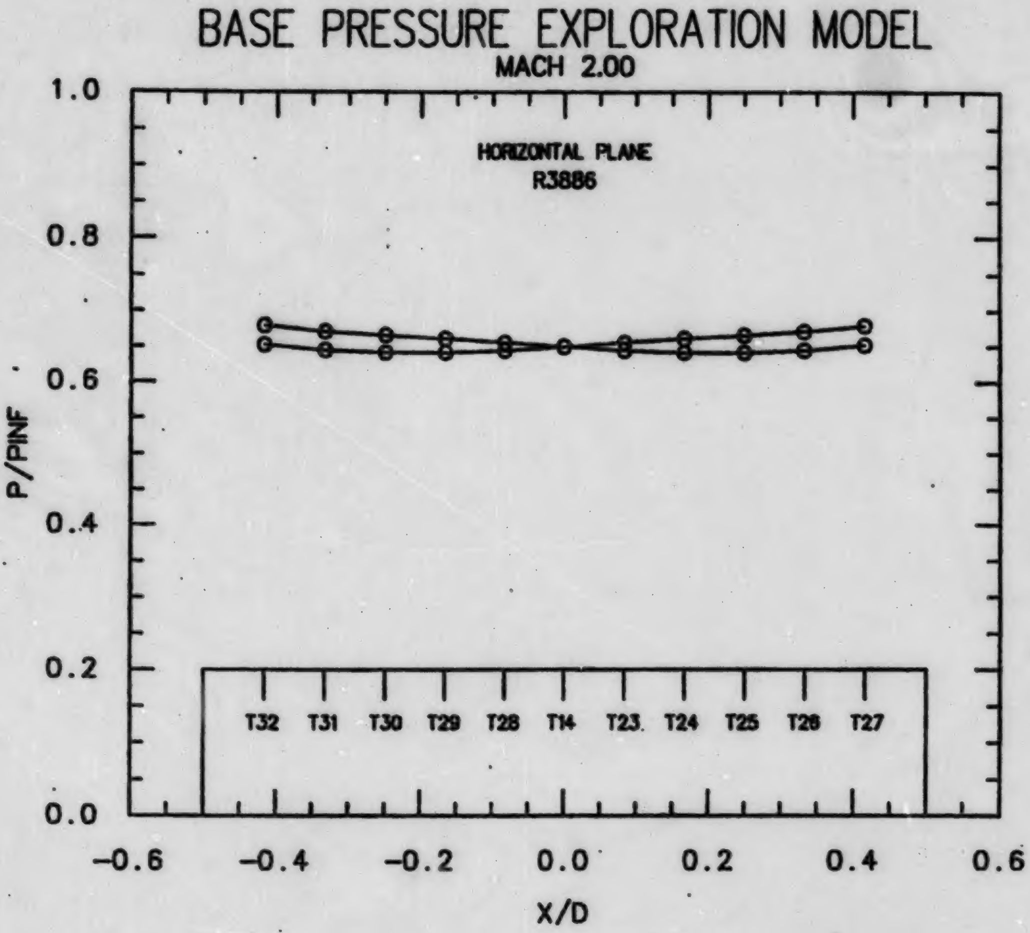

FIGURE 70 - Example of surface pressure ratio distribution graphical layout, Base Pressure Exploration Model, symmetrical plot to verify upstream sting alignment

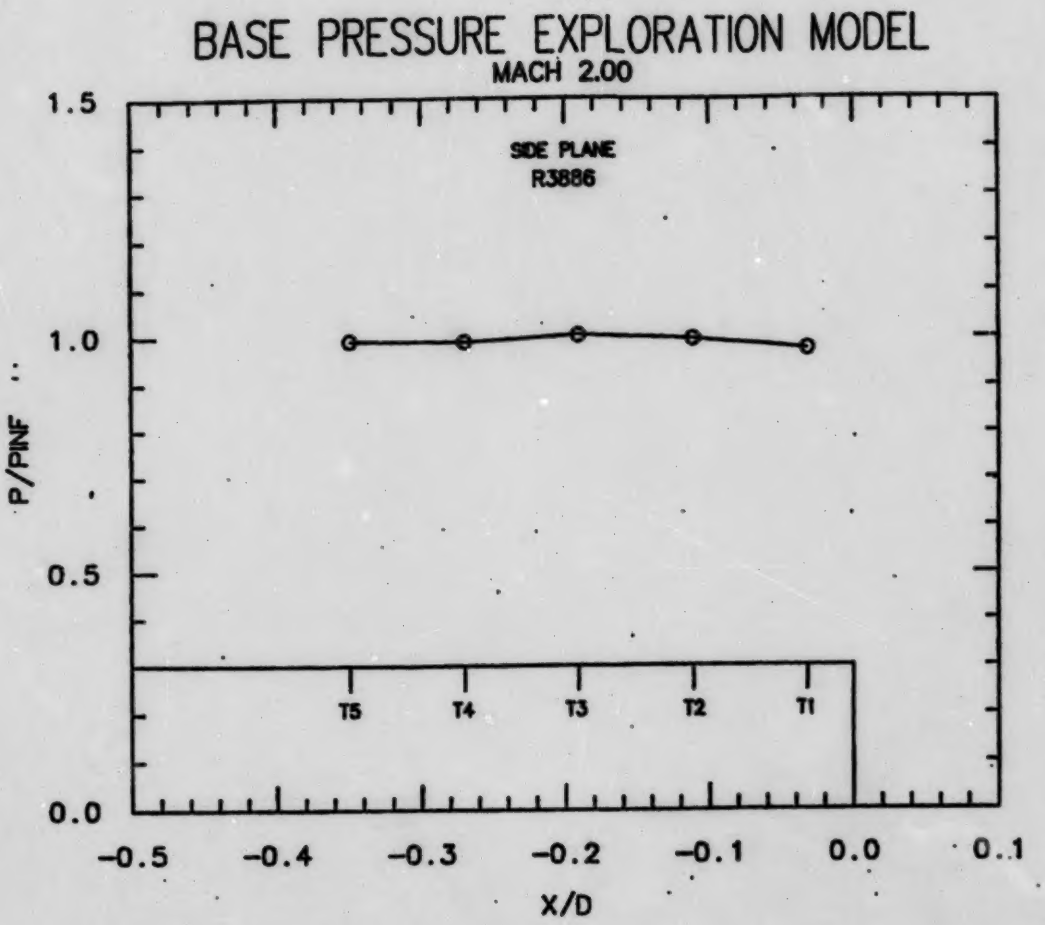

FIGURE 71 - Example of surface pressure ratio distribution graphical layout, Base Pressure Exploration Model

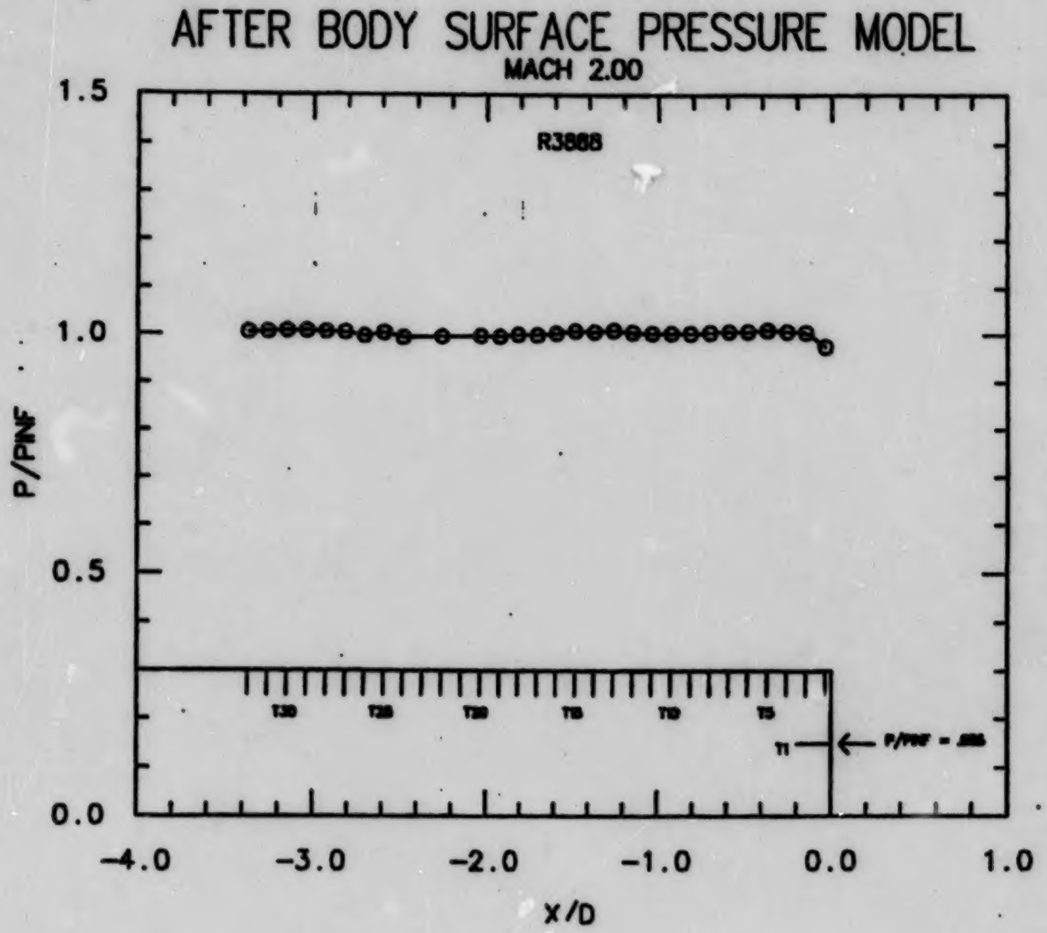

FIGURE 72 - Example of surface pressure ratio distribution graphical layout, Afterbody Surface Pressure Model

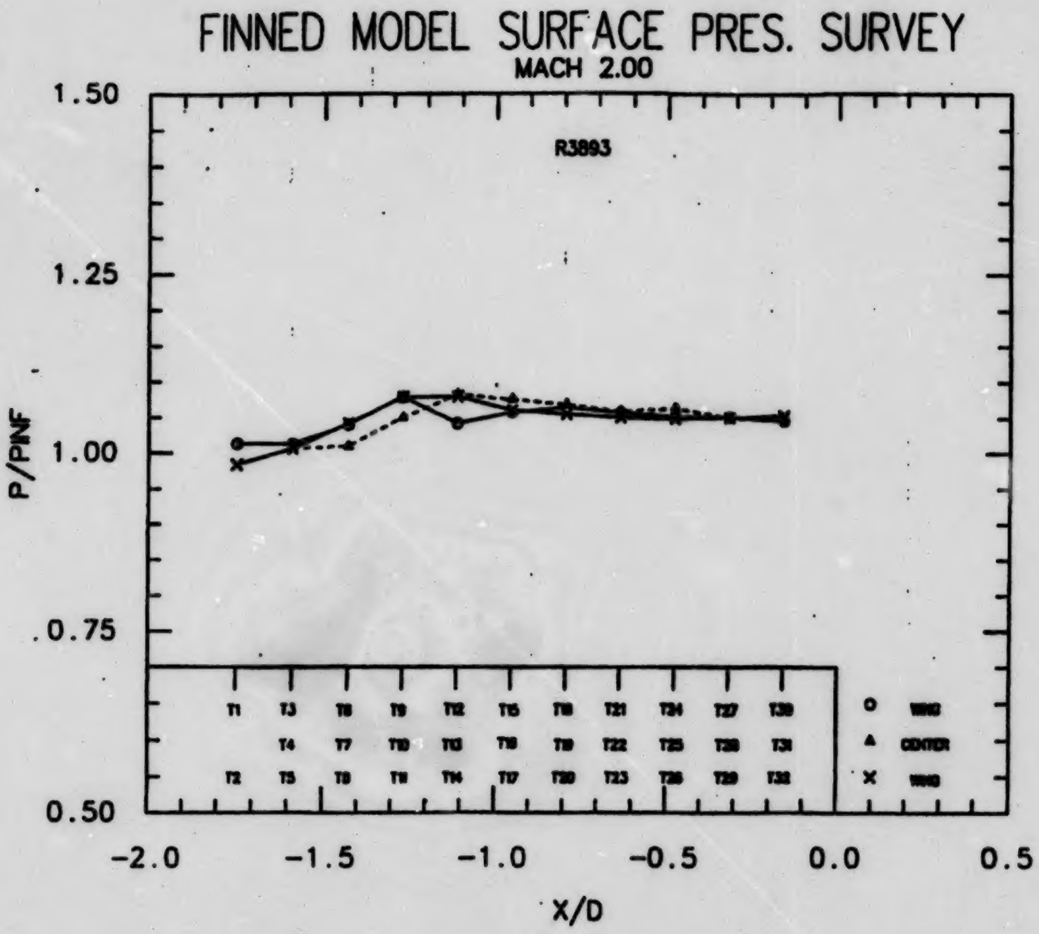

FIGURE 73 - Example of surface pressure ratio distribution graphical layout, Finned Afterbody Model, between fins pressure survey

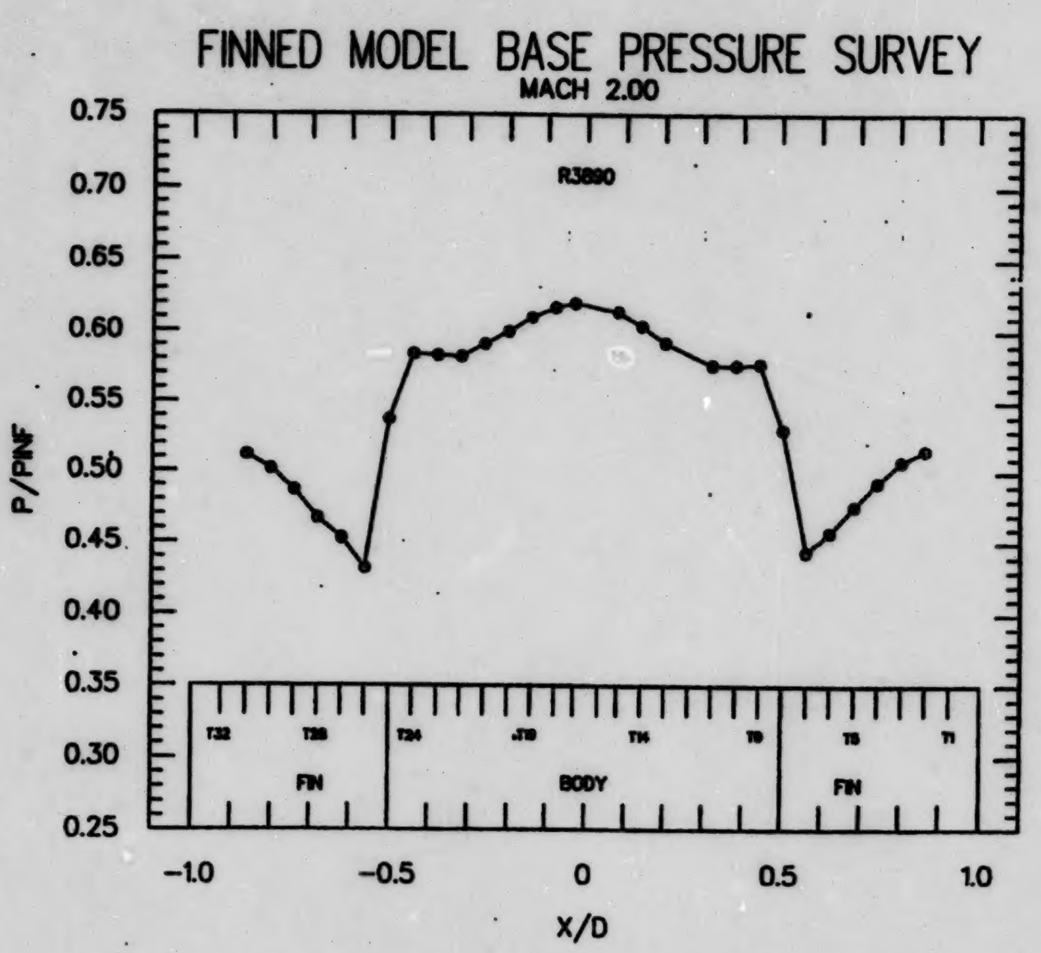

FIGURE 74 - Example of surface pressure ratio distribution graphical layout, Finned Afterbody Model, fins and base pressure survey

10.0 BOUNDARY LAYER CHARACTERIZATION AND PRESSURE DISTRIBUTION MEASUREMENT ERRORS

This section attempts to determine the run-to-run repeatability or " precision " of measurements made in present test series. Results are under the form of ratios " P_{tap}/P_∞ ". Measurement errors can be split in two sources:

a - Systematic Error which represents results dispersion introduced all along the chain of instrumentation elements or modules. This error is usually repetitive and its variance quantitatively known in advance.

b - Residual Error which represents results dispersion that could not be explained by behavior of measurement instrumentation. Small variations of test conditions (from mechanical sources or atmospheric fluctuations) or the aerodynamic phenomena natural instability are the cause of the difference between overall measurement errors and systematic errors.

The residual error and systematic error combine together to produce the measurement total error which is observed while compiling results. The standard deviation of measurement total error is related to the residual error and systematic error standard deviations as the following:

$$\text{Measurement total error} = \sqrt[2]{(\text{Residual error})^2+(\text{Systematic error})^2}$$

As experimental measurements are concerned, the concept of " precision " is related to the probable difference between result values that were measured during one test run and the average values that would have been obtained after repeating the same run for a large number of times. It is not possible to determine the " absolute accuracy " as true values are not known for free flight conditions as well as for idealized wind tunnel test conditions. There are inaccurate flow parameters which are inherent to the wind tunnel test section, like Mach number and Reynolds number, that result in a different environment than atmospheric flight conditions.

Also, the test section flow angularity combined with incorrect angles of attack (pitch and yaw) themselves induced by misalignment between component fixations within the model/sting support combination system, are other sources of measurement errors.

In order to evaluate data dispersion due to variations in the measurement systems, several runs should have been repeated (for a minimum of three times) for the same test conditions. Since such a procedure was not applied in present test series, to the exception of fin trailing edge and base pressure survey (model no. 5), tests results from repeated runs preformed after the completion of present test series were used to extrapolate the measurement test error. These runs were made in very similar tests conditions (i.e. Mach 2.0, similar boundary layer, same models).

The statistical methodology to evaluate aerodynamic coefficient and pressure distribution measurement errors is presented in Appendix F. Although some typical test runs were repeated several times in order to investigate result dispersion, statistical analysis provided result interval limits (confidence level of 95.0%), related to the case of a single individual test run. This data, which is presented in Tables III to V, is expressed in percentage of experimental values. The interval limits are defined as the upper and lower values of results that correspond to the specified level of confidence. Their values were calculated as per the methodology described in Appendix H.

Tables III and IV shows that the fin trailing edge and the base pressure distribution tests provided results with a similar level of precision. Although the model base/afterbody was aligned by the method described in Appendix B, there was no way to compensate for pitch and yaw model angular alteration that could supervene during model disassembly/re-assembly cycle. Base pressure measurements were therefore affected by some model residual misalignments, the magnitude being dependant on the relative position of each individual pressure tap.

Statistical results presented in TABLE V show that the velocity ratio U/U_{inf} was within ± 3.5% for a level of confidence of 95%. This is not bad at all when considering that the velocity ratio

U/U_{inf} is the result of elaborate calculations involving measurements of the test section static pressure, the pitot tube total pressure and the model surface static pressure at the location of the pitot tube.

Because two test runs were made for several test conditions, average values determined from data results are of a higher precision than for the case of a single test run as calculated in Appendix F. Table VI presents a compilation of the predicted measurement errors for the averaged values. The methodology, which is explained in Appendix F, consists in transforming the average values of interval limits related to a single run.

TABLE III
Base Pressure Distribution Test Error

(Results are expressed in % of measured values)
(Level of confidence of 95.0%)

MACH NUMBER Mach number total error single run case	TAP no:1 Base center tap pressure ratio P_{tap}/P_∞ single run case
2.001 ±0.384%	±2.691%

TABLE IV
Fin Trailing Edge and Base Pressure Distribution Test Error

(Results are expressed in % of measured values)
(Level of confidence of 95.0%)

Mach NUMBER	TAP no:2 pressure ratio P_{tap}/P_∞	TAP no:9 pressure ratio P_{tap}/P_∞	TAP no:17 pressure ratio P_{tap}/P_∞	TAP no:24 pressure ratio P_{tap}/P_∞	TAP no:31 pressure ratio P_{tap}/P_∞
1.999 0.542% single run case	3.76%	4.52%	2.44%	1.54%	3.40%
0.313% average of 3 test runs	2.17%	2.61%	1.41%	0.889%	1.96%

TABLE V
Boundary Layer Velocity Profile Test Error

At the height where Y/R = .1365

(Results are expressed in % of measured values)
(Level of confidence of 95.0%)

MACH NUMBER Mach number total error	U/U_{inf} Velocity ratio	LnU/U_{inf}	MBL Mach number inside boundary layer
2.005 ±0.916%	±3.481%	±7.822%	±2.647%

TABLE VI

Compilation of Pressure Measurement Test Error

On the values of averaged data results from repeated runs

TEST ERROR ON SURFACE PRESSURE COEFFICIENT, LEVEL OF CONFIDENCE OF 95%	
Base afterbody model designation	% ERROR Number of runs
Model no. 2 - BASE PRESSURE EXPLORATION MODEL	±1.90% 2
Model no. 3 - AFTER-BODY SURFACE PRESSURE MODEL	±1.90% 2
Model no. 4 - FINNED AFTER-BODY MODEL, BETWEEN FINS PRESSURE SURVEY	±1.90% 2
Model no. 5 - FINNED AFTER-BODY MODEL, FINS AND BASE PRESSURE SURVEY	±1.81% 3

11.0 DISCUSSIONS

These test series were made to provide complementary results to a data bank in support to a cooperative programme between DREV and ISL, rather than with the objective of identifying a specific aerodynamic phenomenon.

ISL has a recognized expertise in laser anemometry and in surface pressure distribution measurement in their 0.2 m x 0.2 m blow down facility at high Reynolds numbers (high pressure reservoir that blow through test section, down to atmospheric pressure). DREV, for its part, has many years of expertise with aerodynamic coefficient measurement through the use of wind tunnel balances and also in pressure distribution measurement at low Reynolds numbers (that are 20 times lower than in ISL facility) in its 0.6 m x 0.6 m indraft wind tunnel (atmospheric air that blow through test section, down to a vacuum reservoir).

Results obtained from the present test series are also intended to form a basis of comparison for computational fluid dynamics (CFD) studies made at DREV on projectile base flow. The challenge for this comparison is enhanced by the complexity of base flow recirculating phenomena. The numerical simulations shall take into account the specific conditions encountered in the DREV wind tunnel facility. Although the real projectile could fly at different Mach numbers, if the computation Mach number can be compatible with that of the wind tunnel experiment, comparison between CFD and experiment can be meaningful. This aspect shall be covered in a separate publication by the project scientific authority.

During this tests series, the behavior of the base pressure was one of the subjects of interest. The results obtained (finned and finless models) were compared (Fig. 75) to other experimental data on the base pressure ratio for a flat base configuration (Ref. 11). The base pressure ratios that were obtained in the Phase I of the project are also plotted (Ref. 8) in Fig. 75. In that case, the model was held in the test section by a sting support which induced interference on the base flow and affected the base pressure measurements.

One primordial objective of the upstream sting support concept was to provide a mean to measure the base pressure without the interference of a standard sting holder. It can be observed from Fig. 75 that for tests at Mach 2.0, the base pressure measurements made with the finless model installed on a standard sting (Phase I) produced results rather close to those obtained with the upstream sting while the finned model results present much differences. Nothing can be discussed for the other results obtained from Phase I at other Mach numbers since no corresponding tests were made with the upstream sting.

From Fig. 75, it can be observed that the base pressure ratios obtained from the base pressure distribution tests in the DREV wind tunnel are scattered around those values proposed by Ref. 11. Discrepancies could possibly be attributed to differences in the test conditions, such as the Reynolds number and characteristics of the boundary layer approaching the model base. Figure 76 (Ref. 11) shows that the ratio of momentum thickness over base radius for test conditions at Mach 2.0 in the DREV tunnel was about 10 times higher than that of the tests related to in Fig. 75 (Ref. 11).

At the present state of knowledge, theories suggest that primordial dependence of the base pressure ratio would be on the relative location of the recompression zone downstream of the model base and value of recompression (or reattachment) pressure. (See Refs. 11, 18, 19, 20, 21, 28, 31, 32, 33). It is generally recognized that:

a- a turbulent boundary layer results into a slightly higher base pressure than a laminar one,

b- a thick boundary layer results into a slightly higher base pressure than a thin one,

c- a higher Mach number results into a much lower base pressure.

The boundary layer retained for pressure tests was considered turbulent and it was not possible to observed the laminar/turbulent dependence on the base pressure.

For most practical purposes, experimental studies recognize that, for a given Mach number ($\gamma=1.4$), the pressure ratio

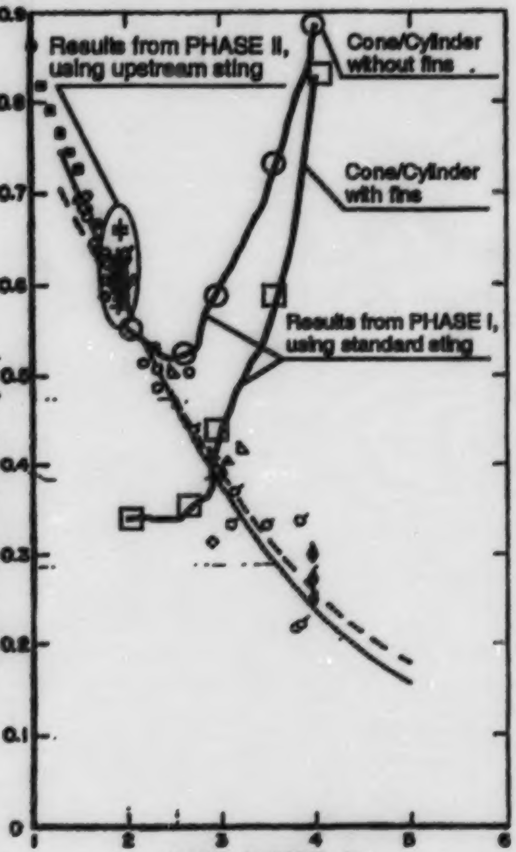

FIGURE 75 - Base pressure vs Mach number specific to axisymmetric base and slender bodies of revolution (flat base) ; data obtained from various sources (Ref. 11) and compared to measurements from present test series (Phase II) and Phase I (standard sting holder)

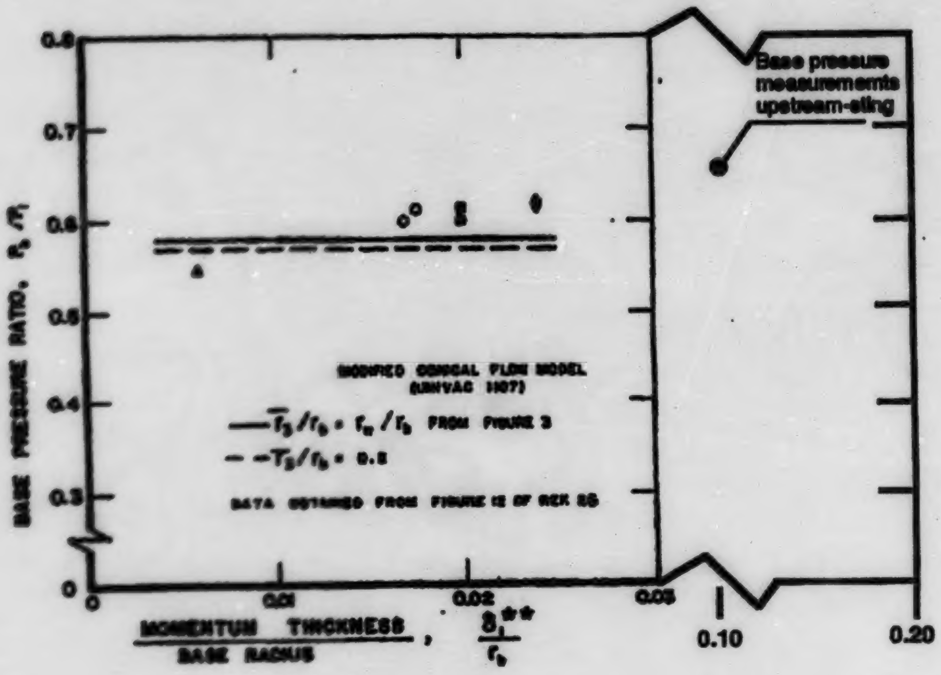

FIGURE 76 - Effect of initial turbulent boundary layer on base pressure for a Mach number of 2.0 and $\gamma = 1.4$. Symbols are for experimental results and lines for theoretical calculations based on various assumptions on relative location of recompression zones downstream model base; data from present test series plotted over

on the base can be considered constant (Ref. 11). It is also well known that the base pressure depends on the relative thickness and character (i.e. laminar, transitional or turbulent) of the boundary layer approaching a blunt base. As an indication, Fig. 75 shows some theoretical and experimental comparisons of base pressure ratio variation with Mach number, and for different conditions of approaching boundary layer. It can be observed that the base pressure is mainly influenced by the Mach number, and the relatively small scatter of experimental data points representative of various conditions of approaching boundary layer suggests its relatively secondary effect.

As an initial reference of comparison, Fig. 76 (Ref. 11) suggests a theoretical and experimental base pressure ratio $\approx$ 0.6 for conditions at Mach 2.0, with very little dependance on boundary layer relative momentum thickness. DREV tunnel data were plotted over for comparison purpose. As per Ref. 11, if the boundary layer is turbulent and its thickness about ten times momentum thickness, data from Fig. 76 covers the range from approximately 0.006 to 0.024 times the base radius, as the boundary layer thickness is concerned. In present test series, the boundary layer thickness at Mach 2.0 was 0.99 times the body radius which was about 9.4 times the momentum thickness (δ_2/base radius = 0.107).

Although Ref. 11 does not support the applicability of two-dimensional base pressure solutions or experiments to axisymmetric base recompression (of bodies of revolution), Fig. 77 (Ref. 28) presents a two-dimensional theoretical influence of the boundary layer momentum thickness on the base pressure coefficient (reduced with respect to dynamic pressure) for various Mach numbers. It indicates increments of base pressure coefficient (to be differentiate with base pressure ratio) as a function of relative momentum thickness increment. The reference datum corresponds to a boundary layer whose momentum thickness $\delta_2/d = .003$.

From the tests that were made with various intensities of upstream sting surface aspiration in order reduce the boundary layer thickness, it is evident that the capacity was marginal. This problem came from the suction intensity which was proportional to the difference between the static pressure in the test

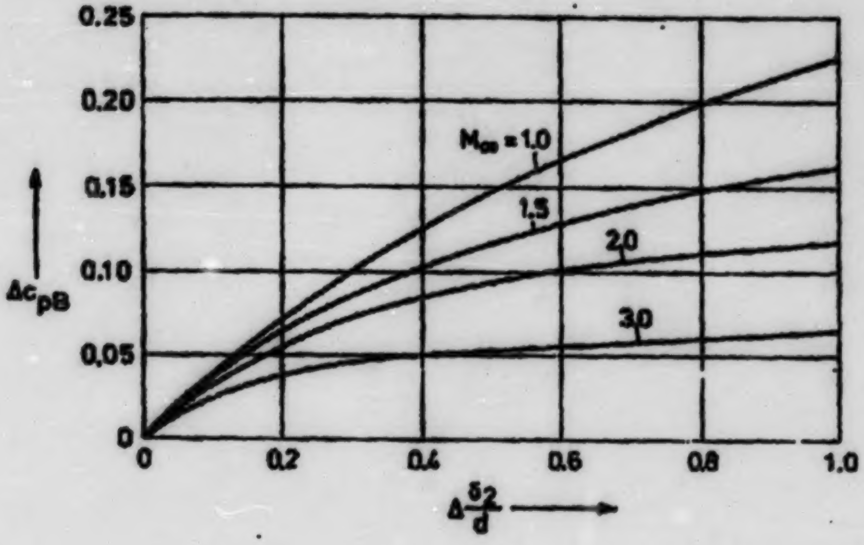

FIGURE 77 - Suggested theoretical influence of the boundary layer momentum thickness on the base pressure coefficient for various Mach numbers, and with respect to datum boundary layer having a momentum thickness $\delta_2/d = .003$

section and that of the suction tubing connected to a vacuum reservoir. The vacuum reservoir pressure cannot be less than zero and since the test section static pressure was very low, it produced a weak suction.

The low Reynolds numbers encountered in the DREV facility test section favoured the development of a rapidly growing boundary layer between the nose of the upstream sting and the aspiration downstream module (Ref. 40). It resulted that the volumetric capacity of the aspiration was marginal to obtain a realistic boundary layer and insufficient to produce a thin velocity profile. The upstream sting aspiration system was of a great help to reduce the thickness of the approaching boundary layer but it remained thicker than expected for a real projectile in free flight.

At the end of the tests series, it was deduced that more aspiration holes should have been drilled in the aspiration downstream module in order to increase the suction intensity. This recommendation was followed and the number of canted holes was doubled to a number of 368. More tests were made (Ref. 41) and it was observed that with the new arrangement, it was possible to achieve boundary layer thicknesses farther reduced by 20%.

This experiment has demonstrate the valuable potential of DREV new upstream sting to perform measurements of afterbody/base pressure distribution. It made possible to modify the approaching boundary layer from laminar to turbulent and its thickness can be controlled by a factor of 2 to 3 (with respect to non-aspirated conditions). By then, surface pressure measurements are made independent of discrepancies between wind tunnel and free flight Reynolds numbers. Since the boundary layer velocity profile is produced artificially, there was no other observed influence of the low test section Reynolds number than inherent difficulty to properly aspire the initial boundary layer.

Concerning the base/afterbody pressure measurement errors, the percentage of the interval limits with respect to average measurement value were around 2.7%, for levels of confidence of 95.0% and related to the case of a single individual test run. Since in all test conditions, more test runs were performed (repeated), the percentage of the interval limits with respect to average measurement value were around 1.9%, again for levels of confidence of 95.0%. These statistics give only an indication on the stability and repeatability of measurements and don't mean that the experimental approach adopted is not questionable.

12.0 CONCLUSIONS

The fundamental logic of the complete test series was based on the assumption that the best measured value of the base pressure should be made in the following conditions:

a- The test setting should provide a measurement of the base pressure without any interference on the base flow (like the one produced from a standard sting holder protruding from a model base).

b- Because of the known influence (although limited) of the characteristics of the boundary layer approaching a projectile base on the base flow, it should be possible to perform boundary layer measurements on the after body. Also, some means should be available to alter or to change the characteristics of the boundary layer near the model base.

With such conditions, wind tunnel tests with some novel means to hold the model were mandatory, (in comparison with an aeroballistic range facility where velocity profile measurements would have been impossible).

In order to not disturb the natural base flow by any kind of downstream sting-support, the approach adopted was unique for the support/balance/model design. The base models were physically a cylindrical prolongation of an upstream/sting which was also cylindrical and of a same calibre.

This upstream sting was fitted with holes canted against the flow and connected to a proper aspiration system in order to reduce the boundary layer thickness around the base/afterbody test model.

It was possible to characterize the boundary layer approaching the model base by measuring air flow velocity profile from the free stream down to model surface. It was made with special pitot tubes (circular/conical and duck beak configured, total pressure only) at a station located 1.75 body calibre from model base. By varying the aspiration intensity and using different transition strip settings, it was possible to produce a boundary layer velocity profile of reference to which all subsequent pressure distribution measurements were related to.

Because of the large number of runs necessary to characterize a single boundary layer in a first time and thereafter to measure the base pressure distribution drag then obtained, only one boundary layer velocity profile was investigated at Mach 2.0 and considered turbulent.

From numerous tests reported in the literature, it was observed that the primordial factor that govern the base pressure is mainly the Mach number. The second factor is the base configuration and the third would be the approaching boundary layer. In summary, for a cylindrical afterbody with a flat base, it can be said that the following conditions would prevail:

a- a higher Mach number results into a lower base pressure and the effect is important,

b- a turbulent boundary layer results into a slightly higher base pressure than a laminar one,

c- the base pressure is slightly higher with thicker boundary layer.

Results from present test series and Ref. 6 show that base pressure was lower for a higher suction intensity of the boundary layer approaching the model base. And this was observed for both turbulent and laminar boundary layers. These results confirm the condition mentioned in " c " above since a higher suction produce a thinner boundary layer.

It was observed that the base pressure measurements from these test series (finned and finless models) are scattered around those published results (Ref. 11). Nothing can be concluded from this since the boundary layer in current test series was probably thicker, owing to the difficulty to make it thin by aspiration.

The suction intensity was weak, being proportional to the small difference of pressure between the test section static pressure and that of the suction tubing which was connected to a vacuum reservoir.

The low Reynolds numbers encountered in the DREV facility test section favoured the development of a thick initial boundary layer (Ref. 40) and the suction capacity was marginal to obtain a realistic thickness. Although the upstream sting aspiration system was of a great help to reduce the thickness of the approaching boundary layer, it was thicker than expected for the case of a real projectile in free flight.

At the end of the tests series, it was concluded that more aspiration holes would help to increase the suction intensity. This recommendation was followed and the number of canted holes was doubled. Subsequent tests showed that boundary layer thicknesses were further reduced by 20%.

It is also concluded that as long it is possible to manipulate the boundary layer with the aspiration system and the addition of transition strips in order to produce the desired characteristics, the tests section Reynolds number would not have any influence on the afterbody model surface pressure measurements. Nevertheless, the test section low Reynolds numbers, by producing thick boundary layers, make it difficult to aspire enough air volume to produce a representative approaching boundary layer. It is probable that at test Mach numbers of 3.0 to 4.0, the suction intensity would be insufficient to produce a realistic boundary layer and the feasibility would have to be explored.

As the test setting is concerned, it must be said that it would be much easier and lot more reliable, with the new DREV system, to measure a drag force by using a standard wind tunnel balance, than to have to measure a base pressure distribution and integrate it. There already exists a new DREV upstream sting/base drag measurement system that can provide a direct measurement of the base drag force component in isolation. It could drive future interests as the base flow surveys and search for a low drag base/afterbody configuration might be concerned. A first tentative was made with success (Ref. 41).

In the past, the principal deterrents to formulating an adequate theoretical solution to the axisymmetric base pressure problem were the lack of understanding of non-constant pressure mixing and the mechanism of recompression. Furthermore, experimental data are available for only a few axisymmetric configurations (Ref. 15). The lack of data of this type is understandable in view of the experimental difficulties involved, and it is why a wind tunnel test setting dedicated to base flow studies was developed at DREV.

13.0 ACKNOWLEDGEMENTS

The author wishes to thank Messrs. R. Langlois and J. Bernier for their valuable contribution in the development of this project. Also, Mr R. Bilodeau's patient work to program the new data acquisition system and general operation of the wind tunnel facility was a primordial contribution to this project. Thanks are addressed to Messrs. A. Jacques, J. Lecours, D. Nadeau, B. Paradis and J. - M. Rioux for their outstanding contributions in designing models, adjusting and installing them in the wind tunnel that were essential to the success of this wind tunnel experiment.

14.0 REFERENCES

1. Dupuis, A. D. and Hathaway, W., " Aerodynamic Characteristics of a Finned Projectile at Supersonic and Hypersonic Speeds from Free-Flight Tests ", DREV - R - 9404, October 1994, UNCLASSIFIED

2. Dupuis, A. D. and Berner, C., " Experimental and Numerical Investigation of a Finned Projectile at Mach 2 ", 14th International Ballistics Symposium, Québec City, Canada, 26-29 Sept., 1993, UNCLASSIFIED

3. Berner, C., Demautis, C., Duffner, P., " Vol de deux projectiles séparés par une faible distance. I1-Visualisation des écoulements et mesures de pression autour de projectiles de référence ", Institut franco-allemand de recherches de St-Louis, ISL, Rapport - R107/92, August 15, 1992, UNCLASSIFIED

4. Berner, C., Demautis, C., Duffner, P., " Vol de deux projectiles séparés par une faible distance. I2-Mesures du champ des vitesses autour des projectiles de référence ", Institut franco-allemand de recherches de St-Louis, ISL Report/94, 1994, UNCLASSIFIED

5. Berner, C., " Numerical Investigation of the DREV/ISL Reference Projectiles ", ISL Report/96, 1996, UNCLASSIFIED

6. Berner, C. and Dupuis, A. D., " Wind Tunnel Investigation and Analysis of the DREV - ISL Reference Projectiles ", DREV - R - 9520, June 1996, UNCLASSIFIED

7. Meunier, IGA, Schulte Dipl.-Ing. from ISL and Peebles, K., from DREV, " Projet de Coopération Scientifique entre CRDV et ISL ", Franco-Canadian Accord under the auspices of Theme 25 - Aeroballistics, Defence Research Establishment Valcartier (DREV), Canada and the French-German Research Institute (ISL), France, January 1990, UNCLASSIFIED

8. Girard, B., " Wind Tunnel Tests on DREV - ISL Reference Models at Supersonic Speeds (Series ISLFPWT- 1) ", DREV - TM - 9704, August 1997, UNCLASSIFIED

9. Hutt, G. R. and East, R. A., " Dynamic Pitch Stability Measurements of Slender Cone-Cylinder Finned Bodies at High Mach Number ", The University of Southampton, Hants, UK, Aeronautics and Astronautics Department, 9th International Symposium on Ballistics, Royal Military College of Science, Shrivenham, Proceedings, Held in UK, pp. 2-9 to 2-17, 29th April -1st May 1986, UNCLASSIFIED

10. Hutt, G. R. and East, R. A., " Dynamic Stability on Finned Bodies at Hypersonic Mach Number ", The University of Southampton, Hants, UK, Aeronautics and Astronautics Department, TTCP Technical Panel W-2, Proceedings - Volume I, Held in the USA, pp. 59-73, 25 October - 1 November 1985, UNCLASSIFIED

11. Mueller, Thomas J., " Determination of the Turbulent Base Pressure in Supersonic Axisymmetric Flow ", University of Notre Dame, Notre Dame, Indiana USA, AIAA Paper No. 67-446, AIAA 3rd Propulsion Joint Specialist Conference, Washington, D.C./July 17-21, 1967, UNCLASSIFIED

12. Zumwalt, G. W., " Analytical and experimental Study of the Axially-Symmetric Supersonic Base Pressure Problem", Ph. D. Thesis, University of Illinois, Dissertation, Department of Mechanical Engineering, MIC 59-4589, University Microfilms, Inc., Ann Harbor, 1959, UNCLASSIFIED

13. Beheim, M. A., " Flow in the Base Region of Axisymmetric and Two-Dimensional Configurations ", Lewis Research Center, NASA TR R-77, 1961, UNCLASSIFIED

14. McDonald, H., " An Analysis of the Turbulent Base Pressure Problem in Supersonic Axi-Symmetric Flow ", Report Ae.200, British Aircraft Corp., Preston Division, Lancashire, England, April 1964, UNCLASSIFIED

15. Vereshchagina, L. I., " On Base Pressure for Solids of Revolution in a Supersonic Gas Flow ", Herald of Leningrad University, Issue 3, No. 13, pp 208-214 (See STARR N66-17406 08-23), UNCLASSIFIED

16. Badrinarayanan, M. A., " An Experimental Investigation of Base Flows at Supersonic Speeds ", Journal of the Royal Aeronautical Society, Vol. 65, pp. 475-482, July 1961, UNCLASSIFIED

17. Love, E. S., " Base Pressure at Supersonic Speeds on Two-Dimensional Airfoils and on Bodies of Revolution with and without Fins Having Turbulent Boundary Layers, NACA TN-3819, January 1957, UNCLASSIFIED

18. Chapman, D. R., " An Analysis of Base Pressure at Supersonic Velocities and Comparison with Experiment ", NACA Report 1051, 1951, (Supersedes NACA TN-2137, 1950), UNCLASSIFIED

19. Potter, J. L., Whitfield, J. D., Strike, W. T., " Transition Measurements and the Correlation of Transition Sensitive Data ", AEDC-TR-59-4, February 1959, UNCLASSIFIED

20. Graham, D. K., Binion, T. W. Jr., " Base Drag Measurements on an Ogive Cylinder Model with Base Nozzle Flow ", AEDC-TDR-64-8, May 1964, UNCLASSIFIED

21. Karpov, B. G., " The Effect of Various Boattail Shapes on Base Pressure and Other Aerodynamic Characteristics of a 7-Caliber Long Body of Revolution at M=1.70 ", Ballistic Research Laboratories Report No. 1295, August 1965, UNCLASSIFIED

22. Nash, J. F., " An Analysis of Two-Dimensional Turbulent Base Flow Including the Effect of the Approaching Boundary Layer ", NPL Aero. Report 1036, A. R. C. 24000, July 1962, UNCLASSIFIED

23. McDonald, H., " Turbulent Shear Layer Reattachment with Special Emphasis on the Base Pressure Problem ", British Aircraft Corp., Preston Division, Lancashire, England, August 1963, UNCLASSIFIED

24. Roshko, A., Thomke G. J., " Flow Separation and Reattachament Behind a Downstream-Facing Step ", Douglas Report SM-43056-1, January 1964, UNCLASSIFIED

25. Roshko, A., Thomke G. J., " Observations of turbulent Reattachment Behind an Axisymmetric Downstream-Facing Step in Supersonic Flow ", Douglas MSSD Report SM-43068, April 1965, UNCLASSIFIED

26. McDonald, H., " The Turbulent Supersonic Base Pressure Problem; a Comparison between a Theory and some External Evidence ", British Aircraft Corp., Report Ae 194, Preston Division, Lancashire, England, April 1965, UNCLASSIFIED

27. Nash, J. F., " Comments on " Review of Recent Development in Turbulent Supersonic Base Flow ", AIAA Journal, pp. 574-575, March 1966, UNCLASSIFIED

28. Tanner, M., " Boundary- Layer Thickness and Base Pressure ", Institut für Theoretische Strömungsmechanik, DFVLR Göttingen, Federal Republic of Germany, AIAA Technical Notes 1985, UNCLASSIFIED

29. Tanner, M., " Steady base Flows ", Progress of Aerospace Sciences, Vol. 21, No. 2, pp. 81-157, 1984, UNCLASSIFIED

30. Goecke, S., " Flight-Measured Pressure Characteristics of Aft-Facing Steps in High Reynolds Number Flow at Mach Numbers of 2.20, 2.50 and 2.80 and Comparison with Other Data", NASA TM-72855, 1978, UNCLASSIFIED

31. Korst, H. H., " A Theory for Base Pressures in Transonic and Supersonic Flow ", Journal of Applied Mechanics, Vol. 23 pp. 593-600, 1956, UNCLASSIFIED

32. Nash, J. F., " An Analysis of Two-Dimensional Turbulent Base Flow, Including the Effect of the Approaching Boundary Layer", British Aeronautical Research council, R and M 3434, 1966, UNCLASSIFIED

33. Roberts, J. B., " On the Prediction of Base Pressure in Two-Dimensional Supersonic Turbulent Flow ", British Aeronautical Research Council, R and M 3434, 1966, UNCLASSIFIED

34. Tanner, M., " Theoritical Prediction of Base Pressure for Steady Base Flow ", Progress of Aerospace Sciences, Vol. 14, pp. 177-225, 1973, UNCLASSIFIED

35. Hong Yong, Shik, " A Study of Axially-Symmetric Supersonic Base Flow With Turbulent Initial Boundary Layer ", Phd Thesis 1968, University of Washington USA, UMI Dissertation Information Service, Ann Harbor Michigan, 1991, UNCLASSIFIED

36. Seginer, A. and Ringel, M., " Magnus Effects at High Angles of Attack and Critical Reynolds Numbers ", Technion - Israel Institute of Technology, Haïfa, Israel, J. Spacecraft, Vol. 23, No. 3, pp. 237-244, May-June 1986, UNCLASSIFIED

37. Dupuis, A.D. and Giraud, M., " Sur les Méthodes Pratiques d'Évaluation du Coéfficient de Trainée de Frottement d'un Projectile en Vol Libre ", France, Institut Saint-Louis de Recherches, 1989, UNCLASSIFIED

38. Wuest, W., " Measurements of Flow Speed and Flow Direction by Aerodynamic Probes and Vanes ", Germany, Göttingen, Space Aerodynamics Dept., Paper presented at the 30th Flight Mechanics Panel Meeting in Montreal, Canada, 30th May-2nd June 1967, UNCLASSIFIED

39. Schlichting, H., " Boundary-Layer Theory ", Translated by Dr J. Kestin, Brown University in Providence, Rhode Island, McGRAW-HILL Series in Mechanical Engineering, McGraw-Hill Inc., pp. 229, 230, USA,1968, UNCLASSIFIED

40. Schlichting, H., " Boundary-Layer Theory ", Translated by Dr J. Kestin, Brown University in Providence, Rhode Island, McGRAW-HILL SERIES IN MECHANICAL ENGINEERING, McGraw-Hill Inc., pp. 26, 28, USA,1968, UNCLASSIFIED

41. Girard, B., " Direct Base Drag Measurement Wind Tunnel Tests of Projectile Base Configuration (Series BDWT-1) ", DREV - TM - 1999-028, February 1999, UNCLASSIFIED

APPENDIX A

Summary of Runs

TRIAL ISLPWT-2

BOUNDARY LAYER CHARACTERIZATION AND PRESSURE WIND TUNNEL SURVEY

Base afterbody model designation:

a- Boundary layer characterization

Model no. 1 - BOUNDARY LAYER EXPLORATION AFTERBODY MODEL

b- Base/afterbody pressure distribution

Model no. 2 - BASE PRESSURE EXPLORATION MODEL

Model no. 3 - AFTERBODY SURFACE PRESSURE MODEL

Model no. 4 - FINNED AFTERBODY MODEL, BETWEEN FINS PRESSURE SURVEY

Model no. 5 - FINNED AFTERBODY MODEL, FINS AND BASE PRESSURE SURVEY

SUMMARY OF RUNS

TRIAL ISLPWT-2

BOUNDARY LAYER CHARACTERIZATION

BOUNDARY LAYER EXPLORATION

Model No. 1
Aspiration setting:
Main body and afterbody aspiration modules installed

RUN NUMBER	MACH NUMBER	ASPIRATION VALVE SETTING deg	TRANSITION STRIP	Y in	$\frac{U}{U_\infty}$
R3851	1.89	0	YES	.0475	0.3187
R3852	1.89	0	YES	.0675	0.3390
R3853	1.89	0	YES	.0075	0.1665
R3854	1.89	0	YES	.0875	0.3644
R3855	1.89	0	YES	.1075	0.3849
R3856	1.89	0	YES	.5075	0.6444
R3857	1.89	0	YES	.7575	0.8495
R3858	1.89	0	YES	1.0230	0.9552
R3859	1.89	90	YES	1.0230	0.9617
R3861	1.89	0	NO	.5075	0.7262
R3864	1.89	0	NO	.5075	0.7305

BOUNDARY LAYER EXPLORATION

Model No. 1
Aspiration setting:
Afterbody aspiration module only

RUN NUMBER	MACH NUMBER	ASPIRATION VALVE SETTING deg	TRANSITION STRIP	Y in	$\frac{U}{U_\infty}$
R3885	2.00	90	YES	.0075	0.5212
R3884	2.00	90	YES	.0475	0.6619
R3883	2.00	90	YES	.0675	0.6975
R3882	2.00	90	YES	.1075	0.7385
R3881	2.00	90	YES	.1475	0.7762
R3880	2.00	90	YES	.1875	0.8145
R3879	2.00	90	YES	.2275	0.8485
R3878	2.00	90	YES	.2675	0.8682
R3877	2.00	90	YES	.2875	0.8800
R3876	2.00	90	YES	.3475	0.9062
R3875	2.00	90	YES	.4275	0.9276
R3865	2.00	90	YES	.5075	0.9446
R3872	2.00	90	YES	.6230	0.9664
R3871	2.00	90	YES	.7230	0.9792
R3870	2.00	90	YES	.8230	0.9872
R3869	2.00	90	YES	.9230	0.9933
R3868	2.00	90	YES	1.0230	0.9978

SUMMARY OF RUNS

TRIAL ISLPWT-2

BASE PRESSURE DISTRIBUTION DEPENDENCE SURVEY

BASE PRESSURE EXPLORATION

Model No. 2
Aspiration setting:
Main body and afterbody aspiration modules installed

RUN NUMBER	MACH NUMBER	NOMINAL ANGLE OF INCIDENCE deg	ASPIRATION VALVE SETTING deg	TRANSITION STRIP	BASE PRESSURE CENTRE TAP P_{base}/P_{∞}
R3837	1.96	0.00	0	NO	0.621
R3838	1.97	0.50	0	NO	0.609
R3839	1.94	0.20	0	NO	0.592
R3840	1.94	0.10	0	NO	0.600
R3841	1.95	0.10	0	NO	0.601
R3842	1.96	0.00	0	NO	0.617
R3843	1.96	0.05	0	NO	0.620
R3844	1.95	0.05	30	NO	0.618
R3845	1.95	0.05	60	NO	0.611
R3846	1.95	0.05	0	YES	0.611
R3847	1.94	0.05	30	YES	0.600
R3848	1.94	0.05	60	YES	0.597
R3849	1.95	0.05	90	YES	0.593
R3850	1.96	0.05	90	NO	0.600

BASE PRESSURE EXPLORATION

Model No. 2

Aspiration setting:
Afterbody aspiration module only

RUN NUMBER	MACH NUMBER	NOMINAL ANGLE OF INCIDENCE deg	ASPIRATION VALVE SETTING deg	TRANSITION STRIP	BASE PRESSURE CENTRE TAP P_{base}/P_{∞}
R3886	2.00	0.05	90	YES	0.650
R3887	2.00	0.05	90	YES	0.657

AFTERBODY SURFACE PRESSURE MEASUREMENT

Model No. 3

Aspiration setting:
Afterbody aspiration module only

RUN NUMBER	MACH NUMBER	NOMINAL ANGLE OF INCIDENCE deg	ASPIRATION VALVE SETTING deg	TRANSITION STRIP	BASE PRESSURE CENTRE TAP P_{base}/P_{∞}
R3888	2.00	0.05	90	YES	0.655
R3889	2.00	0.05	90	YES	0.655

AFTERBODY BETWEEN FINS PRESSURE SURVEY

Model No. 4
Model roll index 45 deg, i.e. fins were oriented to form an "X" with between fins pressure taps pointing upwards

Aspiration setting:
Afterbody aspiration module only

RUN NUMBER	MACH NUMBER	NOMINAL ANGLE OF INCIDENCE deg	ASPIRATION VALVE SETTING deg	TRANSITION STRIP	BASE PRESSURE CENTRE TAP P_{base}/P_{∞}
R3893	2.00	0.05	90	YES	N/A
R3894	2.00	0.05	90	YES	N/A

FINS AND BASE PRESSURE SURVEY

Model No. 5

Model roll index 0.0 deg, i.e. fins were oriented to form a "+" with the fin fitted with pressure taps oriented vertically

Aspiration setting:
Afterbody aspiration module only

RUN NUMBER	MACH NUMBER	NOMINAL ANGLE OF INCIDENCE deg	ASPIRATION VALVE SETTING deg	TRANSITION STRIP	BASE PRESSURE CENTRE TAP P_{base}/P_∞
R3890	2.00	0.05	90	YES	0.658
R3891	2.00	0.05	90	YES	0.623
R3892	2.00	0.05	90	YES	0.616

APPENDIX B

Upstream Sting Alignment

UPSTREAM STING ALIGNMENT PROCEDURE

As this afterbody/base flow wind tunnel test had to be made at 0 deg incidence and 0 deg in yaw with respect to flow in the test section, the procedure to follow in order to make sure of a good upstream sting alignment is described below.

Figures 10, 12 and13 show the 8 (3/8 x 24 NF) bolts, on each side of test section, that allow to release retention friction from upstream sting pivot attachment in order to make an adjustment in pitch. Also, the 2 bolts (1/2 x 20 NF) located horizontally on each side of the test section and that can be loosen for an adjustment in yaw, can be seen in Figs. 10 and 12. The maximum adjustment in pitch was approximately ± 5 deg, and there was a possibility of ±1.5 deg in yaw.

This alignment process was based on the response of the model base pressure distribution (radially) with respect to the incidence angles in pitch and yaw. By then, the use of the base pressure exploration model (afterbody model no:2) for a short series of runs provided the data to extrapolate the upstream sting attitude resulting in a symmetrical base pressure distribution, vertically and horizontally. Once found, the final settings provided an upstream sting alignment that was parallel to the flow in the test section. The treatment of data to reduce the base pressure measurement data is presented in section 8.0.

Figure B1 indicates the tendencies of the base pressure radial distribution with respect to misalignment angle. Afterwards, the results were plotted twice: from right to left and from left to right on a same graph in order to obtain an " X " effect that visually amplified the differences in the base pressure measurements. When the upstream sting adjustments provided results showing an " X " plot that closed on a single line (or almost), the alignment was assumed " good " (see Fig. B2).

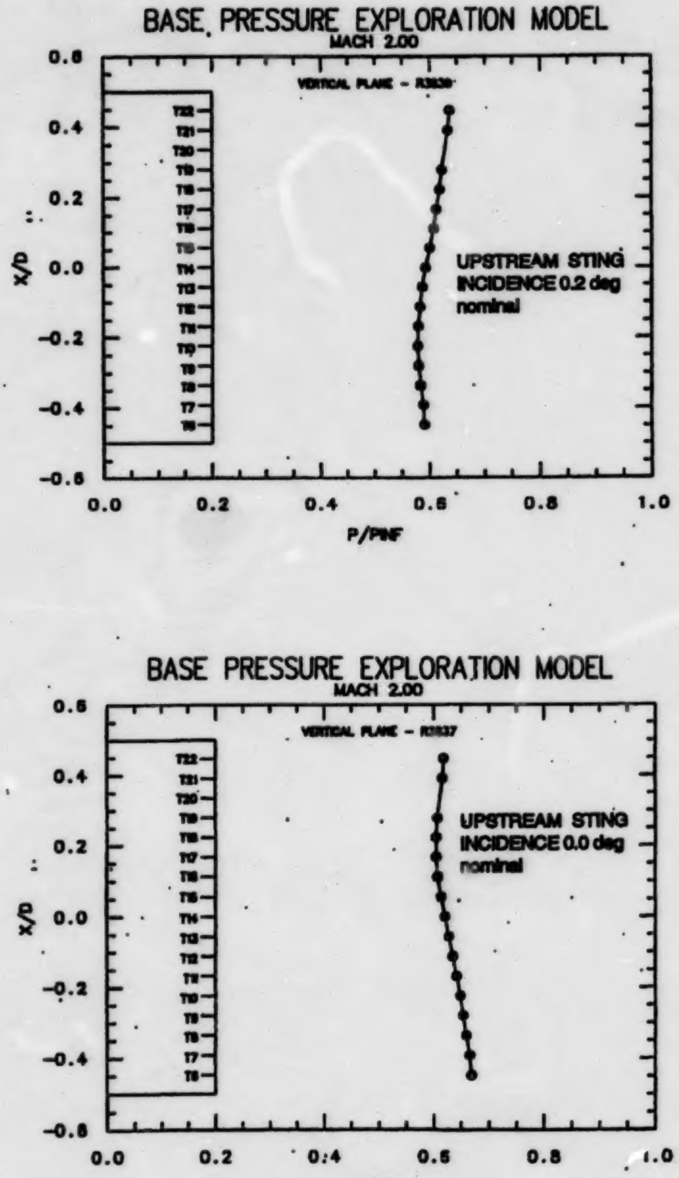

FIGURE B1 - Base flow pressure response with respect to upstream sting alignment

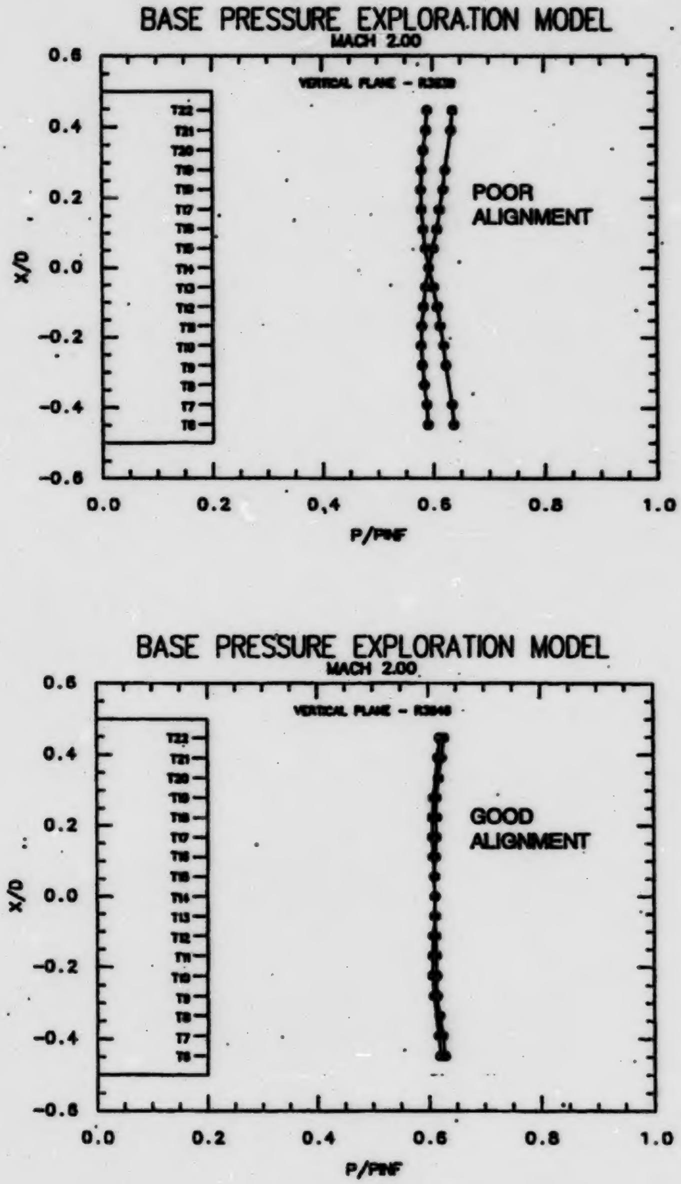

FIGURE B2 - Base pressure response to upstream sting alignment

APPENDIX C

Boundary Layer Aspiration

STEPS SEQUENCE
TO ADJUST BOUNDARY LAYER ASPIRATION

NOTE: The understanding of this appendix will be eased by previously reading Chapters 4.0 and 7.0.

This appendix presents the step sequence that was followed in order to generate the turbulent boundary layer velocity profile and thicknesses (total, displacement and momentum) that were compatible with the specified conditions of the projected base pressure measurements described in Chapter 5.0. The various potential capabilities that were available to modify the boundary layer (around afterbody model installed on the upstream sting) can be listed as follows:

a - If the boundary layer was found laminar, i.e. the exponent " n " of: $\frac{U}{U_\infty} = \left(\frac{Y}{\delta}\right)^{\frac{1}{n}}$ was sensibly less than 7.0, then the flow around afterbody model had to be tripped by gluing a sand paper collar (no: 100 grit) around the afterbody and located at a distance of 4D from the model base.

b - If the boundary layer was found to thick, i.e. $\frac{\delta}{R} \geq 1.4$ (the height from model surface where $\frac{U}{U_\infty} \approx 0.99$ was larger than 1.4 times model radius), then making use of the aspiration system reduced the boundary layer thickness. But, there was also a risk for the boundary layer to come back to laminar again.

c - It was beleived (and it happened so) that the optimized solution or best compromise was a combination of aspiration and afterbody flow tripping (by the use of a sand paper collar).

The initial departure conditions, before to perform the boundary layer exploration, were realized by purposely tripping and/or aspiring the flow in such a combination to produce a base pressure ratio $\left(\frac{P}{P_\infty}\right) \approx 0.6$ at the center of model base (Ref. 11).

In order to minimize guessing, it was agreed to follow the procedure sequence steps listed below:

1 - By using the base pressure exploration model (Fig. 30) assembled on the upstream sting fitted with the main body section dedicated to aspiration (Fig. 18) and also the length adjusting anchorage with aspiration holes (Fig. 20), then a base pressure survey was performed with a special attention to the pressure ratio $\frac{P}{P_\infty}$ encountered at the model base center tap.

2 - If the base center tap pressure ratio was found to be higher than values specified over (and preliminary test runs had confirmed so) the boundary layer was assumed to be to thick and also probably turbulent already. Then, another test run had to be made again by having the flow purposely tripped with a sand paper collar (no: 100 grit) located at 4D from model base. The base center tap pressure ratio then obtained had to be (and was so) higher than previously.

3 - Then, by having already made sure that the flow was turbulent with the flow tripping collar mentioned over, a short run series had to be made with various boundary layer aspiration intensities, and this up to obtaining the correct value for the base center tap pressure ratio ≈ 0.6 at Mach 2.0. Aspiration intensities were regulated by using the aspiration ball valve rotation angle (in deg.) as a reference (Fig. C1). Larger the opening angle, more important was the aspiration, although it does not mean intensities increased linearly with the valve opening angle.

4 - Then, the boundary layer characterization process described in Chapters 4.0 and 7.0 were made. The first

results were found satisfactory, i.e " n " ≈ 7.0 , boundary layer thickness ratio ≈ 1.4. If they had not been found satisfactory, the procedure would have been repeated with a different combination of sand paper collar and aspiration intensities up to satisfaction - if at all possible.

Note: It was found that a transition strip made of a sand paper collar (no: 100 grit) had to be used in combination with only the length adjusting anchorage with aspiration holes and a full aspiration intensity with the ball valve handle at 90 deg.

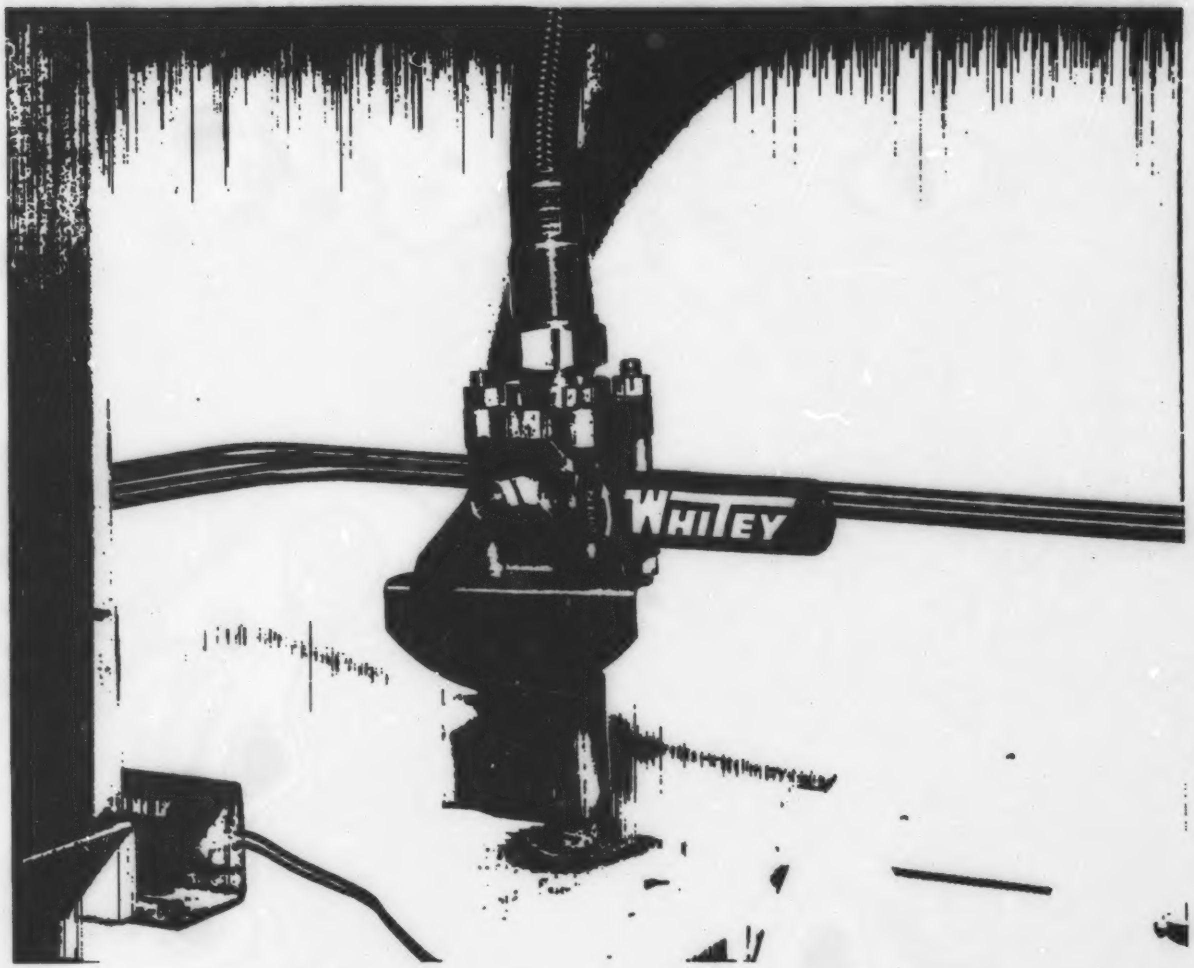

FIGURE C1 - Upstream sting aspiration system ball valve. Shown here fully closed with needle at 0 deg.

APPENDIX D

Boundary Layer - Summary of Results

BOUNDARY LAYER CHARACTERIZATION - SUMMARY OF RESULTS

Results presented in Figs. D1 to D5 give characterization of the approaching boundary layer conditions referred to in Chapters 4.0 and 5.0.

Y/R	Y	U/Uinf	LnY	LnU/Uinf	LnY/d'
0.0095	0.0075	0.5212	-4.8929	-0.6517	-4.6439
0.0603	0.0475	0.6619	-3.0470	-0.4127	-2.7981
0.0857	0.0675	0.6975	-2.6956	-0.3602	-2.4467
0.1365	0.1075	0.7385	-2.2303	-0.3031	-1.9813
0.1873	0.1475	0.7762	-1.9139	-0.2533	-1.6650
0.2381	0.1875	0.8145	-1.6740	-0.2052	-1.4250
0.2889	0.2275	0.8485	-1.4806	-0.1643	-1.2316
0.3397	0.2675	0.8682	-1.3186	-0.1414	-1.0697
0.3651	0.2875	0.8800	-1.2465	-0.1278	-0.9976
0.4413	0.3475	0.9062	-1.0570	-0.0985	-0.8080
0.5429	0.4275	0.9276	-0.8498	-0.0752	-0.6008
0.6444	0.5075	0.9446	-0.6783	-0.0570	-0.4293
0.7911	0.6230	0.9664	-0.4732	-0.0342	-0.2242
0.9181	0.7230	0.9792	-0.3243	-0.0211	-0.0754
1.0451	0.8230	0.9872	-0.1948	-0.0129	0.0542
1.1721	0.9230	0.9933	-0.0801	-0.0067	0.1688
1.2990	1.0230	0.9978	0.0227	-0.0022	0.2717
1.4260	1.1230	1.0001	0.1160	0.0001	0.3650
1.5530	1.2230	1.0015	0.2013	0.0015	0.4503

FIGURE D1 - Boundary layer characterization, summary of results, note: $d' \equiv \delta$ in expression $\mathrm{Ln}\frac{Y}{d'}$, see Section 7.6

UNIT: INCHES

Y	density	delta1	d1xdy	delta2	d2xdy
0.0000	0.6735	1.0000	0.0000	0.0000	0.0000
0.0075	0.6318	0.6771	0.0063	0.1592	0.0006
0.0275	0.6579	0.6321	0.0131	0.1645	0.0032
0.0475	0.6899	0.5761	0.0121	0.1637	0.0033
0.0675	0.7088	0.5489	0.0113	0.1624	0.0033
0.1075	0.7333	0.5210	0.0214	0.1609	0.0065
0.1475	0.7587	0.4881	0.0202	0.1565	0.0063
0.1875	0.7879	0.4436	0.0186	0.1474	0.0061
0.2275	0.8170	0.3954	0.0168	0.1354	0.0057
0.2675	0.8354	0.3680	0.0153	0.1281	0.0053
0.2875	0.8471	0.3475	0.0072	0.1221	0.0025
0.3475	0.8749	0.2986	0.0194	0.1072	0.0069
0.4275	0.8996	0.2554	0.0222	0.0932	0.0080
0.5075	0.9207	0.2143	0.0188	0.0792	0.0069
0.6230	0.9498	0.1471	0.0209	0.0552	0.0078
0.7230	0.9681	0.0998	0.0123	0.0378	0.0047
0.8230	0.9801	0.0664	0.0083	0.0253	0.0032
0.9230	0.9894	0.0374	0.0052	0.0143	0.0020
1.0230	0.9965	0.0131	0.0025	0.0050	0.0010

```
D1XDY (total) =  0.2517  TRAPEZOIDAL INTEGRATION METHOD
D2XDY (total) =  0.0830  H = 3.0325
Delta 1 =  0.2492
Delta 2 =  0.0840
      H =  2.9658
```

FIGURE D2 - Boundary layer characterization, summary of calculations as per methodology described in Section 7.7; trapezoidal integration method (D1XDY , D2XDY), Simpson triplets non-symmetrical method (Delta 1, Delta 2).

UNIT: mm

Y	density	delta1	d1xdy	delta2	d2xdy
0.0000	0.6735	1.0000	0.0000	0.0000	0.0000
0.1900	0.6318	0.6771	0.1593	0.1592	0.0151
0.6980	0.6579	0.6321	0.3325	0.1645	0.0822
1.2060	0.6899	0.5761	0.3069	0.1637	0.0834
1.7140	0.7088	0.5489	0.2858	0.1624	0.0828
2.7300	0.7333	0.5210	0.5435	0.1609	0.1642
3.7460	0.7587	0.4881	0.5126	0.1565	0.1613
4.7620	0.7879	0.4436	0.4733	0.1474	0.1544
5.7780	0.8170	0.3954	0.4262	0.1354	0.1436
6.7940	0.8354	0.3680	0.3878	0.1281	0.1338
7.3020	0.8471	0.3475	0.1817	0.1221	0.0635
8.8260	0.8749	0.2986	0.4923	0.1072	0.1747
10.8580	0.8996	0.2554	0.5630	0.0932	0.2036
12.8880	0.9207	0.2143	0.4768	0.0792	0.1750
15.8220	0.9498	0.1471	0.5302	0.0552	0.1973
18.3620	0.9681	0.0998	0.3135	0.0378	0.1182
20.9020	0.9801	0.0664	0.2111	0.0253	0.0802
23.4420	0.9894	0.0374	0.1318	0.0143	0.0503
25.9800	0.9965	0.0131	0.0640	0.0050	0.0245

```
D1XDY (total) =  6.3926  TRAPEZOIDAL INTEGRATION METHOD
D2XDY (total) =  2.1082  H = 3.0323
Delta 1 =  6.3293
Delta 2 =  2.1341
      H =  2.9658
```

FIGURE D3 - Boundary layer characterization, summary of calculations as per methodology described in Section 7.7; trapezoidal integration method (D1XDY , D2XDY), Simpson triplets non-symmetrical method (Delta 1, Delta 2).

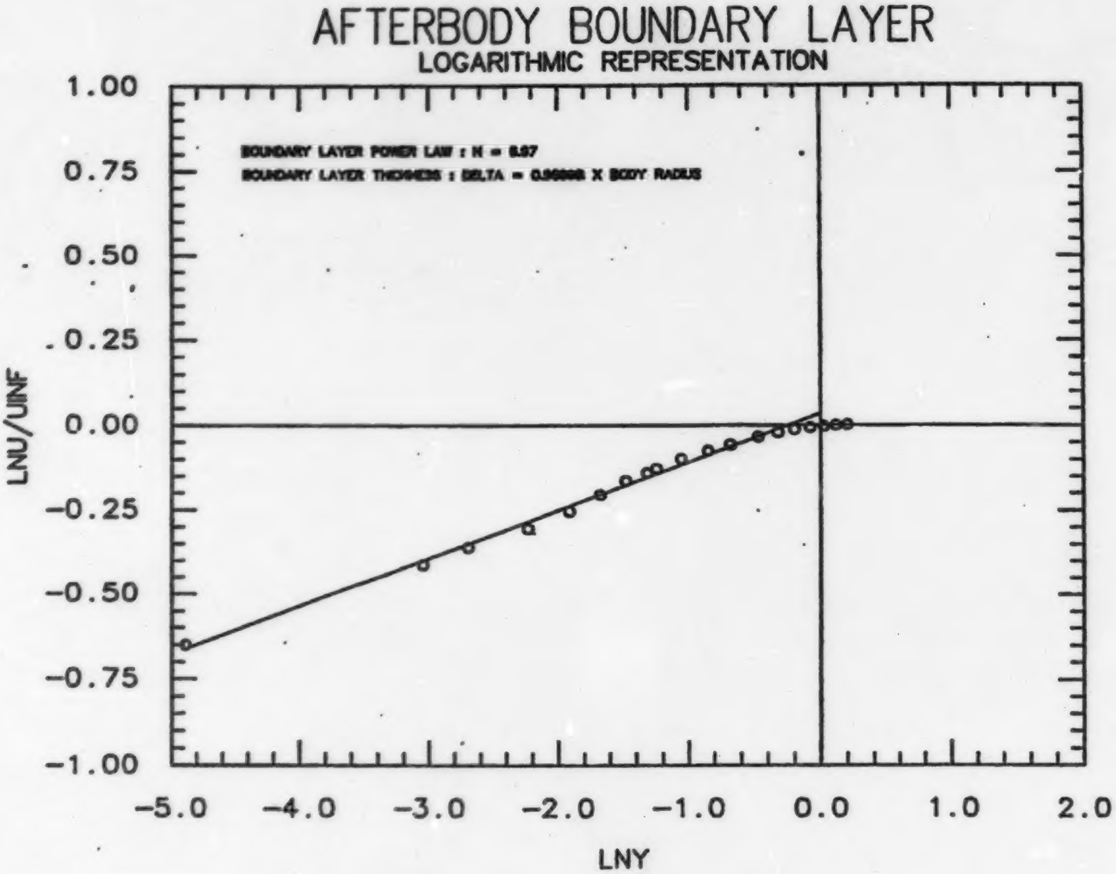

FIGURE D4 - Boundary layer characterization, velocity profile logarithmic representation, see Section 7.6

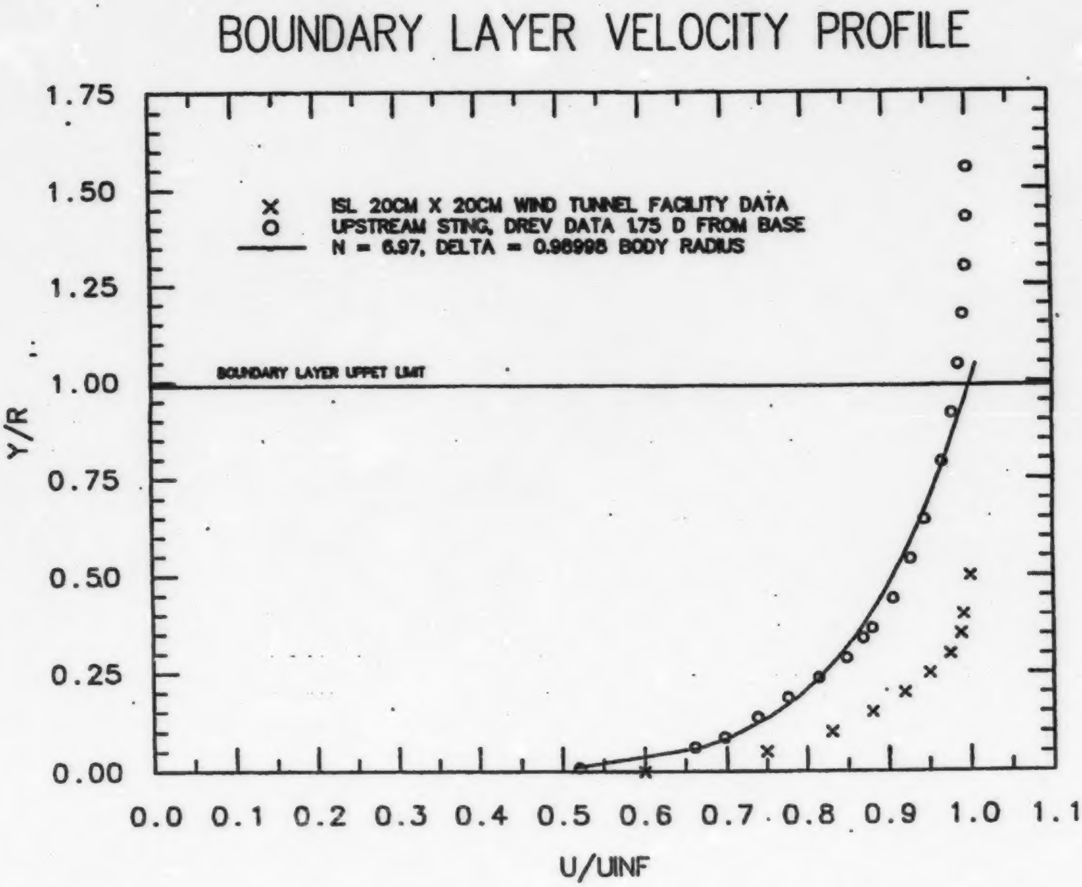

FIGURE D5 - Boundary layer characterization, comparison with velocity profile in ISL tunnel facility and with power law approximation

APPENDIX E

Base Pressure - Summary of Results

SURFACE PRESSURE DISTRIBUTION

Results presented in Fig. E1 to E6 are complementary to the data given in Section 9.2 and Appendix A, and show near afterbody surface pressure and base pressure tendencies with respect to boundary layer aspiration intensity. Graphical results of Section 9.2 are related to test settings (aspiration, transition strip) that produced the specific boundary layer characteristics for which the final afterbody and base pressure experiments were performed. It was assumed that the static pressure dependence on approaching boundary layer characteristics for the finned afterbody models should have been rather similar to results obtained with models without fins, although measurements were not done.

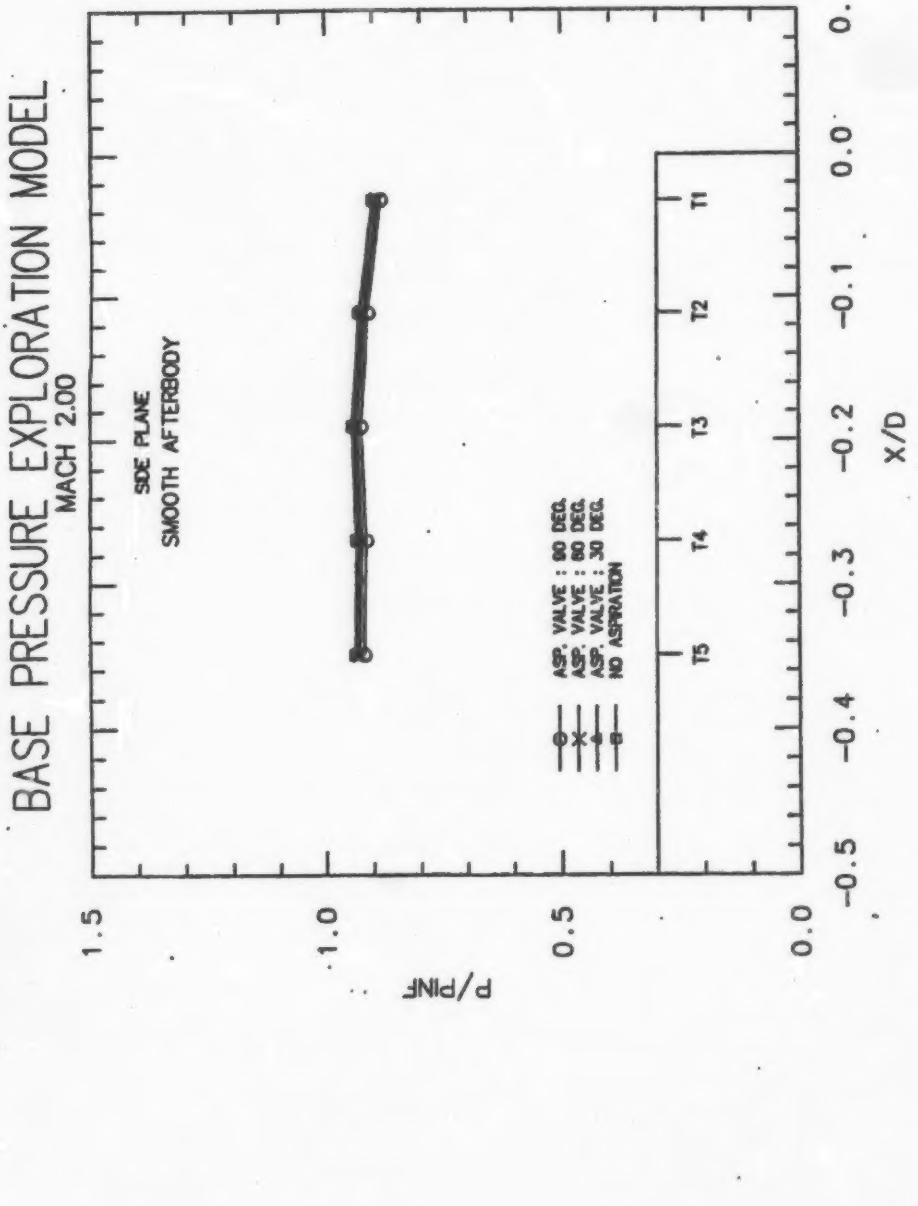

FIGURE E1 - Near base /afterbody surface pressure tendencies with respect to boundary layer aspiration intensity

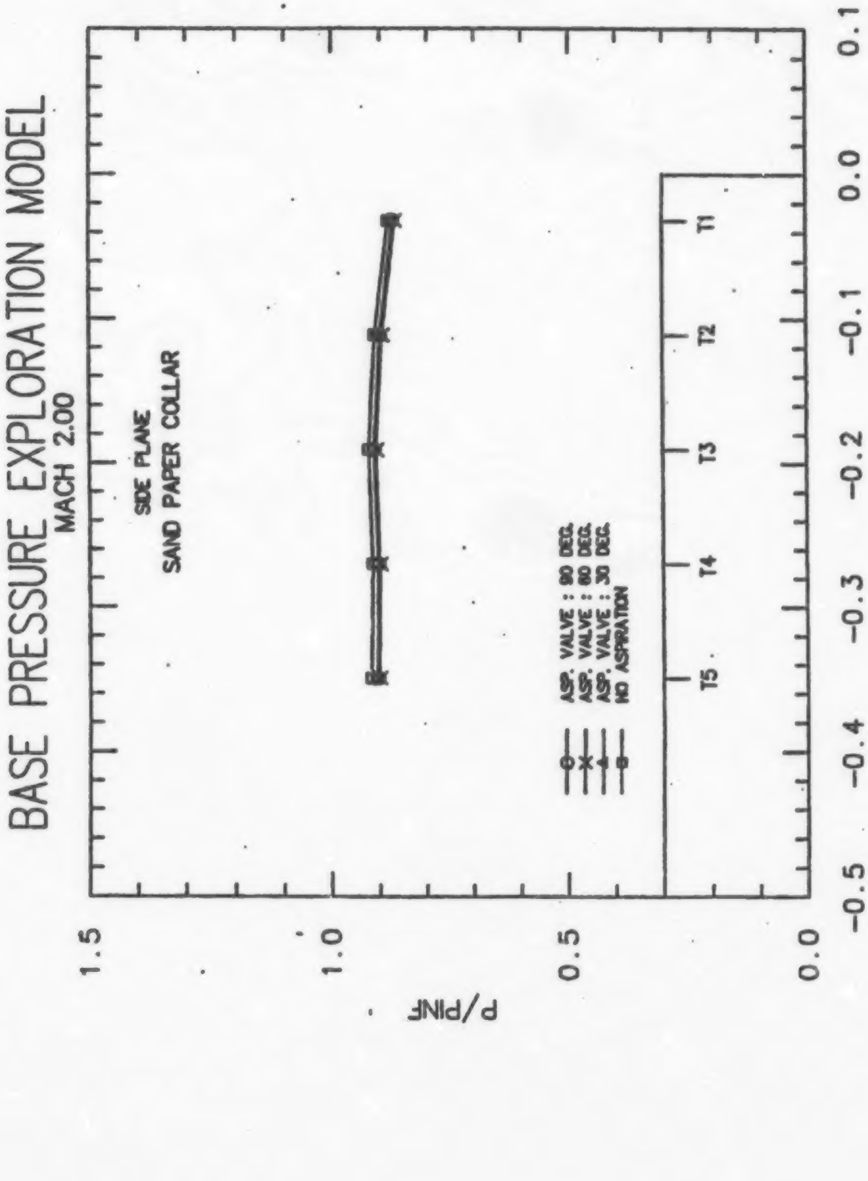

FIGURE E2 - Near base /afterbody surface pressure tendencies with respect to boundary layer aspiration intensity

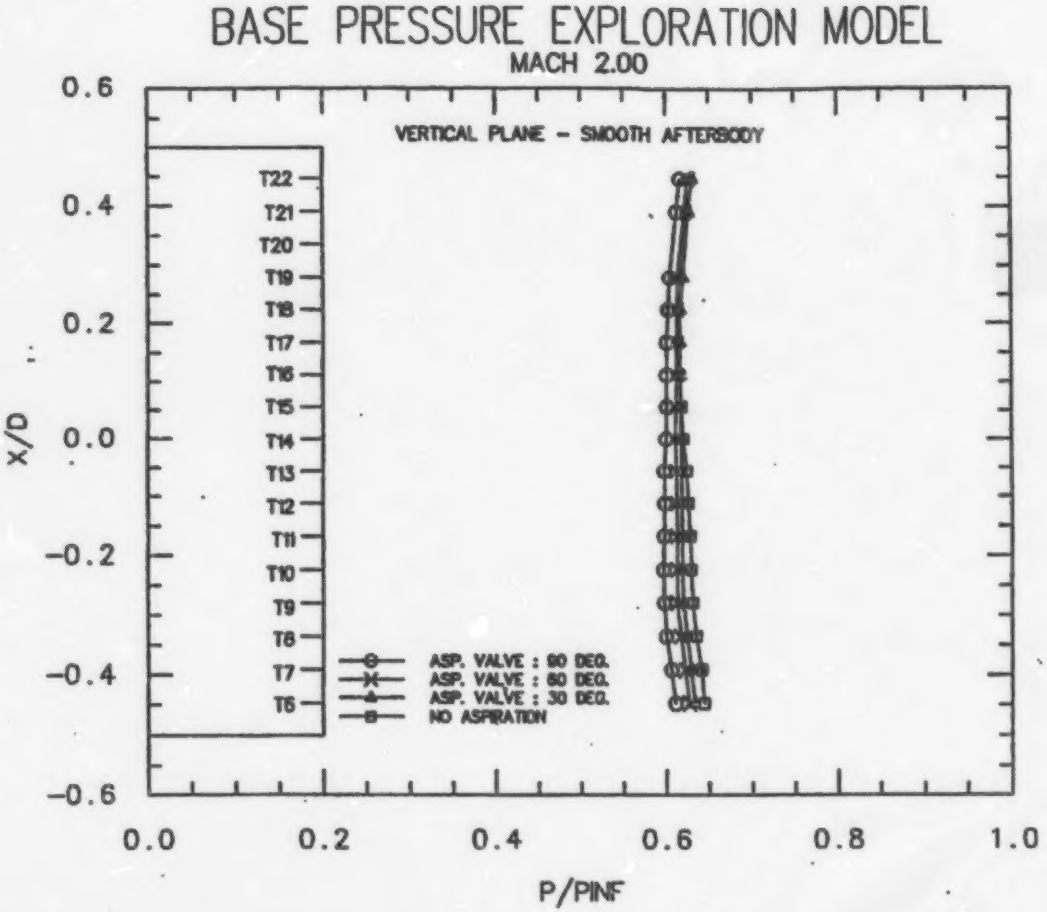

FIGURE E3 - Model base surface pressure tendencies with respect to boundary layer aspiration intensity

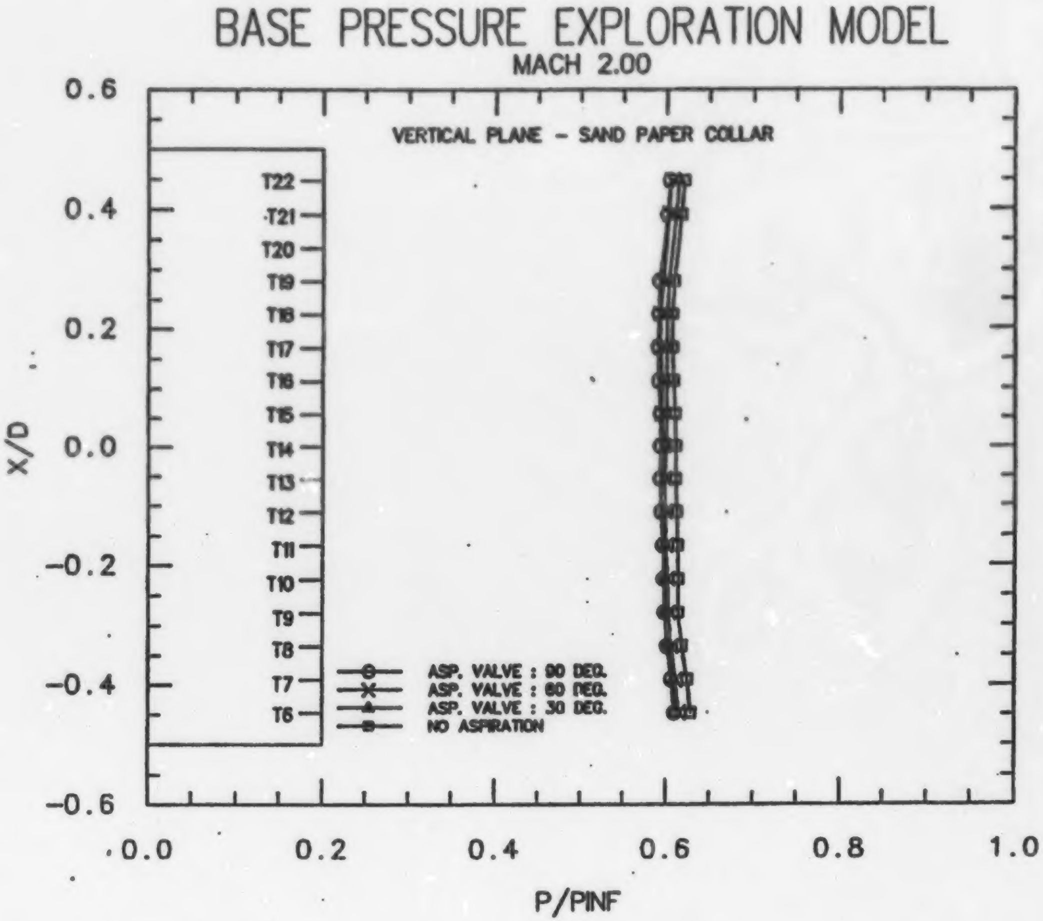

FIGURE E4 - Model base surface pressure tendencies with respect to boundary layer aspiration intensity

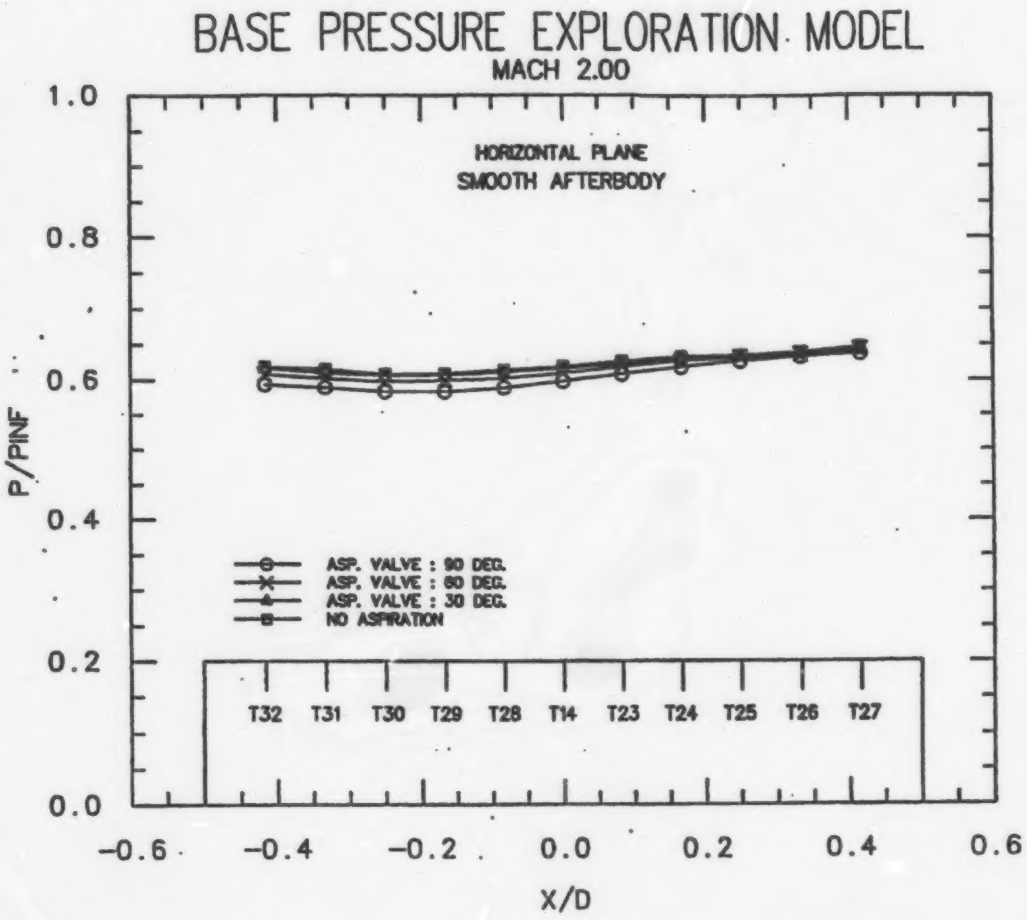

FIGURE E5 - Model base pressure tendencies with respect to boundary layer aspiration intensity

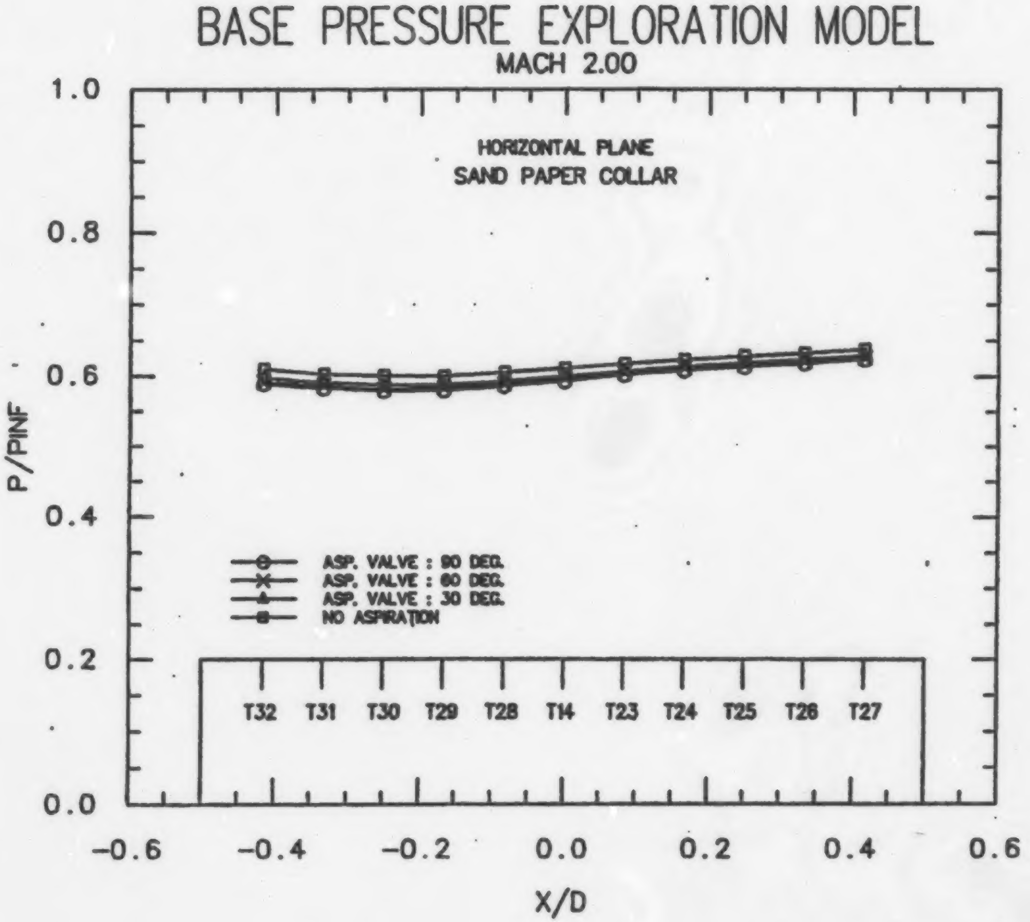

FIGURE E6 - Model base pressure tendencies with respect to boundary layer aspiration intensity

APPENDIX F

Measurement Errors

STATISTICAL METHODOLOGY TO EVALUATE BOUNDARY LAYER VELOCITY PROFILE AND PRESSURE DISTRIBUTION MEASUREMENT ERRORS

During base pressure and boundary layer velocity profile test runs, the afterbody model was set at 0.0 deg of angle of attack, and series of measurements were recorded for each set of test conditions. It was assumed, for statistical calculations, that normally only one test run was to be made for each set of experimental conditions. Several wind tunnel test runs of typical interest must be intentionally repeated in order to provide additional data to determine the 95.0% confidence interval limits to be used for the prediction of future single observation (single run) tests. A minimum of three repeats is necessary. The interval limits are defined as the upper and lower values of results that correspond to the specified level of confidence. The higher is the level of confidence (i.e. 97.5%, 99.0%, 99.9% etc...) and the larger shall be the interval length, which is defined as the difference between the interval limits.

Tables FI present statistical results related to fin trailing edge and base pressure tests in which test conditions stayed constant and several measurements were made. The statistical calculations were made by using the methodology demonstrated below. Since only three repeats had been done for these test conditions, it was found that percentages of errors then obtained were probably larger than in reality. It was then decided to use data from test run that were repeated 9 times and that are considered as typical of base pressure distribution measurement. It was obtained from wind tunnel tests preformed afterwards the present test series, at a same Mach number and same test setting (no fin configuration). Related tests conditions produced a boundary layer velocity profile rather similar to the one reported in Appendix D. Calculations based on this data is assumed to give a very representative base pressure distribution test error. Statistical results then obtained are presented in Table FII where a reduction of about 25% for the measurement error can be observed. Measurement error presented in Tables FI and FII give a good indication of the measurement error relative to pressure measurement performed along the surface of the model afterbody.

A similar approach was adopted relatively to the boundary layer velocity profile tests and statistical results are givenin Table FIII. Typical test runs of interest were then repeated and it was the average pressure values from each run that were used toperform the statistical calculations.

n = 3 or 4 etc... ≡ number of repeated wind tunnel tests to investigate interval limits relative to a specific level of confidence.

$X_1, - - X_k$ measured data for angle of attack: *alpha*$_1$, - - *alpha*$_k$

$X_{1,1} - - X_{1,4}$ measured data for angle of attack: *alpha*$_1$ and n=1 to 4

$\sigma^2 = \mathrm{VAR}(X_i)$ while assuming a constant value for each particular variable at specific test conditions

$$S^2 = \sum_1^n \frac{(X_{1,i} - \overline{X_1})^2}{n-1} \text{ estimator of } \sigma^2 \text{ where } \overline{X_j} = \sum_{i=1}^n \frac{X_{j,i}}{n} \quad \text{where } j = 1,2\ldots k$$

$$\mu_i = \text{idealized value of } X_j = \lim_{n \to \infty} \left(\sum_{i=1}^n \frac{X_{j,i}}{n} \right)$$

$\dfrac{X_j - \mu_j}{\sigma}$ obey the normal law N(0 , 1)

$$\sum_1^n \frac{(X_{1,i} - \overline{X}_1)^2}{\sigma^2} = \left(\frac{n-1}{\sigma^2} \right) S^2 \quad \text{obey } \chi^2_{n-1} \text{ theorem}$$

then:

$$\frac{\dfrac{X_j - \mu_j}{\sigma}}{\sqrt[2]{\dfrac{S^2(n-1)}{(n-1)\sigma^2}}} = \frac{X_j - \mu_j}{S}$$

obey law t(n-1)

$$P\left[-a \le \frac{X_j-\mu_j}{S} \le a\right] = P\left[-aS \le X_j-\mu_j \le aS\right] =$$

$$= P\left[-aS-X_j \le -\mu_j \le aS-X_j\right] = P\left[X_j-aS \le \mu_j \le X_j+aS\right]$$

where: $a = t\left(1 - \alpha/2\ ;\ n-1\right)$

$$P\left[X_j-t\left(1 - \alpha/2\ ;\ n-1\right)S \le \mu_j \le X_j+t\left(1 - \alpha/2\ ;\ n-1\right)S\right] \ge \left(1 - \alpha\right)$$

$\alpha = 0.05$

$1 - \alpha = 0.95$

$1 - \frac{\alpha}{2} = 0.975$

$n - 1 = 2$ or 3 etc... $\equiv \nu$

Law for percentiles of the " t " distribution gives:

$t(0.975, 2) = 4.303$
$t(0.975, 3) = 3.182$
$t(0.975, 4) = 2.776$
$t(0.975, 5) = 2.571$
$t(0.975, 6) = 2.447$
$t(0.975, 7) = 2.365$
$t(0.975, 8) = 2.306$
$t(0.975, 9) = 2.262$
$t(0.975, 16) = 2.120$

$t(0.90, 2) = 1.886$
$t(0.90, 3) = 1.638$
$t(0.90, 4) = 1.533$
$t(0.90, 5) = 1.476$
$t(0.90, 6) = 1.440$
$t(0.90, 7) = 1.415$
$t(0.90, 8) = 1.397$
$t(0.90, 9) = 1.383$
$t(0.90, 16) = 1.337$

The following equation :

$$\boxed{\mu_j = X_j \pm t\,(0.975\,,\,\nu)\,S}$$

applies for a confidence level of 95.0% and where there are 2.5%

of chances that the true experimental value that should have been measured would be lower than the defined low interval limit, and 2.5% of chances that it would be higher than the upper interval limit.

Because, for several test conditions 2 runs were normally made instead of a single individual run, it was worthwhile to determine the 95.0% confidence interval limits to be used for the prediction of future average values from multiple test data results. In these cases where the data results of K observations (or K wind tunnel test runs) were averaged, it was possible to adapt the interval limits as follows:

$$\frac{X_j-\mu_j}{\sigma} \text{ becomes } \frac{\overline{X}_j-\mu_j}{\frac{\sigma}{\sqrt{K}}} \text{ where } \overline{X_j}=\sum_{i=1}^{K}\frac{X_{j,i}}{K}$$

$$\frac{\frac{\overline{X}_j-\mu_j}{\frac{\sigma}{\sqrt{K}}}}{\sqrt[2]{\frac{S^2(n-1)}{(n-1)\sigma^2}}}=\sqrt{K}\,\frac{(\overline{X}_j-\mu_j)}{S}$$

$$P\left[X_j-aS \le \mu_j \le X_j+aS\right] \text{ becomes } P\left[\overline{X}_j-a\frac{S}{\sqrt{K}} \le \mu_j \le \overline{X}_j+a\frac{S}{\sqrt{K}}\right]$$

$$\boxed{\mu_j=\overline{X}_j+-\,t\,(\,0.975\,,\,v\,)\,\frac{S}{\sqrt{K}}}$$

This means that the values identified as $\mu_j=\overline{X}_j \pm$ and $\frac{t(0.975\,,\,n-1)S}{\overline{X}_j}$ in the Tables mentioned over and corresponding to the single run case had to be multiplied by the factors specified below:

K number of test runs	Multiple factor to transform single run test interval limits into multiple runs test interval limits
2	0.7071
3	0.5774
4	0.5000
5	0.4472
6	0.4082

TABLE FI

Fin Trailing Edge and Base Pressure Distribution Test Error

Mach 2.0

RUN NUMBER	Mach NUMBER	TAP no:2 pressure ratio P_{tap}/P_{∞}	TAP no:9 pressure ratio P_{tap}/P_{∞}	TAP no:17 pressure ratio P_{tap}/P_{∞}	TAP no:24 pressure ratio P_{tap}/P_{∞}	TAP no:31 pressure ratio P_{tap}/P_{∞}
R3890	1.997	0.516	0.577	0.620	0.584	0.512
R3891	1.999	0.520	0.579	0.624	0.585	0.515
R3892	2.002	0.511	0.570	0.617	0.581	0.507
$\overline{X}_j =$	1.9993	0.5157	0.5753	0.6203	0.5833	0.5113
$S^2 =$	6.333-6	2.033-5	3.6556-5	1.2333-5	4.3333-6	1.6333-5
$S =$	2.5166-3	4.5092-3	6.0461-3	3.5119-3	2.0817-3	4.0415-3
$\mu_j=\overline{X}_j \pm$ single run case	1.0829-2	1.9403-2	2.6017-2	1.5112-2	8.9574-3	1.7390-2
$\frac{t(0.975\ ,\ 2)S}{\overline{X}_j}$ single run case	0.542%	3.76%	4.52%	2.44%	1.54%	3.40%
$\frac{t(0.975\ ,\ 2)S}{\overline{X}_j}$ average of 3 test runs	0.313%	2.17%	2.61%	1.41%	0.889%	1.96%

TABLE FII

Base Pressure Distribution Test Error

Mach 2.0, repeated 9 times

This data is presented here as typical of base pressure distribution measurement and was obtained from wind tunnel tests preformed afterwards the present test series. Related tests conditions produced a boundary layer velocity profile rather similar to the one reported in Appendix D. Calculations based on this data is assumed to give a very representative base pressure distribution test error.

RUN NUMBER	Mach NUMBER	TAP no:1 Base Center tap pressure ratio P_{tap}/P_{∞}
R5467 BP.20.1.01.1	2.00	0.650
R5468 BP.20.1.01.2	2.00	0.655
R5469 BP.20.1.01.3	2.00	0.653
R5470 BP.20.1.01.4	2.01	0.658
R5471 BP.20.1.02.1	2.00	0.650
R5472 BP.20.1.02.2	2.00	0.652
R5473 BP.20.1.03.1	2.00	0.650
R5474 BP.20.1.03.2	2.00	0.652
R5475 BP.20.1.04.1	2.00	0.654
$\overline{X}_j =$	2.001	0.653
$S^2 =$	1.111-5	5.800-5
$S =$	3.333-3	7.616-3
$\mu_j = \overline{X}_j \pm$ single run case	±7.687-3	±1.756-2
$\frac{t(0.975\ ,\ 8)S}{\overline{X}_j}$ single run case	±0.384%	±2.691%

TABLE FIII

Boundary Layer Velocity Profile Test Error

Mach 2.0, Y/R = .1365, repeated 4 times

This data is presented here as typical of boundary layer velocity profile measurement and was obtained from wind tunnel tests preformed afterwards the present test series. Related tests conditions produced a boundary layer velocity profile rather similar to the one reported in Appendix D. Calculations based on this data is assumed to give a very representative boundary layer velocity profile test error.

RUN NUMBER	Mach number	U/U_{inf}	LnU/U_{inf}	MBL Mach number inside boundary layer
R5239	2.00	0.7768	-0.2526	1.355
R5240	2.01	0.7780	-0.2510	1.359
R5251	2.01	0.7698	-0.2616	1.340
R5252	2.00	0.7683	-0.2636	1.336
$\overline{X}_j =$	2.005	0.7732	-0.2572	1.3475
$S^2 =$	3.333-5	7.1568-5	3.9973-5	1.2567-4
$S =$	5.774-3	8.4598-3	6.3224-3	1.1210-2
$\mu_j = \overline{X}_j \pm$ single run case	±1.837-2	±2.6919-2	±2.0118-2	±3.5671-2
$\frac{t(0.975\ ,\ 3)S}{\overline{X}_j}$ single run case	±0.916%	±3.481%	±7.822%	±2.647%

INTERNAL DISTRIBUTION

DREV TM-1999-134

1 - Director General
1 - Deputy Director General
1 - Chief Scientist
6 - Document Library
1 - B. Girard (author)
1 - G. Bérubé
1 - R. Bilodeau
1 - R. Delagrave
1 - G. Dumas
1 - A. Dupuis
1 - E. Fournier
1 - A. Jeffrey
1 - F. Lesage

EXTERNAL DISTRIBUTION

DREV TM-1999-134

1 - DRDIM
1 - DRDB
1 - DSTA
1 - DSTL

1 - Dr. C. Berner
1 - Bibliothèque ISL
Institut Franco-Allemand de Recherches
5, rue du Général Cassagnou
B.P. 34
68301 - Saint-Louis (France)

1 - Dr. N. D'Souza
Les Technologies Industrielles SNC Inc.
Usine Le Gardeur
5, montée des Arsenaux
Le Gardeur, Qc
J5Z 2P4

1 - Dr. L. Chan
High Speed Aerodynamic Laboratory
Institute for Aerospace Research
National Research Council Canada
Montreal Road
Ottawa, Ontario
K1A 0R6

UNCLASSIFIED
SECURITY CLASSIFICATION OF FORM
(Highest Classification of Title, Abstract, Keywords)

DOCUMENT CONTROL DATA

1. ORIGINATOR (name and address)
Defense Research Establishment Valcartier
(DREV)

2. SECURITY CLASSIFICATION (including special warning terms if applicable)
UNCLASSIFIED

3. TITLE (its classification should be indicated by the appropriate abbreviation (S, C, R or U)
WIND TUNNEL TESTS ON DREV-ISL REFERENCE AFTERBODIES AT MACH 2.0
(SERIES ISLPWT-2)

4. AUTHORS (Last name, first name, middle initial. If military, show rank, e.g. Doe, Maj. John E.)
Girard, Bertrand

5. DATE OF PUBLICATION (month and year)
Marsh 2000

6a. NO. OF PAGES
196

6b .NO. OF REFERENCES
41

7. DESCRIPTIVE NOTES (the category of the document, e.g. technical report, technical note or memorandum. Give the inclusive dates when a specific reporting period is covered.)
Memorandum

8. SPONSORING ACTIVITY (name and address)
DREV

9a. PROJECT OR GRANT NO. (Please specify whether project or grant)
PSC 31D

9b. CONTRACT NO.
N/A

10a. ORIGINATOR'S DOCUMENT NUMBER
DREV TM-1999-134

10b. OTHER DOCUMENT NOS
N/A

11. DOCUMENT AVAILABILITY (any limitations on further dissemination of the document, other than those imposed by security classification)

☒ Unlimited distribution
☐ Contractors in approved countries (specify)
☐ Canadian contractors (with need-to-know)
☐ Government (with need-to-know)
☐ Defense departments

12. DOCUMENT ANNOUNCEMENT (any limitation to the bibliographic announcement of this document. This will normally correspond to the Document Availability (11). However, where further distribution (beyond the audience specified in 11) is possible, a wider announcement audience may be selected.)
Full unlimited announcement

13. ABSTRACT (a brief and factual summary of the document. It may also appear elsewhere in the body of the document itself. It is highly desirable that the abstract of classified documents be unclassified. Each paragraph of the abstract shall begin with an indication of the security classification of the information in the paragraph (unless the document itself is unclassified) represented as (S), (C), (R), or (U). It is not necessary to include here abstracts in both official languages unless the text is bilingual).

Supersonic wind tunnel tests were made in the DREV 0.6 m x 0.6 m trisonic facility in contribution to a research programme between DREV and the Institut de Recherches de St-Louis (ISL), France under the auspices of Theme 25 - Aeroballistics of the Franco-Canadian Accord. The aim was to compare with similar tests performed at ISL with DREV-ISL reference models that were defined to normalize experimental results from DREV and ISL and with an interest to the influence of Reynolds number. The cooperative agreement was to study base flow recirculation phenomena and wake interaction from preceeding projectile on the following one of projectiles flying in formation or tandem projectiles. This memorandum describes Phase II of the wind tunnel tests made at Mach 2.0 to characterize the boundary layer approaching a flat base and to perform surface pressure distributionmeasurements on the base/afterbody of DREV-ISL reference models. They reproduced the afterbody of the "Southampton University Calibration Model" with/without trapezoidal fins. This wind tunnel test runs series (made at subcritical Reynolds numbers) provided data complementary to the ISL facility's (obtained at supercritical Reynolds numbers). The results describe the boundary layer velocity profile and related characterization. A total of 57 runs were made for a variety of roll angles. Equations used for treatment of data are presented together with test conditions and a summary of results. Also, a description of the instrumentation test settings and several model drawings were incorporated.

14. KEYWORDS, DESCRIPTORS or IDENTIFIERS (technically meaningful terms or short phrases that characterize a document and could be helpful in cataloguing the document. They should be selected so that no security classification is required. Identifiers, such as equipment model designation, trade name, military project code name, geographic location may also be included. If possible keywords should be selected from a published thesaurus, e.g. Thesaurus of Engineering and Scientific Terms (TEST) and that thesaurus-identified. If it is not possible to select indexing terms which are Unclassified, the classification of each should be indicated as with the title.)

AERODYNAMICS, ARMOR PIERCING AMMUNITION, ARTILLERY SHELLS, WIND TUNNEL MODELS, ANTITANK AMMUNITION, SUBCALIBER PROJECTILES, WARHEADS, PROJECTILES, MACH 2.0, KINETIC ENERGY PROJECTILE, SUPERSONIC, AERODYNAMIC COEFFICIENTS, BODIES OF REVOLUTION, DRAG, AERODYNAMIC CONFIGURATIONS, SUPERSONIC WIND TUNNELS, LAMINAR BOUNDARY LAYER, TURBULENT BOUNDARY LAYER, BOUNDARY LAYER CONTROL, STATIC PRESSURE, GUNNERY, GUNS (ORDNANCE), WIND TUNNELS, CYLINDRICAL BODIES, LIFTING BODIES, SLENDER BODIES, AERODYNAMIC FORCES, AERODYNAMIC DRAG, AERODYNAMIC LOADS, BLOW DOWN, TEST FACILITIES, BLUNT BODIES, AFTERBODIES, FLOW SEPARATION, PITOT TUBES, BOUNDARY LAYER FLOW, MODEL TESTS, ABSOLUTE PRESSURE, BASE PRESSURE, DYNAMIC PRESSURE, DIFFERENTIAL PRESSURE, GAS LAWS, PRESSURE MEASUREMENT, STATISTICAL ANALYSIS, TURBULENT FLOW, NONUNIFORM FLOW, FLIGHT CHARACTERISTIC, AEROBALLISTICS, BOUNDARY LAYER, VELOCITY PROFILING, BASE FLOW, VELOCITY

(Thesaurus of Engineering and Scientific Terms,
Engineering Joint Council, March 1969)

#513130